ISBN 978-82-471-2900-5 (printed ver.)
ISBN 978-82-471-2901-2 (electronic ver.)
ISSN 1503-8181

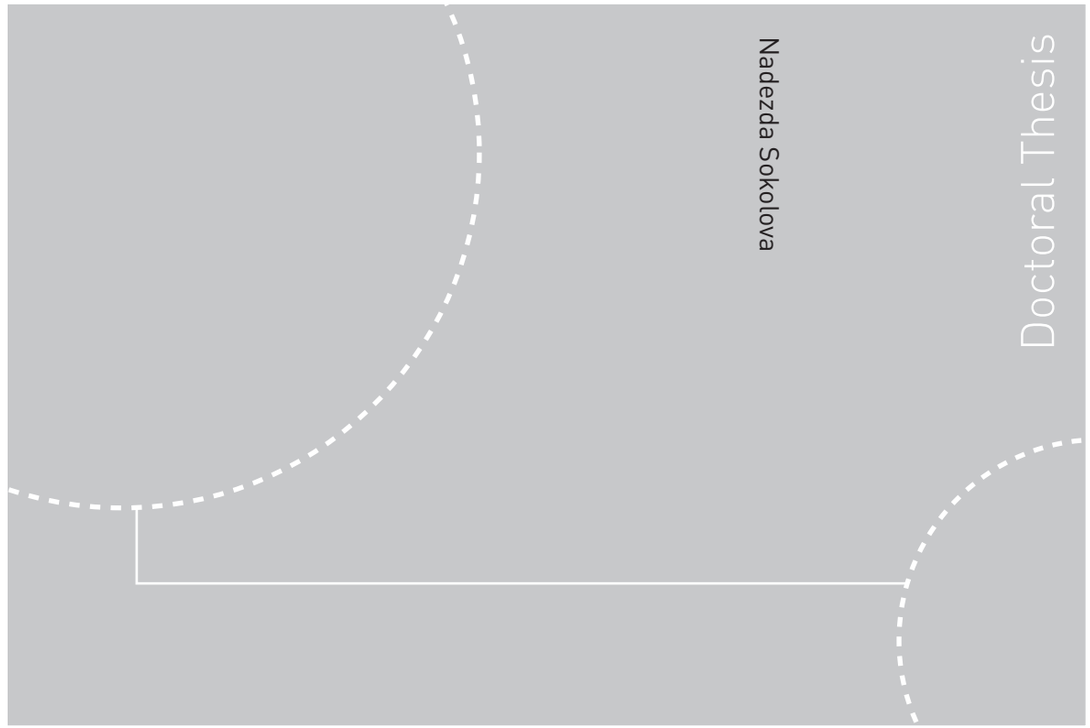

Doctoral theses at NTNU, 2011:176

Nadezda Sokolova

Theoretical Analysis of the Process of Doppler and Doppler Rate Estimation in Standard and High Sensitivity GNSS Receivers

NTNU
Norwegian University of Science and Technology

Doctoral theses at NTNU, 2011:176

NTNU

NTNU
Norwegian University of Science and Technology
Thesis for the degree of doctor philosophiae
Faculty of Information Technology, Mathematics and Electrical Engineering
Department of Electronics and Telecommunications

NTNU
Norwegian University of Science and Technology

Nadezda Sokolova

Theoretical Analysis of the Process of Doppler and Doppler Rate Estimation in Standard and High Sensitivity GNSS Receivers

Thesis for the degree of doctor philosophiae

Trondheim, June 2011

Norwegian University of Science and Technology
Faculty of Information Technology,
Mathematics and Electrical Engineering
Department of Electronics and Telecommunications

NTNU
Norwegian University of
Science and Technology

NTNU
Norwegian University of Science and Technology

Thesis for the degree of doctor philosophiae

Faculty of Information Technology, Mathematics and Electrical Engineering
Department of Electronics and Telecommunications

ISBN 978-82-471-2900-5 (printed ver.)
ISBN 978-82-471-2901-2 (electronic ver.)
ISSN 1503-8181

Doctoral Theses at NTNU, 2011:176

Printed by Tapir Uttrykk

ABSTRACT

Due to the capability of the Global Positioning System (GPS) to provide accurate, stable long-term navigation information, the use of a GPS receiver as a velocity and acceleration sensor has gained an increasing research interest. Navigation and control, airborne gravimetry and integration with inertial navigation systems (INS) are just some of the potential applications.

GPS velocity and acceleration measurements are typically determined using Doppler and Doppler rate observations provided by the receiver carrier tracking loops. Thus, the final quality of the velocity/acceleration measurements depends on the variance of the Doppler and Doppler rate observations and on the approach used for the velocity/acceleration computation. It is therefore desirable to be able to predict the quality of Doppler and Doppler rate observations, not only for quality control and for estimating the uncertainty of this information, but also for properly weighting the measurements in the LS and KF solution.

This thesis introduces a cohesive analysis describing the noise propagation process from the input of the carrier tracking loops to the final Doppler and Doppler rate estimates. Two different approaches used by GNSS receivers are considered namely the sequential carrier tracking, including the standard and memory discriminator based approaches, and block processing techniques. For each approach, a theoretical framework for Doppler estimation relating the variance and biases of the Doppler estimates to C/N_0, the user dynamics and the algorithm parameters is introduced.

Also, based on the proposed theoretical framework a new approach to loop filter design providing control over the noise variance of the Doppler measurements is introduced.

The developed theoretical framework and the proposed approach to loop filter design have been verified by performing a number of static and dynamic pedestrian-based field tests and simulations with the major focus on the environments with strong signal attenuation and multipath.

PREFACE

This thesis is submitted in fulfillment of the requirements for the degree of *philosophiae doctor* (PhD) at the Department of Electronics and Telecommunications, Norwegian University of Science and Technology (NTNU). Doctoral work presented in this thesis has been performed with Professor Börje Forssell, (Radio Systems group, Department of Electronics and Telecommunications) as main supervisor. Most of the practical experiments presented in this work were performed at the Position Location And Navigation (PLAN) group, University of Calgary, Canada, where I have stayed as a visiting graduate student.

The work has been funded by the Norwegian Research Council (NRC), via the project High Accuracy LOcalization (HALO) for handheld terminals conducted by NTNU in conjunction with Telenor R&D, Radionor and Kongsberg-Seatex.

ACKNOWLEDGEMENTS

I would like to acknowledge the following persons and parties for their invaluable contributions to this thesis:

- My supervisor, Professor Börje Forssell for sharing his knowledge and for giving me countless opportunities to develop new skills.
- Dr. Daniele Borio, who has been an infinite source of ideas for discussion that led to so many research opportunities. Much of the knowledge that I required for this research has been developed through my collaboration with this person.
- The head of the PLAN group, Professor Gérard Lachapelle for providing an opportunity to work in the group, and also providing the access to the GSNRx^{TM} software and hardware equipment of the NavLab.
- My friends and colleagues at NTNU, especially IET for your support and encouragement. I owe the completion of this thesis to you all.

Lastly, I would like to thank everybody who was important to the successful realization of thesis, as well as expressing my apology that I could not mention everyone.

TABLE OF CONTENTS

LIST OF TABLES

LIST OF FIGURES

ACRONYMS AND ABBREVIATIONS

Abbreviation	Definition
A-GPS	Assisted GPS
C/N_0	Carrier-to-Noise density ratio
CRLB	Cramer Rao Lower Bound
E911	Enhanced 911
FLL	Frequency Lock Loop
FCC	Federal Communications Commission
FFT	Fast Fourier Transform
FIR	Finite Impulse Response
GNSS	Global Navigation Satellite System
GPS	Global Positioning System
HSGPS	High Sensitivity GPS
IF	intermediate frequency
INS	Inertial Navigation System
KF	Kalman Filter
LOS	Line-Of-Sight
MA	moving average
ML	maximum likelihood
MMSE	minimum mean square error
MSE	mean square error

NCO	numerically controlled oscillator
PLL	Phase Lock Loop
PRN	Pseudo Random Noise
SDR	Software Defined Radio
SNR	signal-to-noise ratio
WLS	weighted least squares

LIST OF SYMBOLS

Symbol	Definition
A	signal amplitude
A_c	signal amplitude at the correlator output
$B(z)$	transfer function of a loop filter
B_d	Doppler bandwidth
$B_{\dot{f}}$	Doppler rate bandwidth
B_n	loop bandwidth
G_d	discriminator gain
$I(z)$	transfer function of an integrator
K	number of complex correlator outputs
L	order of the loop
$N(z)$	transfer function of the NCO
$N_d[k]$	equivalent phase noise
$N_f[k]$	equivalent frequency noise
$N_{\dot{f}}$	equivalent frequency rate noise
P	prompt complex correlator output
R	covariance matrix of observations
R_v	variance-covariance matrix of the unknowns

S_L	squaring loss
T_c	coherent integration time
T_s	sampling interval
W	analysis window length
$\mathbf{a}^{(k)}$	k^{th} satellite acceleration vector
a	user acceleration
f_{IF}	intermediate frequency
$\hat{f}$	final Doppler frequency estimate
$\dot{\hat{f}}$	final Doppler frequency rate estimate
f_s	sampling frequency
f_{cp}	carrier phase derived Doppler measurement
f_d	true Doppler frequency
$\dot{f}_d$	true Doppler frequency rate
f_{raw}	raw Doppler measurement
$\dot{f}_{raw}$	raw Doppler rate measurement
$h^{(k)}$	user-to-satellite LOS unit vector
$\mathbf{v}$	user velocity vector
$\mathbf{v}^{(k)}$	k^{th} satellite velocity vector
α	forgetting factor

$\delta[\cdot]$	Kronecker delta
ε_f	systematic errors in Doppler measurements
$\varepsilon_{\dot{f}}$	systematic errors in Doppler rate measurements
ε_ϕ	residual phase error
ϕ_{ob}	carrier phase observation
$\hat{\phi}$	phase estimate
λ_{L1}	L1 wavelength
τ_0	delay experienced by the received signal

CHAPTER 1: INTRODUCTION

1.1. Background and Justification

The determination of velocity and acceleration from Global Positioning System (GPS) measurements is very important for many applications including navigation, airborne gravimetry and geophysics. GPS velocity and acceleration measurements are typically determined using Doppler and Doppler rate observations which, in turn, are estimated by directly processing carrier tracking loop outputs or, alternatively, obtained by differentiating carrier phase observations (Serrano et al 2004, Serrano et al 2004a, Wieser 2007), once to get the line of sight velocity and twice, for acceleration.

The feasibility of GPS-based velocity and acceleration estimation with mm/s and mm/s^2 accuracy respectively has long been shown using differential techniques (Cannon et al 1997, Ryan et al 1997, Bruton 2000). But during the last several years, low-cost GPS receivers capable to provide accurate Doppler, or carrier phase measurements from which Doppler and Doppler rate measurements can be derived became available for mass market. The achievable accuracy of low-cost GPS-based velocity and/or acceleration estimates has been investigated by Psiaki et al (1999), Serrano et al (2004a, b), Petovello et al (2003) and van Graas & Soloviev 2004, showing that it is possible to achieve accuracies of a few millimetres per second in velocity and acceleration at the millimetres per second squared level depending on the receiver quality, whether in stand-alone or relative and static or kinematic mode. Due to cost-effectiveness, ease in operation and maintenance, as well as capability to provide a long-term stable reference the use of GPS receivers rather than speedometers and/or accelerometers has become a very attractive option (Serrano et al 2004a, Weiser 2007).

While the use of velocity and acceleration measurements provided by GPS for dynamic applications is rather straightforward, in airborne gravimetry GPS observations are used to derive the Earth's gravity field where acceleration measurements derived from the GPS

observables are used to compensate for the motion of the aircraft isolating the desired gravity component (Bruton 2000, Kennedy 2002). This information depending on the required accuracy and resolution is used in geodesy, geophysics and oceanography. However, despite the beneficial effect that GPS brought to the field of airborne gravimetry due to its capability to provide an accurate measure of the absolute position, velocity and acceleration of the aircraft over the long-term, the accuracy of GPS acceleration measurements continues to pose a major challenge (Psiaki et al 2000).

At the same time, escalating requirements from the Federal Communications Commission for the provisioning of Enhanced 911 (E-911) services and the increasing demand for Location Based Services (LBS) in signal degraded environments have been driving the development of positioning technologies where GPS-based techniques have become very attractive due to the great effort made by the industry to miniaturize front-ends and processing cores into one single chipset while increasing both acquisition and tracking sensitivity and the availability of the position solution especially in urban environments. However, GPS-based positioning techniques still encounter issues in urban canyon and indoor areas where LBS users are very likely to be. In such environments, already attenuated GPS signals are further affected by strong multipath and fading making user location a real challenge. To enhance the sensitivity and thus the availability of the position solution using GPS in these adverse environments, High Sensitivity (HS) techniques based on the use of either long integration times (Peterson et al 1997), or massive parallel correlation/block processing (van Diggelen 2001, van Graas et al 2005) have been developed.

In this regard, Doppler rate measurements can be used to improve tracking loop performance as suggested in (Kazemi et al 2009). In particular, Doppler rate information is used to aid the Numerically Controlled Oscillator (NCO) in order to produce a linearly varying local carrier frequency. This reduces the accumulated signal power losses introduced by the mismatch between locally generated and incoming signals. This is

especially valuable in the case of High-Sensitivity (HS) GPS receivers where loops employing long integration time and low update rates are used (Kazemi et al 2009).

An alternative solution to achieve performance in degraded GPS signal environments is by integrating different technologies such as, for example, standard or HSGPS with dead-reckoning sensors such as Inertial Navigation Systems (INS) (Mezentsev 2005, Bancroft et al 2008). Traditionally, a GPS/INS integrated system employs GPS derived pseudorange measurements to aid the INS system. But indoors and in urban areas pseudorange measurements are heavily degraded by errors such as multipath, non-line of sight signals as well as from degraded satellite geometry (Kubo 2009). To circumvent this problem velocity information derived from GPS Doppler measurements (Moafipoor et al 2004), raw Doppler measurements (Petovello et al 2003) or time-differenced carrier phase measurements (Wendel et al 2006) can be used as alternative aiding sources. The advantage of this approach is that Doppler multipath effects are a function of receiver velocity, and therefore for low dynamic navigation in the indoor and urban environments should remain minimal. But for successful implementation of an integrated system, the accuracy of aiding information is critical as an aiding source with poor accuracy will not be able to restrain the INS navigation error growth *(*El-Sheimy 2009*)*.

Typically, both acceleration and velocity of the user are determined using either a Least Squares (LS) or Kalman Filter (KF) estimation technique. According to estimation theory, weighting the measurements properly should lead to better estimates (Gelb 1974). A precise observation should have a higher weight and thus contribute more to the computed parameters than an imprecise one. Knowledge of the accuracy of the Doppler/Doppler rate observables is also important in view of statistical failure detection and identification. Inaccurate variance information may cause outliers to remain undetected and accurate observations to be rejected. Thus, in order to obtain precise and reliable velocity/acceleration estimates it is essential not only to have accurate Doppler and/or Doppler rate information, but also a figure of merit providing an estimate of the uncertainty of this information that can be used for appropriate weighting of the measurements.

Therefore, it is advantageous to have a theoretical framework that will allow one to effectively evaluate and predict the quality of Doppler and Doppler rate measurements providing bounds on the acceleration and velocity accuracy.

1.2 Limitations of the Previous Research

Intense research activities have been focused on the area of Doppler and Doppler rate estimation using GPS. However, most of the previous studies have been essentially limited to hardware receivers (Ryan et al 1997, van Graas & Soloviev 2003, Serrano et al 2004, Zhang et al 2005). Hardware receivers with proprietary algorithms and post-processing software do not provide any insight on how Doppler and Doppler rate measurements are formed, preventing an accurate analysis at the tracking loop level. Moreover, a hardware GPS receiver doesn't allow one to access the Doppler-rate measurements directly from the tracking loops of the receiver. Therefore, to obtain the user's acceleration either a double time differentiation of the GPS derived position or, preferably, differentiation of the raw Doppler or double differentiation of the carrier phase measurements has to be performed (Bruton 2000, Zhang et al 2005).

In this way, only the relationship between carrier phase, Doppler and Doppler rate measurements and velocity and/or acceleration estimation has been investigated. In particular, a thorough review of behaviour and magnitude of the GPS Doppler and carrier phase error sources (multipath, satellite geometry, effect of ionosphere, clock errors, etc.) is provided by Bruton (2000) and Wieser (2007). A good study of the process of time differentiation and an overview of existing methods is given in Bruton (2000) with emphasis on determining velocity and acceleration from measurements made by the GPS receivers. An experimental study of the Doppler measurement quality as a function of the Carrier-to-Noise density ratio (C/N_0) is presented in (Petovello et al 2003), but the introduced results are empirical and do not consider the parameters and structure of the carrier tracking loops.

As it has been mentioned above, Doppler and Doppler rate measurements are obtained by processing the outputs of the carrier tracking loops of the receiver, and parameters such as the loop type and order, integration time and loop bandwidth strongly impact their quality. Ward (1998, 2005) investigated the capability of an FLL to provide accurate frequency estimates depending on C/N_0, loop bandwidth and the coherent integration time by performing interpolation of the simulation results using the Monte Carlo techniques. A study of the process of Doppler estimation based on analytical derivations and the use of a Software Defined Radio (SDR) GPS receiver was performed by Sokolova (2009), proposing a theoretical framework allowing the evaluation of Doppler accuracy relating the variance and biases of the Doppler estimates to PLL parameters such as the PLL bandwidth and integration time, as well as the C/N_0 and the user dynamics. But the theoretical framework presented in Sokolova (2009) is valid for PLLs only, and considers only the process of Doppler estimation. Given the benefits provided by the use of the SDR receiver, it is desirable to develop a similar theoretical framework applicable for evaluation of Doppler rate measurements. Moreover, to be able to evaluate the accuracy of the Doppler estimates in the cases when the receiver is losing phase lock, it is desirable to extend such framework to Frequency Lock Loops (FLLs) and FLL-assisted-PLLs.

Finally, most of the previous studies on Doppler and Doppler rate estimation analysis e.g., Ryan et al (1997), van Graas & Soloviev (2003), Serrano et al (2004) were focused on the near Line Of Sight (LOS) conditions only, which are in the absence of multipath and for high to moderate values of C/N_0. The impact of strong signal attenuation and biases introduced by multipath has been rarely addressed. As it has been mentioned in the previous section, performance in degraded signal environments can be achieved using HSGPS. HSGPS is a technology developed to enhance acquisition and tracking thresholds based either on the use of long integration times or massive parallel correlation/block processing. Petovello et al (2003) performed an experimental analysis of Doppler measurements accuracy provided by a low-cost HSGPS hardware receiver, but as discussed above, due to the limitations of hardware receivers only the relationship between the C/N_0

measurements provided by the receiver and Doppler measurements quality could be analysed. A software HSGPS receiver architecture based on memory discriminators proposed by Borio et al (2009) was used in the analysis provided in (Sokolova 2009) where the presented theoretical framework for Doppler evaluation was extended also to include this type of architecture. However, a memory discriminator based HSGPS architecture represents a sequential approach, i.e., the current frequency estimate is obtained by updating previous estimates using the new information provided by the correlator outputs. Another approach, based on massive parallel correlation, can be adopted and used in investigations such as those outlined in van Diggelen (2001) and van Graas et al (2005) to facilitate the complex task of searching for weak GPS signals. In the literature, this technique is often referred to as block or batch processing e.g., van Graas et al (2005). Because of the frequent use of this approach in HSGPS receiver design, it is desirable to develop a theoretical model that will allow the evaluation of Doppler measurement quality applicable to block processing GPS receiver architectures.

It is also important to consider that although the thermal noise is often treated as the dominant source of carrier tracking error, due to the fact that it is common to use low quality oscillators in consumer grade GNSS receivers, the oscillator phase noise can also pose significant difficulties for PLLs (Kaplan 2006). In particular, it can impose an upper limit on the coherent integration period (Gaggero & Borio, 2008), can impose a lower limit on the PLL filter bandwidth (Curran et al 2010) and can limit the range of applications in the case where oscillators are particularly sensitive to high dynamics and vibrations (Filler 1988). Optimisation of PLL filters with respect to the local oscillator is a topic that has been and still is being studied (Kaplan 2006, Curran et al 2010). Analysis of this source of noise jitter, however, falls beyond the scope of this thesis.

1.3 Statement of the Problem

The overall objective of this thesis is to develop, test and verify a comprehensive theoretical framework for the analysis of the process of Doppler and Doppler rate estimation necessary for studying and charactering the impact of the algorithm parameters, C/N_0 and user dynamics on the accuracy of the measurements. The developed theoretical framework should include the analysis of two approaches used in GNSS receivers, namely sequential carrier tracking, including the standard and memory discriminator based approaches, and block processing techniques. In the case of sequential carrier tracking three types of carrier tracking loops should be considered: PLL, FLL-assisted-PLL and FLL.

1.3.1 Objectives and Contributions

Considering the above-mentioned limitations of the research performed previously on Doppler and Doppler rate determination, the objectives and major contributions of this thesis can be summarised as follows:

1. Analysis of the Doppler estimation process in tracking loops of a sequential GPS receiver architecture. Doppler measurements are obtained by processing the carrier tracking loop outputs and parameters such as integration time, loop bandwidth and order strongly impact their quality. The major objective here is to develop a complete theoretical framework allowing the evaluation of Doppler accuracy, relating the variance and biases in the Doppler estimates to the type of loop and its parameters, C/N_0 and user dynamics extending and completing the research performed in (Sokolova 2009). To get a comprehensive framework, the following types of the carrier tracking loops are considered:

- Phase Lock Loop (PLL)
- Frequency Lock Loop (FLL)
- FLL-assisted-PLL

Moreover, two different types of sequential architecture are used in this research, the standard and memory discriminator based one.

2. Noise propagation and Doppler estimation analysis in a block processing architecture. Because of the ability to perform a massive parallel search over the entire range of possible code delays/carrier frequencies and ensure that the correlation peak will always be detected, even in degraded signal environments with significant signal fading, a block processing technique is frequently used in HSGPS receivers. It is, therefore, desirable to perform a study on the noise propagation process in this type of architecture and provide a theoretical model allowing the evaluation of the Doppler measurements obtained from HS receivers employing block processing techniques.

3. Investigation and verification of the loop filter design based on Doppler bandwidth. The flexibility of the controlled-root formulation approach to loop filter design proposed by Stephens & Thomas (1995) and introduction of the Doppler bandwidth parameter (Sokolova 2009) allows one to design the loop filter in a way which provides control over the noise variance of the Doppler frequency measurements.

Doppler bandwidth has been derived as a related design parameter to the loop noise bandwidth with the major difference between these two parameters being that Doppler bandwidth provides a more faithful interpretation of the bandwidth required to track particular system dynamics.

The proposed approach consists of modifying the controlled-root formulation by basing it on the Doppler bandwidth allowing one to configure the tracking loop to output Doppler measurements with a desired level of Doppler jitter. The design criteria behind this approach are specified, and the effectiveness of proposed algorithm analysed using real GPS data.

4. Development and verification of a theoretical framework for the analysis of Doppler rate estimation process in a sequential receiver architecture. Given the flexibility of the SDR GPS receiver it is possible to obtain Doppler rate measurements by evaluating the outputs of the FLL or the FLL-assisted-PLL of the receiver. Also in this

case, tracking loop parameters such as the integration time, loop order and bandwidth, impact the quality of the measurements and it is therefore necessary to perform a complete and cohesive analysis of the noise propagation through the entire estimation process from the input of the carrier tracking loop to the final Doppler rate estimate. To be able to perform such analysis, a general linear model relating the variance and bias of Doppler rate estimates to the C/N_0, the user dynamics and the loop parameters is used. Additionally, in order to get a complete model, the following types of Doppler rate measurements will be considered:

- raw Doppler rate measurements
- Doppler rate measurements derived from carrier phase observations

Finally, to demonstrate the validity and investigate the effectiveness of the developed theoretical model for the analysis of the Doppler rate measurements, it is necessary to perform extensive data collections in various GPS operating environments to be able to test the theory against real data.

1.3 Thesis Outline

In order to provide a comprehensive view of the research performed, the structure and content of the subsequent chapters is outlined in the following.

Chapter 2 focuses on the types of Doppler and Doppler rate measurements. The first one is the raw Doppler and raw Doppler rate measurement type obtained directly from the outputs of the carrier tracking loops. The second one is carrier phase derived Doppler and Doppler rate measurement type obtained by performing a single time differentiation of the carrier phase observables, in the case of Doppler, or double time differentiation in the case of Doppler rate measurements. Relationship between these two measurement types is highlighted and an alternative approach consisting in filtering raw measurements in order to achieve equivalent performance is discussed. Moreover, this chapter gives a brief overview

of existing differentiation methods for velocity and acceleration determination. In addition to this, the underlying theory behind velocity and acceleration estimation process using GPS, and GNSS in general is provided. A review of HSGPS techniques is also provided with specific focus on memory discriminator based and block processing approaches.

Chapter 3 considers sequential carrier tracking, including the standard and memory discriminator based approaches, and block processing techniques introducing theoretical frameworks for Doppler estimation for each of the approaches. In the case of sequential carrier tracking the quality of Doppler measurements is theoretically evaluated by reformulating the standard tracking loop linear theory with respect to the signal Doppler frequency, the frequency noise and the final Doppler frequency measurement provided by the loop. Tracking loops, including PLL, FLL-assisted-PLL and FLL are considered and it is shown that the concept of Doppler bandwidth is general and can be applied to different types of tracking loops. An approach used to extend the theoretical model in order to include the effect of memory discriminators is also detailed. For the block processing approach the Cramer-Rao Lower Bound (CRLB) for frequency estimation is provided and used to derive an approximation of the variance of the frequency estimates generated by block processing techniques. The theory developed is the basic tool extensively used in the rest of the thesis.

Finally, the proposed theoretical framework is validated by using simulated and real life GPS L1 C/A signals and the analysis of the test results presented.

Chapter 4 concentrates on the investigation of an approach to loop filter design based on Doppler bandwidth that will allow one to control the noise variance of the Doppler measurements. Following an introduction of the controlled-root formulation algorithm (Stephens & Thomas 1995) and a discussion of the motivation behind this design, the necessary changes to this algorithm are described and the design criteria specified. Both standard and memory discriminator based PLLs are considered.

The effectiveness of the proposed approach is verified by live GPS L1 C/A data. Methodology for the data analysis is described and the obtained results presented and analyzed in detail in the last part of the chapter.

Chapter 5 considers sequential carrier tracking, including the standard and memory discriminator based approaches, and block processing techniques with respect to the process of Doppler rate estimation. First, the assumption of negligible Doppler rate during the integration period adopted in GNSS receivers is discussed, and the CRLB for the Doppler rate estimates is provided and used as a comparison for the proposed theoretical models. In the case of sequential carrier tracking, the PLL, common-rate FLL-assisted-PLL and FLL are explicitly considered where each type of the tracking loop is approximated as a linear device extracting Doppler rate measurements from the input samples. The linear transfer functions from the input noise to the final Doppler rate estimate are also derived. In order to quantify the portion of noise transferred from the input signal to the final Doppler rate estimates the concept of Doppler rate bandwidth is introduced. For the block processing approach, an expression of the variance of the Doppler rate estimates is derived based on the CRLB for the Doppler frequency measurements introduced in **Chapter 3**. It is noted that theoretical framework introduced in this chapter is a generalization of the analysis provided in **Chapter 3** with respect to Doppler frequency estimation.

Test methodology and equipment setup for the static and dynamic pedestrian-based field tests and simulations that were carried out for evaluation of the developed theory for Doppler rate analysis are also presented in this chapter. The collected data analysis is presented here through comparison of the results obtained empirically with the ones obtained using the theoretical model. Different combinations of tracking loop parameters and different methods for Doppler rate measurements derivation are considered.

Finally, in **Chapter 6**, conclusions are drawn from the performed investigations and directions for further research suggested.

Although this thesis is written as a monograph, it is based on the material published at conferences, in journals:

- Sokolova, N., D. Borio, B. Forssell (2011) "Loop Filter with Controllable Doppler Jitter for Standard and High Sensitivity (HS) GNSS Tracking Loops." To be presented at *2011 International Conference on Indoor Positioning and Indoor Navigation (IPIN)*, 21-23 September, Guimarães, Portugal
- Borio, D., N. Sokolova and G. Lachapelle (2010) "Doppler Measurement Accuracy in Standard and High-Sensitivity GNSS Receivers." accepted for publication at *IET Radar, Sonar & Navigation journal*
- Sokolova, N., D. Borio, B. Forssell, and G. Lachapelle (2010) "Doppler Rate Measurements in Standard and High Sensitivity (HS) GPS Receivers: Theoretical Analysis and Comparison." *Proceedings of IEEE/2010 International Conference on Indoor Positioning and Indoor Navigation (IPIN)*, Zurich, 15-17 September 2010, 9 pp
- Borio, D., N. Sokolova and G. Lachapelle (2009) "Memory Discriminators for Non-Coherent Integration in GNSS Tracking Loops." *ATTI dell'Istituto Italiano di Navigazione*, No 189, July Issue, 80-100
- Borio, D., N. Sokolova and G. Lachapelle (2009) "Doppler Measurements and Velocity Estimation: a Theoretical Framework with Software Receiver Implementation." *Proceedings of GNSS09* (Savannah, GA, 22-25 Sep, Session A4), The Institute of Navigation, 13 pp
- Borio, D., N. Sokolova and G. Lachapelle (2009) "Memory Discriminators for Non-Coherent Integration in GNSS Tracking Loops." *Proceedings of European Navigation Conference 2009 (ENC09),* Naples, Italy (3-6 May), 12 pp

CHAPTER 2: FUNDAMENTALS

To establish the basic notation for this thesis, a description of the signal and system model is given in the first section of this chapter. The major focus of this thesis is on the process of Doppler and Doppler rate estimation in digital carrier tracking loops. Therefore, an overview of available types of Doppler and Doppler rate observables from the loop outputs is presented. As time differentiation plays an important role in the process of deriving Doppler and Doppler rate measurements from the GPS carrier phase observables, a discussion of the choice of the differentiator types suitable for this particular research is also given. Following this, a brief review of the background relevant to the task of velocity and acceleration estimation using GPS observables is provided.

HSGPS techniques with particular attention on memory discriminator-based receiver architecture and a block processing approach for weak signal tracking are reviewed in the last section of this chapter. These two receiver architectures will be considered in the following chapters to extend the developed theoretical model for Doppler and Doppler rate analysis to be applicable to HSGPS techniques. Finally, a short note on future GNSS signal structures in terms of weak signal tracking is provided focusing on is the availability of the pilot channel.

2.1 Doppler and Doppler rate Estimation Process in GNSS Carrier Tracking Loops

2.1.1 Signal and System Model

The complex baseband signal at the input of a digital tracking loop can be expressed as the sum of L useful signal components modulated using Direct Sequence Spread Spectrum (DSSS) techniques and a noise term:

$$s[n] = \sum_{i=0}^{L-1} y_i[n] + w[n]. \tag{2.1}$$

The input signal, $s[n]$, in Eq.(2.1) has already been down-converted and digitized by the receiver front-end. The notation $y[n] = y(nT_s)$ is used to denote a digital sequence sampled at the frequency $f_s = \frac{1}{T_s}$ and n is the discrete time index. Each useful signal component can be modeled as follows (Misra & Enge 2006):

$$y_i[n] = A_i\, d_i\left[n - \frac{\tau_i}{T_s}\right] c_i\left[n - \frac{\tau_i}{T_s}\right] \cos\left(2\pi\left(f_{IF} + f_{d,i}\right)\cdot nT_s + \varphi_i\right), \tag{2.2}$$

where

- A_i is the useful signal amplitude of the i^{th} signal component;
- $d_i(\cdot)$ is the bit sequence modeling the transmitted navigation message;
- $c_i(\cdot)$ is the signal spreading sequence;
- τ_i is the delay experienced by the received signal;
- $f_{d,i}$ and φ_i are the carrier Doppler frequency and phase;
- f_{IF} is the receiver intermediate frequency.

Due to the quasi-orthogonality of the spreading codes, $c_i(\cdot)$, the receiver is able to process each signal component independently. Thus, it is possible to assume the presence of a single useful signal at the correlator output, $(L = 1)$. Herein, the case of a single useful component is considered and the index i is dropped for ease of notation. Moreover, the major focus of this thesis is on the analysis of the estimation process of Doppler and Doppler rate measurements. For this reason, it is assumed that the spreading sequence, $c_i(\cdot)$, of each signal is successfully removed by, for example, the Delay Lock Loop (DLL) used for estimating the code delay, τ_i. Thus, under the assumption of perfect code synchronization and after code wipe-off, the input signal (2.2) becomes:

$$r[n] = Ad\left[n - \frac{\tau}{T_s}\right]\cos\left(\left(f_{IF} + f_d\right)\cdot nT_s + \varphi\right) + \tilde{w}[n], \tag{2.3}$$

where the code dependence has been removed from the useful signal and $\tilde{w}[n] = w[n]\,c\,[n - \tau / T_s]$ is a complex Gaussian process characterized by the same mean and variance of $w[n]$.

Figure 2-1 shows a block diagram of the general structure of a carrier tracking loop which can be applied to both a PLL and an FLL. The loop consists of four main components:

- the integrate and dump (I&D) block used for evaluating the complex correlator output, that is the projection of the incoming signal over the locally generated replica;
- the non-linear discriminator for extracting the phase/frequency error;
- the loop filter, characterized by the transfer function $B(z)$;
- the Numerically Controlled Oscillator (NCO) used for the local carrier generation.

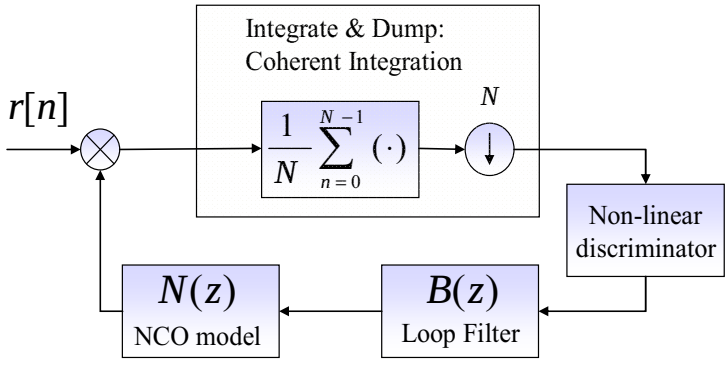

Figure 2-1: General structure of a carrier tracking loop.

In the PLL case, a phase discriminator is used, and the control signal is the phase difference between the incoming and local carriers averaged over the integration interval (Ward 1998, Ward et al 2005). In an FLL, a frequency discriminator is used, and the loop is driven by an estimate of the frequency difference between incoming and local signals.

A combination of these loops can be used and the receiver can switch among different operating modes depending on the frequency uncertainty and the noise level (Ward 1998, Borio et al 2009b). In the presence of large frequency uncertainty, an FLL is typically used due to its large pull-in range (Ward 1998, Ward et al 2005). Once frequency tracking in FLL mode is achieved, the PLL takes over. The FLL mode is also used as a fall-back mode when phase lock is lost. However, since it is usually difficult to transit directly from FLL tracking to PLL tracking, a structure called an FLL-assisted-PLL is generally used as a transition step between the two above-mentioned modes. Rather than using a single loop, it consists of a PLL and an FLL in a coupled mode, to reduce locking times and avoid false locks. As the major task of this section is to provide a general description of the system and signal model used in this thesis, the FLL-assisted PLL is only marginally considered here. A more detailed description of this type of carrier tracking loop structure is provided in **Chapter 3,** while a complete study relative to the structure and performance of standard carrier-tracking loops is presented in (Ward 1998, Ward et al, 2005).

As can be observed from Figure 2-1, the signal $r[n]$ is multiplied by a complex sinusoid and integrated (low-pass filtered) over N samples, for a total duration $T_c = NT_s$, where $T_s = \frac{1}{f_s}$ is the sampling interval of the input signal, $r[n]$, and T_c is the coherent integration time. After integration and decimation, a complex correlator output is obtained and the control signal driving the loop error is extracted by the non-linear discriminator. The control signal is filtered and used for driving the Numerically Controlled Oscillator (NCO) that, in turn, is used for the local carrier generation.

The properties of the loop are mainly influenced by the loop filter, $B(z)$. The order of the loop filter determines the ability of the carrier tracking loop to track signal dynamics, while

the filter coefficients determine the bandwidth of the loop (Stephens & Thomas 1995, Ward et al, 2005). The portion of input noise variance transferred from the input samples to the final phase/frequency estimate is determined by the loop filter bandwidth (Stephens & Thomas 1995). Hereafter, the loop filter bandwidth is denoted by the symbol B_n.

The complex correlator output can be modeled as suggested by van Dierendonck et al, (1996):

$$P = P_I + jP_Q = d\,\frac{\sin(\pi N \Delta f T_s)}{\pi N \Delta f T_s} A_c \exp\{j\phi\} + \eta_P\,, \tag{2.4}$$

where d models the effect of the navigation message, A_c is the amplitude of the correlator output, Δf is the residual frequency error, ϕ is a residual phase error that will be extracted by the non-linear discriminator and η_P is a complex Gaussian random variable derived by processing the noise term $w'[n]$. The phase and frequency information is then extracted from the input correlator output, P, by the carrier tracking loops of the receiver.

Typically, it is assumed that the input signal, $r[n]$, has been normalized such that the real and imaginary parts of η_P have unit variance (van Dierendonck et al 1992), but as the power relationship between signal and noise is preserved by scaling, this choice does not affect the results presented herein. Under this condition and neglecting the impact of front-end filtering, according to (van Dierendonck et al 1992), the amplitude of the correlator output can be expressed as:

$$A_c = \sqrt{2C / N_0 T_c}\,. \tag{2.5}$$

where C/N_0 is the input carrier-to-noise density power ratio. Furthermore, when considering small frequency errors, Δf ,the following assumption can be justified:

$$\frac{\sin(\pi N \Delta f T_s)}{\pi N \Delta f T_s} \approx 1\,. \tag{2.6}$$

When considering a carrier tracking loop with extended integration time, several correlator outputs, obtained from subsequent portions of the input signal, are evaluated and used for producing an improved phase estimate. For this reason, the index $k = 0,1, ..., K$ -1 is introduced, and different correlator outputs are denoted as

$$P_k = P_{I,k} + jP_{Q,k} = d_k A_c \exp\{j\phi\} + \eta_{P,k}, \tag{2.7}$$

where the quantities $\{d_k\}_{k=0}^{K-1}$ are modeled as independent random variables assuming values from the set $\{-1, \ 1\}$ with equal probability. Eq. (2.7) represents the basic signal model used in this thesis. It is noted that in Eq. (2.7) the signal phase, ϕ, is assumed to be approximately constant during the total integration time and thus does not depend on *K*.

2.1.2 Carrier Tracking Loop Observables

2.1.2.1 Doppler frequency observable

There exist two different ways to estimate the signal Doppler frequency in carrier tracking loops of a GPS receiver (Hebert 1997, Serrano et al 2004a). Consider Figure 2-2 that shows a standard structure of a PLL illustrating the types of available observables. The first option is to use the raw Doppler measurements provided by the loop filter output which is an instantaneous measure produced over a very small time interval, namely the coherent integration time, T_c. In the following the loop filter output or raw Doppler estimate will be indicated as:

$$f_{raw}[k]. \tag{2.8}$$

The second method uses time-differenced GPS carrier phase observables allowing the production of smoother Doppler frequency measurements. These carrier phase derived Doppler measurements are given by

$$f_{cp}[k] = \phi_{ob}[k] * \Delta[k], \tag{2.9}$$

where $\phi_{ob}[k]$ is the carrier phase observable, and $\Delta[k]$ is the impulse response of a digital differentiator.

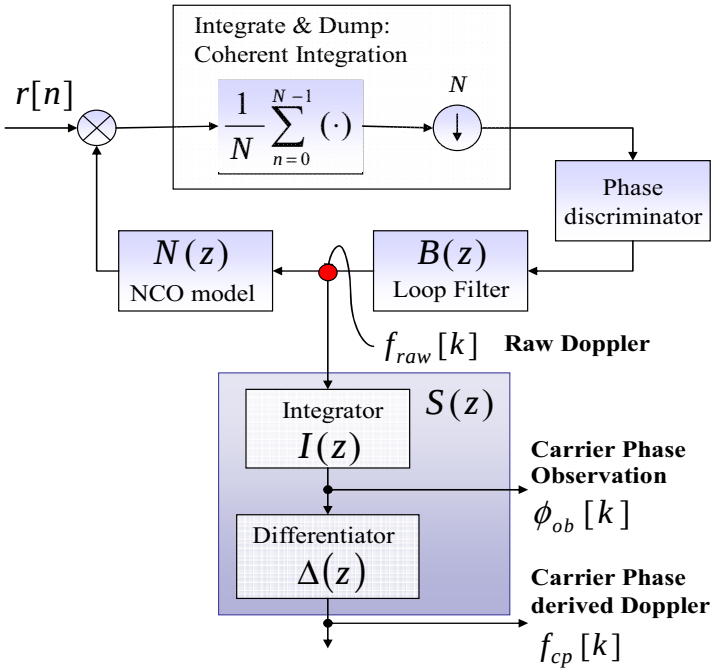

Figure 2-2: Standard PLL structure and available observables.

Carrier phase observables are obtained by integrating raw Doppler measurements:

$$\phi_{ob}[k] = f_{raw}[k] * i[k] = \phi_{ob}[k-1] + T_c f_{raw}[k], \tag{2.10}$$

where $i[k]$ is the impulse response of a digital integrator characterized by the following transfer function

$$I(z) = ZT\{i[k]\} = \frac{T_c}{1 - z^{-1}}. \tag{2.11}$$

$ZT\{\cdot\}$ is used to denote the Z-transform of a discrete time sequence. It is noted that other types of integrators can be used for producing carrier phase observables. In the following, only the case of the integrator with transfer function (2.11) is considered.

In the literature, the second approach has been considered advantageous, mainly because of the achievable accuracy and the noise reduction obtained in the process of computing carrier phase measurements. Differentiating the observables over a short time interval brings some advantageous effects, namely removal of the residual effects of the tropospheric and ionospheric delays and the provision of an ambiguity free solution (Moafipoor et al 2004, Wendel et al 2006).

But as it has been shown in (Borio et al 2009b) and (Sokolova 2009), equivalence with the carrier phase derived Doppler measurements, $f_{cp}[k]$, can be achieved by performing appropriate filtering of the raw Doppler measurements. More specifically, consider for example the integrator model given by Eq.(2.11), and a first order central difference approximation type differentiator $\Delta[k]$ the transfer function of which can be expressed as follows

$$\Delta(z) = z^{-H}\frac{z^{H} - z^{-H}}{2HT_c}, \tag{2.12}$$

where HT_c is the interval between consecutive carrier phase measurements. It should be noted here that an additional delay term, z^{-H}, is included to account for the latency introduced by the receiver for computing the carrier phase difference. In this case, the transfer function between raw and carrier phase derived Doppler measurements can be expressed as:

$$S(z) = I(z)\Delta(z) = \frac{T_c}{1 - z^{-1}}\frac{1 - z^{-2H}}{2HT_c} = \frac{1}{2H}\sum_{i=0}^{2H-1} z^{-i}. \tag{2.13}$$

Eq.(2.13) represents the transfer function of a moving average (MA) filter with the analysis window length equal to $2H$. A GPS receiver can output carrier phase observations at a rate lower than the loop update rate. This corresponds to down-sampling the raw Doppler, $f_{raw}[k]$, by a factor H . The fact that the process of computation of the carrier phase derived Doppler measurements, $f_{cp}[k]$, can be expressed as a MA filter, in the specific case of Eq.(2.12), and a low-pass filter in the general case, indicates the equivalence between carrier phase derived Doppler measurements, $f_{cp}[k]$, and filtered raw Doppler observations. Thus, in the case with the raw Doppler measurements

$$S(z)=1, \tag{2.14}$$

while for the case with the carrier phase derived Doppler measurements relationship defined in Eq.(2.13) applies. Under poor tracking conditions e.g., high user dynamics, heavily attenuated signals or severe multipath effects, it is very likely that PLL looses lock and the receiver will have to use FLL to track the frequency of the received carrier. The difference between these two carrier tracking loops is that the FLL uses a frequency discriminator and an additional integrator is inserted after the loop filter (Ward 1998, Ward et al 2005). In this case, an estimate of Doppler frequency is provided by the integrated output of the FLL filter, as shown in Figure 2-3. Notation given by in Eq.(2.8) will be used for this type of measurement.

2.1.2.2 Doppler rate observable

Due to the limitations imposed by the use of hardware GPS receivers, it has been considered impossible to get direct Doppler rate measurements (Zhang et al 2005, Bruton 2000). In the case of a Software-Defined Radio (SDR) GPS receiver using an FLL, Doppler rate measurements can be obtained directly from the outputs of the FLL loop filter, as shown in Figure 2-3.

Similar to raw Doppler measurements, the Doppler rate measurements are produced over an interval equal to the coherent integration time, T_c, and therefore they can be considered as an instantaneous observation. In this thesis, the FLL filter output or raw Doppler rate estimates will be indicated as:

$$\dot{f}_{raw}[k]. \tag{2.15}$$

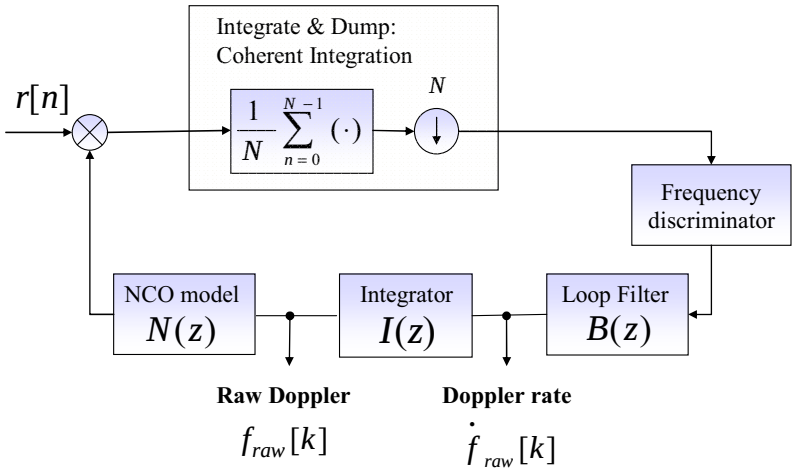

Figure 2-3: Standard FLL structure: the FLL filter output is a raw Doppler rate estimate. Raw Doppler estimates are obtained by integrating the outputs of the filter.

In the absence of the direct Doppler rate measurements approach involving double time differentiation of the carrier phase GPS observables provided by the PLL was typically used (Bruton 2000, Serrano et al 2004b). Differentiating carrier phase observable gives Doppler estimates and, if performed a second time, Doppler rate measurements. As in the case of Doppler measurements, Doppler rate measurements obtained by double differentiation of the carrier phase observables are considered more accurate due to the smoothing effect intrinsic in the processes of their computation. But by performing

appropriate filtering of the raw Doppler rate measurements, also in this case equivalence can be achieved. A more detailed discussion of this topic will be given in **Chapter 5**.

The design of differentiator filters, $\Delta[k]$, suitable for the derivation of Doppler frequency and Doppler rate has been of particular interest in the GNSS receiver community, and several techniques have been proposed. Fenton & Townsend (1994) demonstrated the use of parabolic functions. Both Cannon et al (1997) and Hebert (1997) approached the task using simulated GPS data by applying low-order Taylor series approximations of the derivative (i.e. central difference equations) and by differentiating cubic spline interpolation of the carrier phase data. A Kalman filtering approach was also proposed and applied by Hebert (1997). Bruton (2000) gave a comprehensive review and characterization in the frequency domain of several possible methods of carrying out the differentiation process with specific focus on higher order central difference approximations and curve fitting also known as Savitsky-Golay (Savitzky & Golay 1964) differentiators for high dynamics applications.

2.1.2.3 Differentiator Selection

A common choice of a differentiator for deriving Doppler and Doppler rate measurements from carrier phase observables is a Finite Impulse Response (FIR) differentiator (Bruton 2000, Serrano et al 2004a, Zhang et al 2005). The use of Infinite Impulse Response (IIR) filters has been investigated in (Zhang et al 2005) and found applicable as well as being a good alternative to FIR filters, especially for real-time applications. This approach is not treated in this research due to a less straightforward design than that of FIR filters and frequent necessity to perform reverse time filtering in order to achieve a zero-phase response, as concluded by Bruton (2000).

The frequency response of an ideal uniformly-sampled discrete-time differentiator is given by (Antoniou 1993):

$$H(e^{j\omega T}) = j\omega \text{ for}, 0 \le |\omega| < \frac{\omega_S}{2} \tag{2.16}$$

where ω is the frequency of the spectrum of the signal, $\omega_S = 2\pi / T$ is the sampling frequency in radians per second, and T is the corresponding sampling period. While the ideal differentiator increases its amplification with increasing frequency, realizable FIR differentiators can only approximate the ideal case within a certain bandwidth, above which it attenuates the signal. This practical constraint of differentiator design is useful, as it can be used to suppress noise, particularly in low dynamic applications.

As indicated by Bruton (2000), the key issue in designing a suitable differentiator algorithm is that the differentiator should be close to ideal in the frequency band where the user motion is present. The danger in using a differentiator with a very narrow bandwidth, or smoothing before differentiation, is that higher frequency motion of the user may not be captured, resulting in a poor estimate of the derivative. Using a wider bandwidth ensures that all user motion frequencies will be retained, but more noise will also be allowed to pass into the derivative. Another important consideration is the absolute length of the impulse response. A filter with a short impulse response offers the advantage of a small time delay whereas a filter with a longer impulse response offers the advantage that it can achieve a more accurate magnitude response. Moreover, such errors as cycle slips and gaps in GPS data will affect less data if the length of the impulse response of the filter is small.

In the research presented here to obtain the carrier phase derived Doppler and Doppler rate measurements, FIR filters are considered exclusively, because they can be designed to have a time-symmetric impulse response implying that all spectral components of the input signal are subject to the same delay. Moreover, this thesis is concentrated on low levels of user dynamics characteristic to pedestrian motion. Therefore, consistent with suggestions made by Ryan et al (1997), Cannon et al (1997) and Bruton (2000), and as a compromise between sufficient bandwidth, simplicity, and noise suppression, the first-order central difference approximation and Savitzky-Golay smoothing filter approaches will be used to generate the Doppler and Doppler rate observations.

The impulse response of a first-order differentiator, neglecting the delay introduced in Eq.(2.12), is given by (Hebert 1997):

$$\Delta[k] = \frac{\delta[k+H] - \delta[k-H]}{2HT_c} \tag{2.17}$$

where HT_c is the interval between consecutive carrier phase measurements and $\delta[\cdot]$ is the Kronecker delta.

In the case of a Savitzky-Golay smoothing filter, a sliding window is used to analyze carrier phase observations over a specific time interval. The selected carrier phase observations are then fitted to a polynomial curve. The Doppler estimate is obtained as the time derivative of the interpolating polynomial. A third order polynomial is usually adopted, and overlap between the analysis windows is used to reduce discontinuities between subsequent Doppler estimates (Hebert 1997). A more detailed description of these two differentiator types as applied for derivation of Doppler frequency from GPS carrier phase observables can be found in Bruton (2000) and Sokolova (2009).

2.2 Velocity and Acceleration Estimation from GNSS Carrier Tracking Loop Observables

This section briefly describes the process of estimating velocity and acceleration from the observables provided by the carrier tracking loops of a GPS receiver. Doppler observables are direct measures of the relative velocity between user and satellite, measured along the line-of-sight (LOS). If the satellite velocities and accelerations are known, and the user position is approximately known, these LOS velocities and accelerations can be corrected for the contribution of satellite motion. Therefore, the first step in this process is to compute the satellite velocity and acceleration from the broadcast ephemeris. For a detailed description of satellite velocity and acceleration computation see (Zhang et al 2006) and

(Serrano et al 2004b). The Doppler and Doppler rate measurements then represent essentially the projection of the user acceleration and velocity onto the respective LOS, and the user velocity and acceleration can be computed directly from these projections.

The observation equations relate the observed Doppler and Doppler rate to the user velocity and acceleration and form the basis for estimating the user velocity from GPS observations.

These equations are typically given in the following form (Misra & Enge 2001, Kaplan & Hegarty 2005):

$$\begin{aligned}\dot{\phi}^{(k)} &= \dot{\rho}^{(k)} + \dot{d\rho}^{(k)} + c(\dot{dt}^{(k)} - \dot{dT}) - \dot{d}_{ion}^{(k)} + \dot{d}_{trop}^{(k)} + \dot{\xi} \\ &= \dot{\rho}^{(k)} + c\,\dot{dT} + \dot{\varepsilon}_{\phi}^{(k)}\end{aligned} \tag{2.18}$$

where

- $\dot{\phi}^{(k)}$ is the carrier phase derivative or Doppler measurement,
- $\dot{\rho}^{(k)}$ is the geometric range rate between the receiver and the satellite,
- $\dot{d\rho}^{(k)}$ is the orbital error drift,
- c is the speed of light,
- $\dot{dt}^{(k)}$ is the bias rate of the satellite clock,
- $\dot{dT}$ is the bias rate of the receiver clock,
- $\dot{d}_{ion}^{(k)}$ is the ionospheric delay rate,
- $\dot{d}_{trop}^{(k)}$ is the tropospheric delay rate,
- $\dot{\xi}$ is the receiver system noise,

and $\ddot{\varepsilon}_{\phi}^{(k)}$ denotes the combined error in the satellite clock, receiver system noise, ionosphere and troposphere. A thorough review of the behavior and magnitude of each error source can be found in Raquet (1998) or Bruton (2000). Similarly, the observation equation for the Doppler rate is:

$$\begin{aligned}\ddot{\phi}^{(k)} &= \ddot{\rho}^{(k)} + \ddot{d}\rho^{(k)} + c(\ddot{dt}^{(k)} - \ddot{dT}) - \ddot{d}_{ion}^{(k)} + \ddot{d}_{trop}^{(k)} + \ddot{\xi} \\ &= \ddot{\rho}^{(k)} + c\,\ddot{dT} + \ddot{\varepsilon}_{\phi}\end{aligned} \tag{2.19}$$

with all the quantities in the equation being now of the second order. Some of the error effects in the measurements can be modeled and partially compensated for using appropriate algorithms the description of which can be found in numerous references (e.g., Parkinson et al 1996, Misra & Enge 2001, Kaplan & Hegarty 2005). After modeling the measurements, the observation equations for velocity and acceleration determination can be stated as follows:

$$\dot{\phi}^{(k)} = (\mathbf{v}^{(k)} - \mathbf{v}) \cdot \mathbf{h}^{(k)} + \dot{dT} + \dot{\varepsilon}_{\phi}^{(k)} \tag{2.20}$$

$$\ddot{\phi}^{(k)} = (\mathbf{v}^{(k)} - \mathbf{v}) \cdot \dot{\mathbf{h}}^{(k)} + (\mathbf{a}^{(k)} - \mathbf{a}) \cdot \mathbf{h}^{(k)} + \ddot{dT} + \ddot{\varepsilon}_{\phi}^{(k)} \tag{2.21}$$

where $\mathbf{v}^{(k)}$ and $\mathbf{a}^{(k)}$ stand for the satellite velocity and acceleration vectors; $\mathbf{v}$ and $\mathbf{a}$ for the user velocity and acceleration vectors, to be estimated, and $\mathbf{h}^{(k)}$ is a user-to-satellite LOS unit vector that can be determined from an estimate of the user position given as

$$\mathbf{h}^{(k)} = \frac{\mathbf{u}^{(k)} - \mathbf{u}}{\left\| \mathbf{u}^{(k)} - \mathbf{u} \right\|}, \tag{2.22}$$

where $\mathbf{u}^{(k)}$ and $\mathbf{u}$ are the position of the k^{th} satellite and user, respectively. It should be noted that positioning accuracy of at least 10 m is required for the errors caused by the wrong coordinates to be negligible (Itani et al 2000). As it has been shown by Weiser (2007), an error in the user position of 10 m in any of the coordinate direction may cause an

apparent Doppler shift of up to 1.5 mm/s. Thus, for mm/s level velocity estimation, the receiver position can only be treated as known to within 7 m.

Equations (2.20) and (2.21) are linear in user velocity and acceleration components, so that they can be rewritten as

$$(\dot{\phi}^{(k)} - \mathbf{v}^{(k)} \cdot \mathbf{h}^{(k)}) = -\mathbf{h}^{(k)} \cdot \mathbf{v} + d\dot{T} + \varepsilon_{\dot{\phi}}^{(k)} \tag{2.23}$$

$$(\ddot{\phi}^{(k)} - \mathbf{v}^{(k)} \cdot \dot{\mathbf{h}}^{(k)} - \mathbf{a}^{(k)} \cdot \mathbf{h}^{(k)}) = -\dot{\mathbf{h}}^{(k)} \cdot \mathbf{v} - \mathbf{h}^{(k)} \cdot \mathbf{a} + d\ddot{T} + \varepsilon_{\ddot{\phi}}^{(k)}. \tag{2.24}$$

Denoting $(\dot{\phi}^{(k)} - \mathbf{v}^{(k)} \cdot \mathbf{h}^{(k)})$ and $(\ddot{\phi}^{(k)} - \mathbf{v}^{(k)} \cdot \dot{\mathbf{h}}^{(k)} - \mathbf{a}^{(k)} \cdot \mathbf{h}^{(k)})$, which are the observations corrected for the contribution of satellite motion as $\dot{\phi}'^{(k)}$ and $\ddot{\phi}'^{(k)}$ respectively, the final functional models for velocity and acceleration determination can be written as sets of equations in matrix form as:

$$\dot{\phi}' = \mathbf{H}\begin{bmatrix} \mathbf{v}^T & d\dot{T} \end{bmatrix} + \varepsilon_{\dot{\phi}} \tag{2.25}$$

$$\ddot{\phi}' = \dot{\mathbf{H}}\begin{bmatrix} \mathbf{v}^T & d\dot{T} \end{bmatrix} + \mathbf{H}\begin{bmatrix} \mathbf{a}^T & d\ddot{T} \end{bmatrix} + \varepsilon_{\ddot{\phi}}, \tag{2.26}$$

where

$$\mathbf{H} = \begin{bmatrix} \left(-h^{(1)}\right)^T & 1 \\ \left(-h^{(2)}\right)^T & 1 \\ \vdots & \vdots \\ \left(-h^{(k)}\right)^T & 1 \end{bmatrix} \tag{2.27}$$

is an $(k \times 4)$ matrix characterizing the receiver-satellite geometry. The receiver velocity and acceleration are then typically estimated by implementing epoch by epoch Weighted Least Squares (WLS) solution or Kalman Filter (KF) approach (advanced approaches with less

stringent requirements are beyond the scope of this thesis). Using either of these techniques requires the knowledge of the accuracy of each Doppler/Doppler rate estimate modelling which will be the main topic of the following chapters.

2.3 Overview of High Sensitivity GNSS

During the past several years new techniques have been developed for processing GPS signals with a very low C/N_0. Methods for increasing the length of the integration period beyond classical limits at both acquisition and tracking have received particular attention. For a given integration duration and in the absence of residual frequency/phase errors, the higher the coherent integration time, the better the reduction of the noise power at the output of the correlators with respect to the signal power, i.e. the higher the probability of detection (Julien 2008), or of maintaining lock in a receiver which is already in tracking mode. To enhance acquisition and tracking thresholds and thus the availability of the position solution using GPS, High Sensitivity techniques based on the use of long integration times have been developed (Peterson et al 1997). For weak signal acquisition and tracking, coherent integration and non-coherent accumulation are performed in conjunction to increase the total signal dwell time.
Alternatively, a massive number of correlators can be used to perform a simultaneous parallel search over the entire range of code delays and Doppler frequencies (van Diggelen 2001). All the correlator outputs are evaluated in parallel in this case by jointly processing blocks of input samples and for this reason this approach is often referred to as block or batch processing (van Graas et al 2005).

2.3.1 Coherent processing

In standard receivers the coherent integration time is typically limited to 20 ms because of the presence of the navigation data, and even where the navigation data are known a-priori,

integration is limited by residual frequency errors due to the receiver motion. Moreover, depending on the receiver oscillator quality, the receiver oscillator error can induce an additional reduction in the signal to noise ratio (SNR) that increases with the integration time (Watson 2006). Extension of the integration time beyond the navigation data bit period can be accomplished by detecting, estimating and removing possible bit transitions. The subject of estimation of the received navigation message and removal of the effect of bit transitions have been treated recently in a number of publications including (Soloviev et al 2008), (Petovello et al 2008) and (Borio & Lachapelle 2009).

In general, an initial synchronization is assumed and the bit boundaries are asserted to be known. The basic idea is then to search for the bit sequence that maximizes the signal energy over the entire correlation integration interval consisting of K consecutive correlator outputs integrated over 20 ms. This bit sequence is an estimate of the received navigation message which can then be used to remove the effect of the transmitted bits and further increase the coherent integration time.

An apparent drawback of this approach is that it becomes unreliable for low C/N_0, reducing the gain provided by extended coherent integration, (Petovello et al 2008). Moreover, as this technique requires testing of all possible bit combinations it leads to a computational load growing exponentially with the added number of integrations. For these reasons, to be able to effectively track the signals in degraded environments, other methods such as non-coherent processing have to be considered for the extension of the integration period in tracking loops.

Feasibility of extremely long coherent integration of up to several tens of seconds for positioning indoors has been thoroughly investigated by Watson et al (2006) and Gaggero & Borio, (2008). In both cases data bits have been removed using reference data in a manner similar to AGPS techniques, and ultra-stable reference oscillators were used to avoid losses due to the stability of the local frequency source.

Although signal acquisition indoors has been successfully demonstrated, the achieved position solution accuracy was rather poor, in the best case with relative error of 20 m in

the horizontal plane and 100 m in the vertical plane. In addition to the relative inaccuracy of the above, the position calculations provided in the latter study referenced above required significant external aiding information, and the overall thrust of the work was not directed towards creating a receiver which could operate autonomously within degraded environments. In this work, significant attention is given to approaches that will not only allow receiver operation in degraded signal conditions, but will do so independently of external aiding information.

2.3.2 Non-coherent processing

Non-coherent integration, obtained by applying a non-linear function to the correlator outputs for removing the impact of data bits, can be much longer than coherent integration, but since this procedure involves squaring or other non-linear operations, it also implies squaring losses relative to pure coherent integration of the same net duration (Lachapelle et al 2004). This approach is mostly used for acquiring weak signals (O'Driscoll 2007). Extending the non-coherent integration period at the tracking level has been recently proposed by Borio & Lachapelle (2009).

A solution for non-coherently extending the integration time at the tracking level can be represented by the use of non-linear operations for removing the signal dependence on the data bit. Assuming a random distribution of data bits, the ML estimator for the signal phase can be derived. Navigation data can then be considered as nuisance parameters that do not need to be estimated and therefore can be removed through squaring. According to the comparative analysis presented in (Borio & Lachapelle 2009), the non-coherent architecture results in an effective alternative to coherent integrations enabling less noisy measurements than the ones obtained by means of standard loops.

2.3.3 Memory Discriminator-Based Tracking Loop Architecture

In this thesis, an approach using memory discriminators (Borio et al 2009a) that includes a general low-pass filtering stage for the non-coherent extension of the integration time is considered. The concept of memory discriminators is quite new. It has been first proposed by Borio & Lachapelle (2009) and then further studied and characterized by (Borio et al 2009a) and Sokolova (2009). The major objective of memory discriminators is to introduce extended integration times, without requiring the estimation of the navigation message. This gives origin to tracking loops capable of tracking strongly attenuated signals in the presence of additional impairments such as fading and multipath as well as bear higher dynamics without losing phase lock.

This approach directly derives from the ML phase estimator in the presence of sign transitions. The ML phase estimator is derived assuming that the navigation data bits are randomly distributed. As previously stated, under this assumption the navigation data are considered as nuisance parameters which do not need to be estimated, and therefore can be removed through squaring. This non-coherent ML phase estimator is used as a discriminator for a new type of tracking loop that allows extended non-coherent integrations. In (Borio & Lachapelle 2009), the ML phase discriminator in the presence of bit transitions is derived as:

$$S(\Delta\phi_k) = \frac{1}{2}\arctan_2\left[2\sum_{i=0}^{K-1} P_{I,k-i}P_{Q,k-i}, \sum_{i=0}^{K-1}(P_{I,k-i}^2 - P_{Q,k-i}^2)\right] = \frac{1}{2}\arg\left\{\sum_{i=0}^{K-1} P_{k-i}^2\right\}, \tag{2.28}$$

where $\arctan_2$ is the four-quadrant arctangent (Ward et al 2005), P_k is the complex correlator output, as defined in Eq.(2.7), and $k = 0,1, ..., K-1$ is the index denoting the number of correlator outputs when considering PLL with extended integration time. It

should be noted that for only one complex correlator output, $K=1$, $S(\phi_k)$ equals to the standard *arctan* discriminator

$$S(\Delta\phi_k)=\arctan\left(\frac{P_{Q,k}}{P_{I,k}}\right). \tag{2.29}$$

The discriminator represented by Eq. (2.28) performs bit removal by squaring the complex correlator outputs, P_k, and non-coherent integration by further summing the squared correlator outputs. Finally, the phase is extracted using the *arctan*$_2$ operators.

The process of non-coherent integration is equivalent to low-pass filtering the squared correlator, P_k^2, with a Moving Average filter (MA) of length K (Borio & Lachapelle 2009). In this way, the input of the four-quadrant arctangent is a process that depends on the last K complex correlator outputs. By updating the filter at the correlator rate, $T_c = NT_s$, a first type of memory discriminator is obtained. In this way, longer integration time can be achieved without reduction of the loop's update rate.

Substituting the moving average filter with a general low pass filtering stage leads to a new class of memory discriminators. Thus, the expression for the ML phase discriminator given in Eq. (2.28) can be generalised to

$$S(\Delta\phi_k)=\frac{1}{2}\arg\left\{\sum_{i=0}^{+\infty} f_i P_{k-i}^2\right\}, \tag{2.30}$$

where $\{f_i\}_{i=0}^{+\infty}$ define the low-pass filter impulse response

$$f[n]=\sum_{i=0}^{+\infty} f_i\cdot\delta[n-i]. \tag{2.31}$$

Figure 2-4 illustrates the general structure of a PLL with memory discriminator. As shown on Figure 2-4, this type of discriminator operates by first removing the bit dependence from the correlator outputs by squaring. A low-pass filtering stage responsible for the

discriminator memory is then applied to further extend the integration time. A memory-less discriminator finally extracts the phase information. Similarly, the same method can be applied for frequency and delay estimation as well, as shown by Borio et al (2009a).

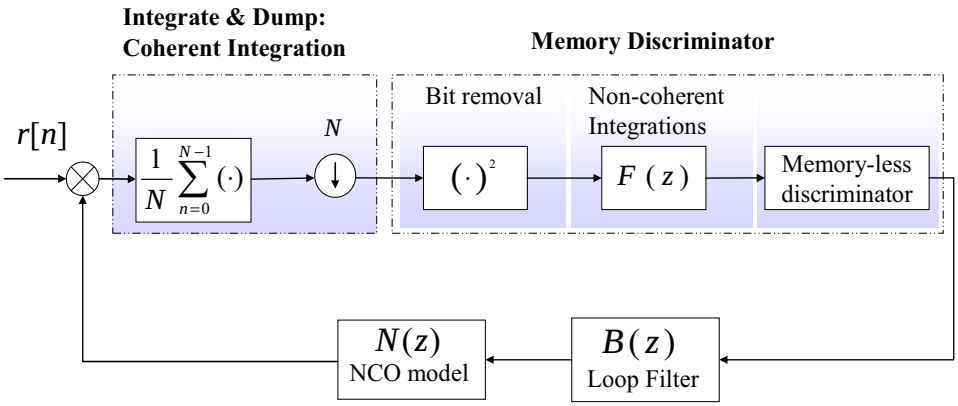

Figure 2-4: PLL with non-coherent integrations (Borio et al 2009a). The integration time is extended non-coherently by the additional filter after the squaring block.

The ML discriminator given in Eq. (2.28) has been derived assuming that the phase is constant during the integration interval. In this case, a uniform filtering is performed and all the input samples are weighted equally. However, including a more general low-pass filtering into the discriminator allows one to progressively de-weight the input observations, so that older samples, P_k, have less impact on the current phase estimate with respect to more recent ones. More specifically, as it has been suggested by Borio et al (2009a), an exponential filter can be used to extend the integration time before extracting the phase/ frequency/delay information. Exponential filtering has been chosen for its reduced computational load and for the possibility of progressively de-weighting the squared correlator outputs, according to the filter forgetting factor, α. The transfer function of an exponential filter can be expressed as follows:

$$F(z) = (1-\alpha)\sum_{i=0}^{+\infty} \alpha^i \cdot z^{-i} = (1-\alpha)\frac{1}{1-\alpha z^{-1}}, \tag{2.32}$$

where $0 \le \alpha < 1$ is the filter forgetting factor, specifying how quickly the filter "forgets" past sample information. Setting $\alpha = 0$ means that no filtering has been performed making the memory discriminator to degenerate into a standard memory-less discriminator. On the other extreme, setting $\alpha = 1$ specifies an infinite memory.

From (2.32) it is possible to determine the filter impulse response that is given by

$$f[n] = (1-\alpha)\sum_{i=0}^{+\infty} \alpha^i \delta[n-i]. \tag{2.33}$$

Figure 2-5 shows an example of the exponential filter impulse responses for different values of α.

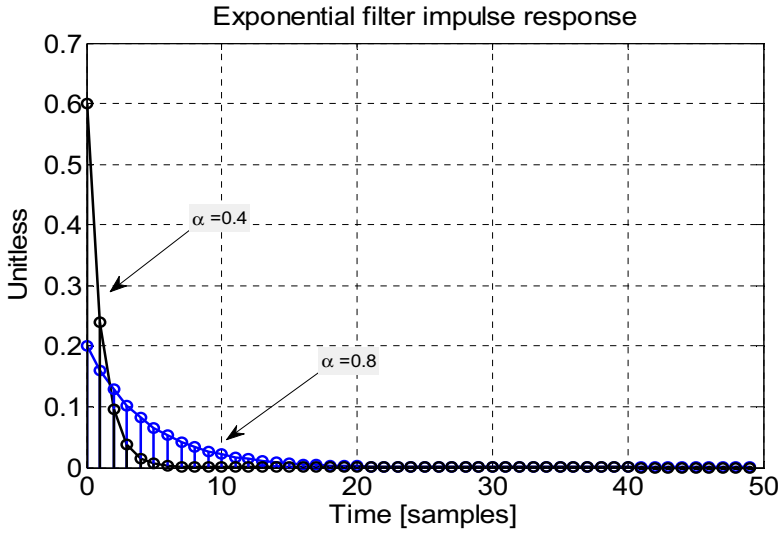

Figure 2-5: Exponential filter impulse response.

Whereas Figure 2-5 illustrates the performance of the memory discriminator based architecture using exponential filtering, Figure 2-6 considers cases of $\alpha = 0.5$ and $\alpha = 0.8$, demonstrating that due to the introduction of an additional filtering stage as a part of the memory discriminator, this type of tracking loop architecture has increased noise rejection

capability and is, therefore, able to provide a faster lock-in time and more accurate Doppler frequency estimates when compared to the standard architecture $(\alpha = 0)$.

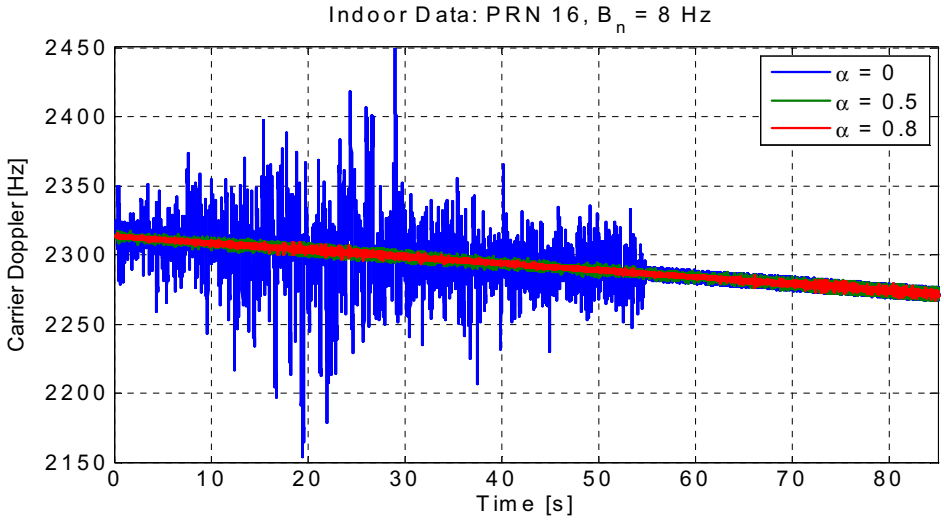

Figure 2-6. Raw Doppler estimated using standard, $\alpha = 0$, and memory discriminators, $\alpha = 0.5$ and $\alpha = 0.8$ for the indoor data. (PRN 16, C/N_0 = 33 dB-Hz), (Sokolova 2009).

An important fact is that memory discriminators introduce additional poles and zeros in the linear transfer function of the loop and a new procedure for the design of the loop filter is required to ensure the stability of the loop. Since standard techniques derived from the transformation of analog filters cannot be directly applied, the controlled-root formulation proposed by Stephens & Thomas (1995) can be modified to account for the effect of the additional poles introduced by the new discriminators (Borio & Lachapelle 2009). In this way, stable loops able to work under strongly attenuated conditions can be obtained. A brief overview of the procedure used for loop filter design and design criteria is given in **Chapter 4** of this thesis, whereas a more thorough explanation can be found in (Borio et al 2009a, Sokolova 2009). Also more details about the performance of the memory discriminator based architecture can be found in (Borio et al 2009a, Sokolova 2009) where

this type of the architecture is evaluated compared to the standard one with the focus on weak signal environments and the impact of different levels of dynamics.

2.3.4 Block Processing

Previous discussion in Section 2.3 was focused on sequential carrier tracking loop approaches where the current phase/frequency estimate is obtained by updating previous estimates using the new information provided by the correlator outputs, Figure 2-1. In this way, only one correlator output is required to produce a new phase/frequency estimate. To be more specific, in this case the acquisition block of the receiver provides the first frequency estimate that is being further refined by the carrier tracking loop.

A different approach based on the use of a massive number of correlators to perform a simultaneous evaluation of GPS signal correlation over the entire range of possible code delays/carrier frequencies is being frequently used in HSGPS receivers (van Diggelen 2001) and (van Grass et al 2005). As has been mentioned above, due to the fact that all the correlator outputs are evaluated in parallel by jointly processing blocks of input samples this approach is referred to as block or batch processing. In this approach, the receiver generates several replicas of the incoming code and carrier and correlates them with the incoming signal. The parameters of the incoming signal are then estimated so as to maximize the correlation function with the local replica. A basic structure of the frequency search algorithm in this type of architecture is illustrated in Figure 2-7.

As it can be seen from Figure 2-7, the Doppler shift of the signal is estimated as the frequency that maximizes the energy of the signal correlation with the local carrier. The Doppler frequency rate, in its turn, is obtained by time differentiating the Doppler estimates. The simultaneous evaluation of a block of correlator outputs is typically performed by employing efficient Fast Fourier Transform (FFT) algorithms. A detailed discussion on FFT-based block processing techniques is presented in Psiaki (2001) and van Graas et al (2005).

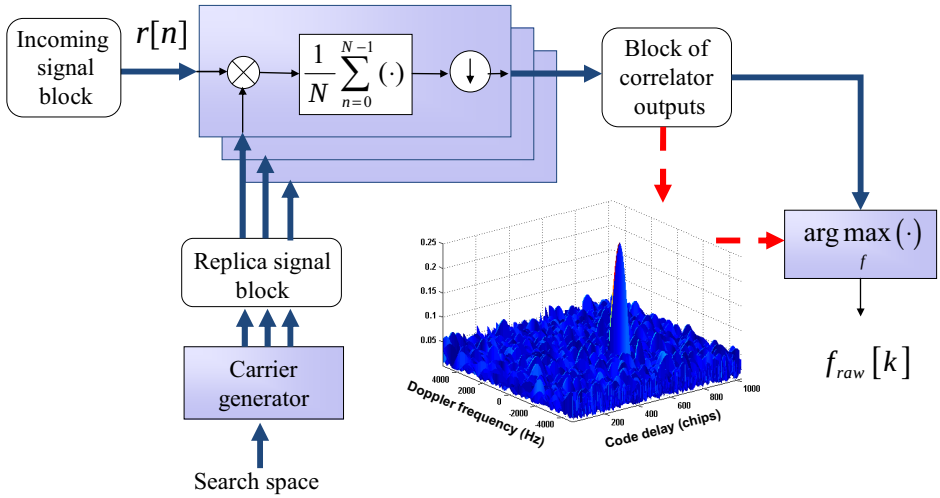

Figure 2-7: General structure of the frequency estimation process in a block processing approach (van Graas et al 2005). A bank of correlators is employed to perform a search over all possible code delays/carrier frequencies.

In degraded signal environments with significant fading as well as in high dynamic situations, a receiver experiences frequent loss of lock. Computing all possible correlations simultaneously ensures that the correlation peak is always detected resulting in lack of signal loss as well as minimization of the tracking dynamic sensitivity. Furthermore, since the block processing approach is based on the evaluation of a block of correlator outputs, and the integration time is typically extended at the correlation level, the same techniques as the ones developed for the sequential architecture for improving the tracking sensitivity can be applied here. Thus, such methods as navigation data bit estimation, discussed in **Section 2.3.1**, use of external aiding to remove the navigation data bits (Turunen 2007), as well as non-coherent processing techniques, can be used. These factors make block processing a very attractive approach to HSGPS implementation.

2.3.5 Note on Future GNSS Signals

Previous subsections are concentrated on the methods for improvement of the GNSS signal tracking sensitivity on the tracking loop/receiver level. In this regard, it is important to mention that a lot of effort is being done also on the system level. The modernized GPS and upcoming GNSS are being designed to solve some of the problems limiting the current GPS performances. The existence of several carrier frequencies for better ionosphere error estimation, and the use of new signal modulations for enhanced tracking performance are two important examples. The latter is mainly of interest when considering applications requiring high sensitivity as well as improved measurement accuracy.

As discussed above, the existing HSGNSS techniques provide substantial improvements but still the presence of data bits remains to be the one of the major limiting factors for weak signal tracking. Therefore, the most important modification in most of the future GNSS signal structures in terms of weak signal tracking is the availability of a dataless, or pilot channel in quadra-phase with the classical channel containing the data (Fontana et al 2001, Spilker & Van Dierendonck 1999, Hein et al 2002).

Under weak signal conditions, the advantages of the pilot channel include the ability to integrate the signal for a longer period, and the use of a pure PLL with more robust carrier phase tracking which is often described as the weakest link in the receiver signal processing blocks (Kaplan 2006).

Moreover, both data and pilot channels undergo exactly the same impairments. This makes the Doppler shift and code delay identical on both cannels. In this way, the pilot channel provides an additional and independent observation for the parameters to be estimated by the receiver. This makes joint data/pilot processing an advantageous option to improve signal tracking performance by reducing the tracking jitter (Muthuraman 2010).

Since this thesis is mainly focused on the GPS L1 C/A signal tracking, only a brief review on the current modernization of the GNSS signal structure is presented. Moreover, the provided discussion is limited to the developments directed for improvement of weak

signal tracking. For more information on the new GNSS signals and their structure and a more complete list of references the reader is referred to (Fontana et al 2001, Spilker & van Dierendonck 1999, Hein et al 2002). More details about combined data/pilot tracking can be found in (Muthuraman 2010).

CHAPTER 3: THEORETICAL FRAMEWORK FOR DOPPLER FREQUENCY ESTIMATION: SEQUENTIAL AND BLOCK PROCESSING ARCHITECTURES

In this chapter two different approaches used by GNSS receivers are considered with respect to the process of the Doppler estimation, namely the sequential carrier tracking, including the standard and memory discriminator based approaches, and block processing techniques. For each approach, a theoretical framework for Doppler estimation relating the variance and biases of the Doppler estimates to C/N_0, the user dynamics and the algorithm parameters is introduced. In the case of sequential carrier tracking, the quality of Doppler measurements is theoretically evaluated by reformulating the standard tracking loop linear theory with respect to the signal Doppler frequency, the frequency noise and the final Doppler frequency measurement provided by the loop.

Three types of tracking loops are explicitly considered: the PLL, common-rate FLL-assisted-PLL and FLL. For the block processing approach, results from previous studies (Rife & Boorstyn 1974, Chan et al 1997) are exploited: the Cramer-Rao Lower Bound (CRLB) for frequency estimation is provided and used to derive a tight approximation of the variance of the frequency estimates generated by block processing techniques.

The second part of the chapter concentrates on the practical verification of the proposed theoretical framework. Test methodology and equipment setup adopted for the performed experiments are described, and the results obtained using the proposed theoretical models for the Doppler variance and bias are compared against the empirical data.

3.1 Theoretical Analysis

The expression of the signal at the input of the processing block responsible for Doppler frequency estimation given in Eq.(2.3), can be written in the following form:

$$r[n] = Ad\left[n - \frac{\tau}{T_s}\right]\cos\left(\left(f_{IF} + f_d\right)nT_s + \varphi\right) + \tilde{w}[n] \tag{3.1}$$

where $d(\cdot)$ is the bit sequence modeling the transmitted navigation message, τ is the delay experienced by the received signal, f_d and φ are the Doppler frequency and carrier phase, whereas f_{IF} is the intermediate frequency to which the signal $s[n]$ (Eq.(2.3)) has been down-converted. $r[n]$ in Eq.(3.1) indicates the signal after code wipe-off and $\tilde{w}[n]$ is, the noise term derived in **Chapter 2**. When the impact of the navigation message, is neglected, the problem of estimating the Doppler frequency, f_d, degenerates to the classical problem of estimating the frequency of a sinusoid in noise (Kay 1993). The above-mentioned estimation problem has been intensively investigated and several results are available in such references as (Rife & Boorstyn, 1974), (Chan et al 1997), (Kay 1993) and (Flower 2002). In (Rife & Boorstyn, 1974), in particular, it has been shown that the Maximum Likelihood (ML) frequency estimator for a sinusoid in noise is given by:

$$f_{ML}[n] = \arg\max_{f_d} \left| \sum_{n=0}^{N-1} r[n] \exp\{-j(f_{IF} + f_d) nT_s\} \right|, \tag{3.2}$$

where N is the number of samples used for frequency estimation. Eq.(3.2) is valid only if the navigation message $d(\cdot)$, is constant during the integration interval, T_c. A more detailed explanation of the derivation of Eq.(3.2) is provided in **Appendix B**.

In this chapter two different techniques, the sequential and block processing approaches, are considered and their relationship with the ML frequency estimator is highlighted.

3.1.1 Sequential Architecture: Carrier Tracking Loop Linear Analysis

In a sequential approach a new frequency estimate is obtained by updating the cost function (Eq.(3.2)) which is sequentially updated using one correlator output at the time. The first frequency estimate provided by the acquisition block is further refined by carrier tracking loops that are a form of local estimators (Rife & Boorstyn, 1974) operating on a frequency uncertainty reduced by the acquisition stage. Thus, this type of receiver architecture is a suboptimal implementation of the ML frequency estimator, (Eq.(3.2)).

To be able to evaluate the quality of Doppler frequency measurements in the case of a sequential GPS receiver architecture, it is necessary to perform a theoretical analysis of the carrier tracking loops with respect to the frequency observables, characterising the noise propagation process from the input signal to the final Doppler frequency estimates. Such an analysis can be performed by extending the PLL linear theory from the phase domain to the frequency domain considering the signal Doppler frequency, the frequency noise and the final Doppler frequency estimate provided by the loop. The basics of the linear loop theory are thoroughly detailed in such references as for example (Borio & O'Driscoll, 2009) and (Julien 2008). The adopted analysis can then be subsequently applied to the FLL and the FLL-assisted-PLL. In order to get a complete model for Doppler frequency analysis and incorporate both the raw and the carrier-phase derived Doppler measurements, the standard linear tracking loop model is further extended to include the effect of a smoothing filter, $S(z)$, to account for the case when Doppler measurements are derived from the carrier phase observations.

3.1.1.1 PLL Linear Model: General Theory

The tracking loop linear theory is generally based on the approximation of the non-linear discriminator by a constant discriminator gain (Gardner 2005). In general, the function of a phase discriminator is to produce an estimate of the phase error, $\Delta\phi$, or an error signal

approximately proportional to it. Typically, this error signal provided by the discriminator is calculated on the basis of an odd discriminator function. Although this function is non-linear, for small phase errors it is possible to obtain a linear discriminator model by assuming that the phase error is close to zero, assumption that is true when the loop is locked without bias. The non-linear function can then be approximated by a constant gain so that:

$$S(\Delta\phi) \approx G_d \Delta\phi + O\left(\Delta\phi^3\right), \tag{3.3}$$

where $O\left(\Delta\phi^3\right)$ is the Landau symbol $O(\cdot)$ indicating the truncation error of the odd discriminator function, and

$$G_d = \left.\frac{\partial S(\Delta\phi)}{\partial(\Delta\phi)}\right|_{\Delta\phi=0}, \tag{3.4}$$

is the discriminator gain also defined as the slope of the discriminator function when the phase error is zero (Kaplan 2006). Both the gain and non-linearity function depend on the type of the used discriminator. A broad overview of the carrier tracking loop discriminators typically used in GNSS, their characteristics and the effect on the tracking capabilities can be found in (Kaplan 2006, Misra & Enge 1996).

Furthermore, normalising the discriminator gain to unity allows one to design the loop filter independently of the discriminator gain. Thus, using this assumption and the fact that the remainder of the PLL is linear, a linear loop model of a standard PLL can be defined as illustrated in Figure 3-1,

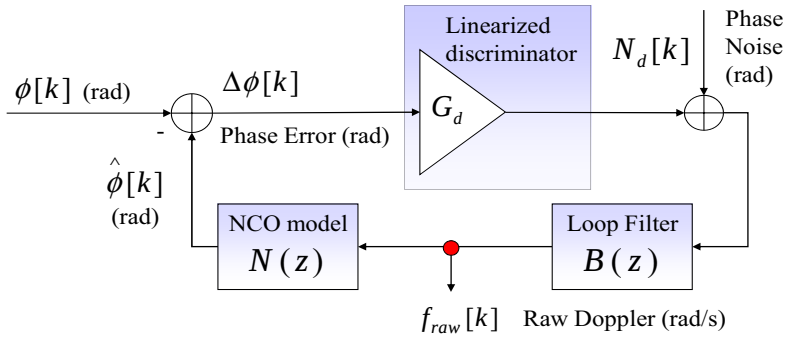

Figure 3-1: PLL equivalent linear model (Sokolova 2009).

where

- $\phi[k]$ is the average phase at the correlator output that the loop is trying to track (the average is computed over the integration time adopted at the correlator level);
- $\Delta\phi[k]$ is the phase error;
- $\hat{\phi}[k]$ is the phase estimated by the loop;
- $N_d[k]$ is a white random process accounting for the noise at the input of the loop and the distortions introduced by the non-linearities in the discriminator;
- $f_{raw}[k]$ is the raw Doppler estimate,
- $N(z)$ and $B(z)$ are the transfer functions characterizing the NCO and loop filter respectively.

As shown in Figure 3-1, the phase error, $\Delta\phi[k]$, is evaluated as the phase difference between the useful signal component of $r[n]$, (Eq.(2.2)), and of the locally generated carrier averaged over the integration interval:

$$\Delta\phi[k] = \phi[k] - \hat{\phi}[k], \tag{3.5}$$

The effect of the noise present in the input signal is modeled by $N_d[k]$ which also accounts for the effect of the non-linear discriminator that amplifies the impact of the input noise (van Dierendonck 1997). Denoting the loop filter impulse response as $b[k]$, raw Doppler measurements can be expressed as:

$$f_{raw}[k] = b[k] * \left(\Delta\phi[k] + N_d[k]\right). \tag{3.6}$$

It is noted that $N_d[k]$ and $\phi[k]$ are updated at a rate equal to $T_c = NT_s$, whereas the input useful signal and noise samples, $r[n]$ and $w'[n]$, are at a rate T_s. This justifies the used of two different time indexes, *k* and *n*. The raw Doppler, $f_{raw}[k]$, is finally integrated by the NCO that produces a new phase estimate $\hat{\phi}[k]$. It should be noted that since the objective of this subsection is to give a general overview of the PLL linear theory, no assumption on the NCO and loop filter models are made. Using the linear model shown in Figure 3-1 this new phase estimate can be expressed in the Z-domain as:

$$\hat{\phi}(z) = N(z) \cdot B(z) \cdot \left[G_d \cdot \left(\phi(z) - \hat{\phi}(z) \right) + N_d(z) \right]. \tag{3.7}$$

Approximation of the non-linear discriminator by a constant gain allows the removal of the non-linearities present in the PLL so that the tracking loop can be approximated by a linear device that computes phase estimates as a linear combination of filtered noise and input signal phase. Thus, assuming the discriminator gain, G_d, to be equal to 1, relationship given in Eq.(3.7) can be re-formulated as follows:

$$\begin{aligned} \hat{\phi}(z) &= \underbrace{\frac{G_d N(z)B(z)}{1 + G_d N(z)B(z)}}_{H_\phi(z)} \cdot \phi(z) + \underbrace{\frac{N(z)B(z)}{1 + G_d N(z)B(z)}}_{H_n(z)} \cdot N_d(z) = \\ &= \frac{N(z)B(z)}{1 + N(z)B(z)} \cdot \left[\phi(z) + N_d(z)\right] \end{aligned}, \tag{3.8}$$

where $H_\phi(z)$ and $H_n(z)$ are the signal and noise transfer functions, respectively. It is noted, that the assumption, $G_d = 1$, is not restrictive since a normalization can be applied to the discriminator in order to achieve the mentioned condition. Given relations defined in Eqs.(3.5) and (3.8), the phase error, $\Delta\phi[k]$, can be then expressed as:

$$\Delta\phi(z) = \left(1 - H_\phi(z)\right)\phi(z) + H_n(z)N_d(z). \tag{3.9}$$

In the discrete time domain Eq.(3.9) takes the following form:

$$\Delta\phi(k) = \left(\delta[k] - h_\phi[k]\right) * \phi[k] + h_n[k] * N_d[k], \tag{3.10}$$

where $h_\phi[k]$ and $h_n[k]$ are the signal and noise impulse responses, respectively and $\delta[\cdot]$ is the Kronecker delta.

Under the assumption that the signal term, $\left(\delta[k] - h_\phi[k]\right) * \phi[k]$, in Eq.(3.10) introduces only a deterministic bias in $\Delta\phi[k]$, the variance of $\Delta\phi[k]$ can be expressed as

$$\begin{aligned} Var\{\Delta\phi[k]\} &= \int_{-0.5}^{0.5} \left|H_n(e^{j2\pi f})\right|^2 df \, Var\{N_d[k]\} \\ &= T_c \int_{-0.5/T_c}^{0.5/T_c} \left|H_n(e^{j2\pi f T_c})\right|^2 df \, Var\{N_d[k]\} \end{aligned} \tag{3.11}$$

where $N_d[k]$ has been assumed to be a white sequence. The term

$$B_n = \frac{1}{2}\int_{-0.5/T_c}^{0.5/T_c} \left|H_n(e^{j2\pi f T_c})\right|^2 df \quad [Hz] \tag{3.12}$$

in Eq.(3.11) defines the loop filter bandwidth and quantifies the amount of noise transferred from the input equivalent noise to the tracking error, $\Delta\phi$.

As shown in Ward et al (2005), the variance of $N_d[k]$ is approximately given by

$$Var\{N_d[k]\} = \sigma_n^2 = \frac{1}{2 \cdot T_c \cdot C/N_0}\left(1 + \frac{1}{2 \cdot T_c \cdot C/N_0}\right) \quad [rad^2], \tag{3.13}$$

and by using Eqs. (3.11), (3.12) and (3.13) it is possible to obtain the standard formula for the phase tracking jitter:

$$\sigma_n = \frac{\lambda}{2\pi}\sqrt{\frac{B_n}{C/N_0}\cdot S_L} = \frac{\lambda}{2\pi}\sqrt{\frac{B_n}{C/N_0}\left(1+\frac{1}{2T_c\,C/N_0}\right)} \quad [rad], \tag{3.14}$$

where S_L represents the squaring loss which, as shown by Lindsey & Chie (1981), in the case when the bandwidth of the integrate and dump filter of the PLL is wide enough not to introduce signal distortion, can be approximated by

$$S_L \approx 1+\frac{1}{2T_c\,C/N_0}. \tag{3.15}$$

3.1.1.2 PLL as a Frequency Filter

The general PLL linear theory discussed in the previous section focuses on the propagation of the phase noise. This section will introduce PLL linear analysis performed with respect to the frequency observables based on the research performed by Sokolova (2009), reformulating the standard PLL model with respect to the signal Doppler frequency, the frequency noise and the final estimate provided by the loop.

In a similar way as in the case of the standard linear model (Figure 3-1), the PLL can also be approximated by a linear device that forms frequency estimates as a linear combination of the filtered version of the true Doppler frequency $f_d[k]$ and filtered frequency noise $N_f[k]$. This relation is illustrated in Figure 3-2, representing the PLL as a frequency filter. It is noted that similarly to the standard PLL linear model, the non-linear discriminator is approximated by a unit gain, and this assumption will be used in all subsequent analyses. With respect to the phase linear model shown in Figure 3-1, an integrator has been added in order to explicitly model the input driving frequency $f_d[k]$. In this case, the phase, $\phi[k]$, is obtained by integrating $f_d[k]$. As suggested in Borio et al

(2009b), the integrator modeling the relation between the frequency and the phase is characterized by the same transfer function of the NCO since both local and incoming signals are processed in the same way through the Integrate and Dump (I&D) component of the PLL.

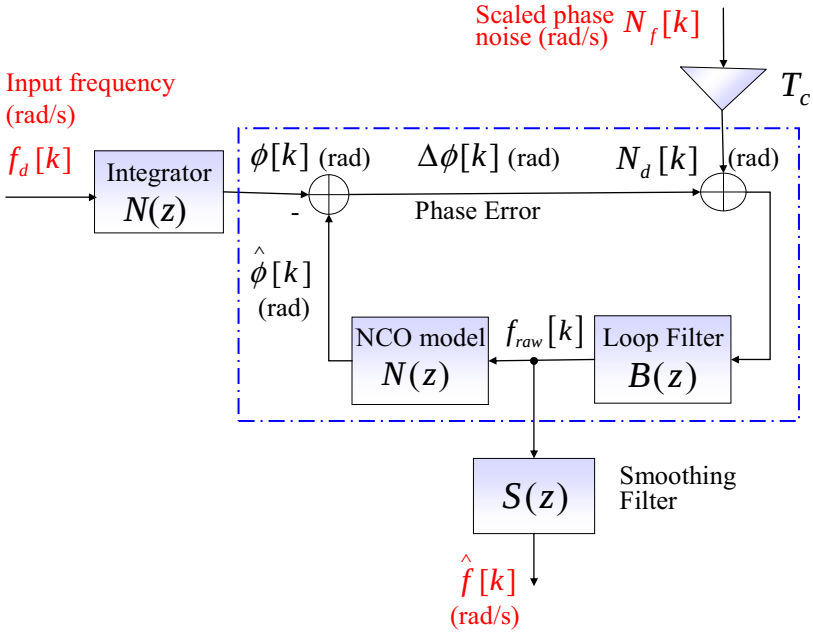

Figure 3-2: PLL as a frequency filter: Doppler frequency estimates are formed as a linear combination of the filtered noise and input signal frequency (Sokolova 2009).

In order to get all quantities at the inputs and the output of the PLL model in the same units of radians per second, a frequency noise term $N_f[k]$ is introduced. This term is obtained by scaling $N_d[k]$ by the coherent integration time T_c as follows:

$$N_f[k] = \frac{1}{T_c} N_d[k]. \tag{3.16}$$

A functional block representing a smoothing filter with transfer function $S(z)$ has also been added to incorporate both the raw and the carrier phase derived Doppler

measurements. In the case of the raw Doppler measurements $S(z)=1$, whereas for the carrier phase derived Doppler measurements $S(z)$ acts as a low pass smoothing filter and, as discussed in **Chapter 2**, the following relationship applies:

$$S(z)=I(z)\Delta(z), \tag{3.17}$$

where $I(z)$ and $\Delta(z)$ are the transfer functions of an integrator and a differentiator defined by Eqs. (2.10) and (2.11). In this case, the final Doppler frequency estimate is given by

$$\hat{f}[k]=s[k]* f_{raw}[k], \tag{3.18}$$

where $s[k]$ is the impulse response of the smoothing filter.

Considering the linear model of a PLL as a frequency filter defined above and illustrated in Figure 3-2, it is possible to show that in the Z-domain, the final frequency estimate is obtained as:

$$\hat{f}(z)=S(z)\cdot f_{raw}(z)=S(z)\cdot\left(B(z)\cdot\left[N_f(z)\cdot T_c+N(z)\cdot\left(f_d(z)-f_{raw}(z)\right)\right]\right). \tag{3.19}$$

Then, similarly to the case of the standard PLL linear model, Eq.(3.19) can be re-formulated as follows:

$$\hat{f}(z)=\underbrace{\frac{S(z)B(z)N(z)}{1+B(z)N(z)}}_{H_f(z)}\cdot f_d(z)+\underbrace{\frac{T_cS(z)B(z)}{1+B(z)N(z)}}_{H_{nf}(z)}\cdot N_f(z), \tag{3.20}$$

where $H_f(z)$ and $H_{nf}(z)$ are the input signal frequency and frequency noise transfer functions. Eq.(3.20) shows that the final frequency estimate, $\hat{f}(z)$, is also given as a linear combination of the filtered input signal frequency and noise. In the time domain this relationship can be expressed as:

$$\hat{f}(k)=h_f[k]* f_d[k]+h_{nf}[k]* N_f[k], \tag{3.21}$$

where $h_f[k]$ and $h_{nf}[k]$ are the frequency and frequency noise impulse responses. In order to evaluate the noise and signal frequency transfer functions it is necessary to define the models for the loop filter and NCO. As mentioned above, the non-linear discriminator is approximated by a unit gain. For the loop filter, the most commonly used approach, namely the integrator-based model is considered:

$$B(z) = \frac{1}{T_c}\sum_{i=0}^{L-1} K_i \frac{1}{(1-z^{-1})^i} = \frac{1}{T_c}\sum_{i=0}^{L-1} K_i \left[\frac{z}{z-1}\right]^i . \tag{3.22}$$

In this case, the loop filter is constrained to be a linear combination of several integrators of different order. L denotes the order of the loop and $\{K_i\}_{i=0}^{L-1}$ are the filter integrator gains.

In the following, for the NCO, a rate-only feedback NCO (Stephens & Thomas 1995) is considered, where the phase estimate is updated according to the following equation:

$$\hat{\phi}[k] = \hat{\phi}[k-1] + \frac{1}{2}\left(f_{raw}[k-1]\cdot T_c + f_{raw}[k-2]\cdot T_c \right), \tag{3.23}$$

where, $f_{raw}[k-1]$ and $f_{raw}[k-2]$ are the Doppler frequencies estimated by the loop at the two previous epochs. In the Z-domain Eq.(3.23) becomes:

$$N(z) = \frac{T_c}{2}\frac{z^{-1}(1+z^{-1})}{(1-z^{-1})} . \tag{3.24}$$

Since the frequency noise, $N_f[k]$, at the input of the extended PLL linear model is a normalized version of the input phase noise, Eq.(3.16), $N_f[k]$ is a zero mean white sequence with variance

$$Var\{N_f[k]\} = \frac{1}{T_c^2}\sigma_n^2 = \frac{1}{T_c^2}\frac{1}{2T_c C/N_0}\left(1+\frac{1}{2T_c C/N_0}\right) \quad \left[\left(\frac{rad}{s}\right)^2\right]. \tag{3.25}$$

Following the same approach as in the case of the standard PLL linear model, it is assumed that the signal term $h_f[k] * f_d[k]$ in Eq.(3.21) does not contribute to the variance of the final frequency estimates. Considering this fact the following relationship is found:

$$Var\left\{\hat{f}[k]\right\} = T_c \int_{-0.5/T_c}^{0.5/T_c} \left| H_{nf}\left(e^{j2\pi fT_c}\right)\right|^2 df \, Var\left\{N_f[k]\right\}. \tag{3.26}$$

Eq.(3.26) is analogue to the expression for the phase variance (Eq.(3.11)), therefore the concept of **Doppler bandwidth** can be introduced as a counterpart of the loop bandwidth, given in Eq.(3.12), for frequency estimation:

$$B_d = \frac{1}{2}\int_{-0.5/T_c}^{0.5/T_c} \left| H_{nf}\left(e^{j2\pi fT_c}\right)\right|^2 df \quad [Hz]. \tag{3.27}$$

The Doppler bandwidth parameter is obtained by considering the transfer function of the overall frequency linear model of the PLL. Thus, it summarizes in a single parameter the ability of the tracking loop to produce smooth frequency estimates including the effects of the loop components and the smoothing filter, $S(z)$, while quantifying the amount of noise transferred from the input equivalent noise to the final frequency estimate. This fact makes it an effective metric for comparing different receivers when the same input C/N_0 and coherent integration time are assumed.

The major difference between the loop noise bandwidth and Doppler bandwidth is that Doppler bandwidth provides a more faithful interpretation of the bandwidth required to track particular system dynamics. A closer illustration of the relationship between these two parameters is provided in the last part of this chapter when discussing the results of the tests performed to validate the proposed theoretical models. It is possible to study the relationship between the loop noise bandwidth and Doppler bandwidth by performing numerical integration of Eqs. (3.12) and (3.27), which is in fact done in **Chapter 4** in regard to a new approach to loop filter design, but further investigation is required to characterise the exact relationship between these two parameters.

Using Eqs. (3.26) and (3.27), the variance of the frequency estimate, $\hat{f}[k]$, can be expressed as

$$Var\left\{\hat{f}[k]\right\} = 2T_c B_d Var\left\{N_f[k]\right\} = \frac{B_d}{T_c^2 C/N_0}\left(1+\frac{1}{2T_c C/N_0}\right) \quad \left[\left(\frac{rad}{s}\right)^2\right]. \tag{3.28}$$

The Doppler jitter then becomes

$$\sigma_f = \frac{1}{T_c}\sqrt{\frac{B_d}{C/N_0}S_L} \quad = \quad \frac{1}{T_c}\sqrt{\frac{B_d}{C/N_0}\left(1+\frac{1}{2T_c C/N_0}\right)} \quad \left[\frac{rad}{s}\right], \tag{3.29}$$

where S_L represents the squaring loss as defined in Eq.(3.15).

As discussed in **Chapter 2**, all Doppler measurements are obtained by processing PLL outputs and therefore parameters of the tracking loop strongly impact their quality. Expressions for the frequency estimate variance and the Doppler jitter introduced above can be effectively used for the assessment of the Doppler measurements quality as a function of the input C/N_0, the coherent integration time and the Doppler bandwidth, B_d.

Doppler Bias Analysis

In a way similar to the variance analysis, biases introduced by the loop can be determined starting from the frequency transfer function, $H_f(z)$. Biases in the Doppler estimates are induced by the transient response of the loop to changes in the input frequency as well as latencies introduced by the smoothing filter, $S(z)$. The ability of the loop to recover from changes in the input Doppler without steady-state errors depends on its order. Systemic errors in the Doppler measurements can be defined as

$$\varepsilon_f = E\left[f_d[k] - \hat{f}[k]\right]. \tag{3.30}$$

Using the relationship from Eq.(3.21), and considering the fact that $N_f[k]$ is zero mean, the Doppler systemic error, Eq.(3.30) can be expressed as:

$$\varepsilon_f[k] = f_d[k] - h_f[k] * f_d[k] = \left(\delta[k] - h_f[k]\right) * f_d[k] = h_\varepsilon[k] * f_d[k], \tag{3.31}$$

where

$$h_\varepsilon[k] = \delta[k] - h_f[k] \tag{3.32}$$

is the bias impulse response. Using the model given by Eq.(3.31), analysis of the bias introduced by the loop due to the variations in the input Doppler can be performed. However, one should note that for this type of analysis a reference for Doppler measurements is required. The computation of this reference will be discussed in the last part of this chapter.

3.1.1.3 Doppler Variance and Bias Analysis: FLL

As discussed in the previous chapter, an FLL operates in a similar way as the PLL. The main differences are the use of a frequency discriminator instead of a phase discriminator and the insertion of an additional integrator after the loop filter. Capability of this type of the carrier tracking loop to provide accurate frequency estimates depending on C/N_0, loop bandwidth and the coherent integration time has been previously investigated by Ward (1998), (Ward et al 2005) by performing interpolation of the simulation results using the Monte Carlo techniques. More specifically, the following expression for the frequency jitter has been suggested (Ward 1998), (Ward et al 2005):

$$\sigma_f = \frac{1}{T_c}\sqrt{\frac{4FB_n}{C/N_0}\left(1 + \frac{1}{T_c C/N_0}\right)} \quad \left[\frac{rad}{s}\right] \tag{3.33}$$

where

F=1 at high C/N_0,

F=2 at near threshold,

where the frequency jitter threshold *(1σ)* is equal to $1/12 \cdot T_c = 0.0833/T_c \quad [Hz]$.

This section introduces a theoretical analysis of the FLL based on the tracking loop linear theory. The main objective with using this approach is to provide an alternative method for the analysis of the noise propagation process in an FLL based on analytical derivations as opposed to the simulation/interpolation approach used in the derivation of Eq.(3.33). The general structure detailing the operations performed by an FLL is shown in Figure 3-3.

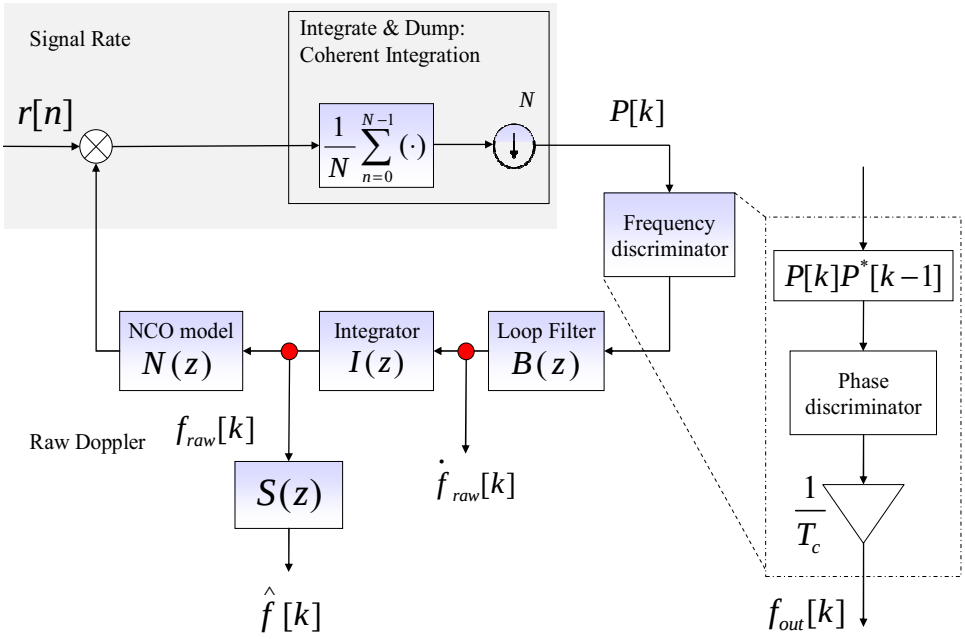

Figure 3-3: General structure of a digital FLL detailing the operations performed by the frequency discriminator, (Borio et al 2010).

A smoothing filter, $S(z)$, is also included into the scheme to account for the fact that frequency estimates can be further smoothed in order to get observations equivalent to carrier phase derived Doppler measurements. As it has been detailed in this figure, the

frequency discriminator implicitly performs a phase differentiation using two subsequent correlator outputs, $P[k]$ and $P[k-1]$. To be more specific, the quantity

$$P[k] \cdot P^*[k-1] \tag{3.34}$$

is evaluated first and its phase is extracted using a phase discriminator. This operation corresponds to evaluation of the phase difference of two subsequent complex correlators:

$$\angle\{P[k] \cdot P^*[k-1]\} = \angle\{P[k]\} - \angle\{P[k-1]\} = \Delta\varphi[k] - \Delta\varphi[k-1]. \tag{3.35}$$

After this phase difference is extracted by the phase discriminator, it is normalised by the coherent integration time, T_c. In this way, the frequency discriminator output is given by:

$$f_{out}[k] = \frac{1}{T_c}\left(\Delta\varphi[k] - \Delta\varphi[k-1]\right) \quad \left[\frac{rad}{s}\right]. \tag{3.36}$$

In a frequency discriminator, only the phase difference $\Delta\varphi[k] - \Delta\varphi[k-1]$ has to be extracted. Performing this phase differentiation helps to mitigate phase wrapping (Flower 2002, Borio et al 2010), a problem that is common for both the PLL and FLL. A phase discriminator is usually able to extract phases in a specific range: $[-\pi, \pi]$ for a four quadrant arctangent, $[-\pi/2, \pi/2]$ for a two quadrant arctangent. So if the phases $\Delta\varphi[k]$ and $\Delta\varphi[k-1]$ were to be extracted directly, then they could differ by an integer number of cycles (2π for a four quadrant arctangent, π for a two quadrant arctangent). In this way, their difference would be evaluated with an error equal to an integer number of cycles. This problem is called phase wrapping. But while in an FLL phase wrapping problem is reduced by performing phase differentiation (Eq.(3.34)), in a PLL, where the phases $\Delta\varphi[k]$ and $\Delta\varphi[k-1]$ are extracted directly, consecutive phase measurements can be affected by an additional difference equal to an integer number of cycles. After being averaged by the loop filter these phase measurements can lead to a biased loop control signal that can cause loss

of lock. This is the main reason why the FLL is more robust when compared to the PLL in terms of frequency tracking (Ward 1998, Ward et al 2005).

As it has been shown in (Borio et al 2010), when the phase error affecting the prompt correlators is small, the frequency discriminator is equivalent to a phase discriminator followed by a differentiator. This differentiator is fully determined by the frequency discriminator structure as indicated in Figure 3-3, and is in fact a first order differentiator that can be defined by a following transfer function:

$$\Delta_f(z) = \frac{1 - z^{-1}}{T_c}. \tag{3.37}$$

In particular, the dot-cross arctangent frequency discriminator can be obtained by applying the first order differentiator defined above to the output of an arctangent phase discriminator (Ward et al. 2005). The discriminator is obtained by using the arctangent addition formula.

This equivalence can be used to develop the FLL frequency linear model. By replacing the frequency discriminator by a phase discriminator followed by the differentiator defined in Eq.(3.37) and considering that this differentiator and the integrator, $I(z) = \frac{T_c}{1 - z^{-1}}$, following the loop filter are complementary operators and their effects cancel in the frequency linear model, it is possible to show that FLL and PLL are characterized by the same linear model with respect to the Doppler frequency. Thus, the expressions for Doppler bandwidth, Doppler jitter and Doppler bias given in Eqs. (3.27), (3.29) and (3.31) also apply to FLL.

This also means that the PLL and FLL with the same loop and Doppler bandwidths will produce frequency estimates with the same jitter. However, it is important to consider that the equivalence between PLL and FLL only holds for the linear frequency model under the assumption of a small phase error.

The validity of the proposed model as defined in Eq.(3.29) with respect to Eq.(3.33) is discussed later in this chapter, where live GPS L1 Coarse Acquisition (C/A) data are used to determine the empirical Doppler jitter.

3.1.1.4 Doppler Variance and Bias Analysis: FLL-assisted-PLL

As it has been briefly introduced in **Chapter 2**, because of the difficulties in direct transition from FLL tracking to PLL tracking, an intermediate tracking loop stage, called an FLL-assisted-PLL, can be used as a transition step between the two tracking modes. In this case, instead of a single loop, a PLL and an FLL are used in a coupled mode, in order to reduce locking times and avoid false frequency locks. A structure of an FLL-assisted-PLL is shown in Figure 3-4.

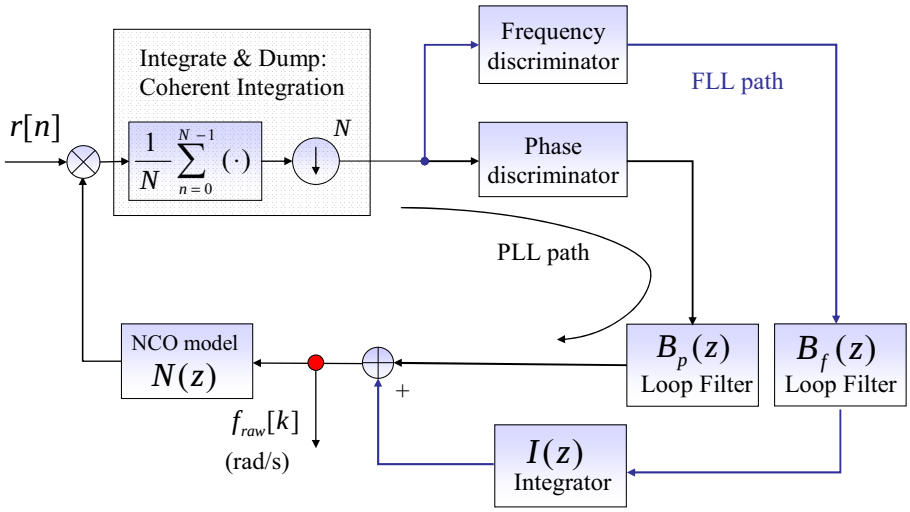

Figure 3-4: A general structure of a common-rate FLL-assisted-PLL.

The basic principle of FLL-assisted-PLL is such that both the phase and frequency discriminators are implemented in the same loop structure. Both the phase and frequency discriminator errors are then applied to their respective loop filter inputs, where an additional integrator follows the loop filter in the FLL part of the structure. In the case when the phase error at the input of the PLL loop filter is zero, the loop becomes a pure FLL, and on the contrary, if the frequency error at the input of the FLL filter is zeroed, the loop becomes a pure PLL. An important consideration about this type of a carrier tracking loop design is that it can be implemented using either common or different loop update rate for the PLL and FLL parts (Ward 1998, Legrand 2002). The design shown in Figure 3-4 represents the so-called common-rate FLL-assisted-PLL, since PLL and FLL branches are updated at the same rate. In particular, the same correlator outputs are used by the frequency and phase discriminators. Different FLL-assisted-PLL schemes can however be adopted (Ward 1998) where PLL and FLL branches are updated at different rates. In (Ward 1998), for instance, the FLL discriminator is updated using a 10 ms coherent integration time whereas the PLL branch uses correlator outputs computed over 20 ms. Monte Carlo simulation performance results for this type of carrier tracking loop design can be found in (Ward 1998). But since it is standard practice to use a common update rate due to simplicity in implementation, only this type of an FLL-assisted-PLL design will be considered in this section.

Frequency linear model of the common rate FLL-assisted-PLL can be derived using the same approach used for the analysis of the FLL and PLL and detailed in the previous sections. The procedure for deriving the frequency linear model is illustrated in Figure 3-5. First, as described in *Section 3.1.3*, the impact of the frequency discriminator in the FLL part of the FLL-assisted-PLL structure is modeled by applying a first order differentiator (Eq.(3.37)) to a phase discriminator. As in the case of the FLL, the impact of this differentiator and the integrator, $I(z)$, following the loop filter cancel out in the frequency linear model since they are complementary operators. In this way, the effect of coupling the

PLL and FLL loops in a single structure can be modeled by using a loop filter the transfer function of which is given by the sum of the FLL and PLL loop filter transfer functions:

$$B_{eq}(z) = B_p(z) + B_f(z), \tag{3.38}$$

where expressions for the PLL and FLL loop filter transfer functions $B_p(z)$ and $B_f(z)$ are given by Eq.(3.22).

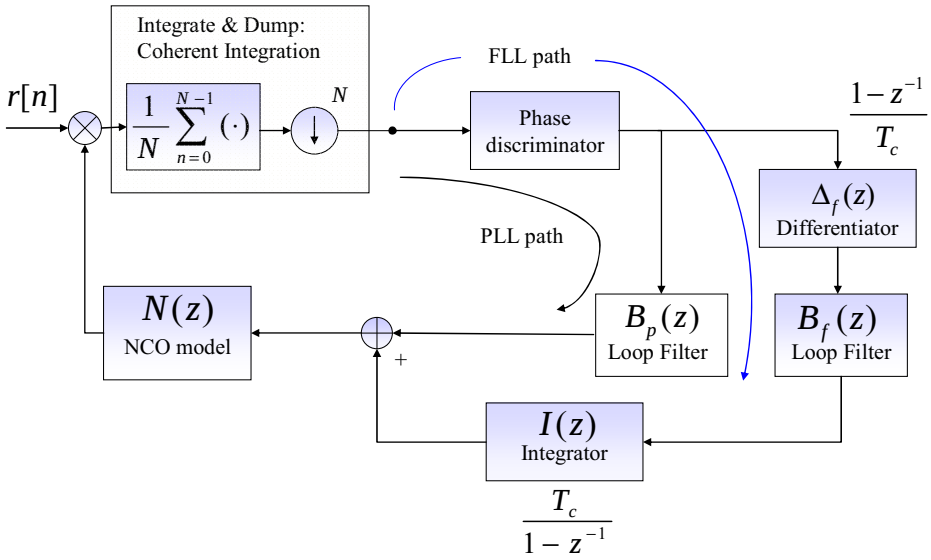

Figure 3-5: Derivation of the common-rate FLL-assisted-PLL frequency linear model: effect of the frequency discriminator is modeled by a phase discriminator followed by a differentiator.

As the input of the frequency and phase discriminators (the output of the I&D block) in an FLL-assisted-PLL is exactly the same as the input of the phase discriminator in a PLL, the noise impact on the input signal can be modeled by $N_f[k]$ that is the scaled phase noise defined by Eq.(3.16). Considering this, and approximating the non-linear phase discriminator by a constant gain, an approximated linear model of a common rate FLL-

assisted-PLL can be finally derived as shown in Figure 3-5, and the signal and noise transfer functions defined as follows:

$$H_f(z) = \frac{S(z)B_{eq}(z)N(z)}{1+B_{eq}(z)N(z)}, \tag{3.39}$$

$$H_{nf}(z) = \frac{T_c\, S(z)B_{eq}(z)}{1+B_{eq}(z)N(z)}. \tag{3.40}$$

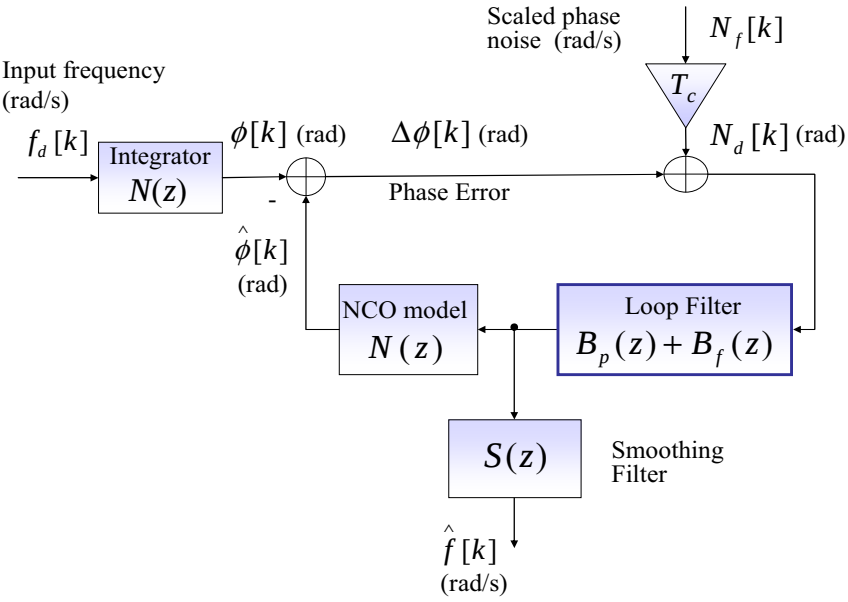

Figure 3-6: Frequency linear model of a common-rate FLL-assisted-PLL.

The derived frequency linear model of a common rate FLL-assisted-PLL shows that it is also possible to represent this type of a carrier tracking loop as a frequency filter, so that the final frequency estimate, $\hat{f}[k]$, can be expressed as a linear combination of the filtered

noise and input frequency. Thus, using the derived signal and noise transfer functions the Doppler variance, jitter and bias can be determined as defined using Eqs. (3.28), (3.29) and (3.31), where the Doppler bandwidth is computed using the noise transfer function defined in Eq.(3.40).

3.1.1.5 Doppler Variance and Bias Analysis Applied to Memory Discriminator Based Tracking Loops

As it has been shown in the previous sections, the proposed analysis approach and the developed model for Doppler variance and bias analysis are general and can be applied to PLL, FLL and the common-rate FLL-assisted-PLL tracking loops. Due to the similarity in the basic structure of different designs of sequential carrier tracking loops, this approach can also be applied for the analysis of the memory discriminator based carrier tracking loops. While in traditional carrier tracking loops the non-linear discriminator can be approximated by a constant gain, in the case of memory discriminators, the additional low-pass filtering stage introduced by this type of algorithms has to be accounted for. As explained in **Chapter 2**, exponential filtering has been chosen to be used as a part of the memory discriminator design responsible for progressively de-weighting the squared correlator outputs and extending the integration time before extracting the phase/frequency information. In this case, the loop linear model is obtained by approximating the loop discriminator with a linear filter (Borio et al 2009a, Sokolova 2009). The transfer function of an exponential filter has been defined in Eq.(2.32).

The generality of the suggested approach allows one to perform analysis of all types of the memory discriminator based carrier tracking loops exploiting the fact that a memory discriminator can be approximated by a linear filter model which can be easily adopted into the linear models of the standard tracking loops. The approximated frequency linear model for a PLL with memory discriminator is illustrated in Figure 3-6.

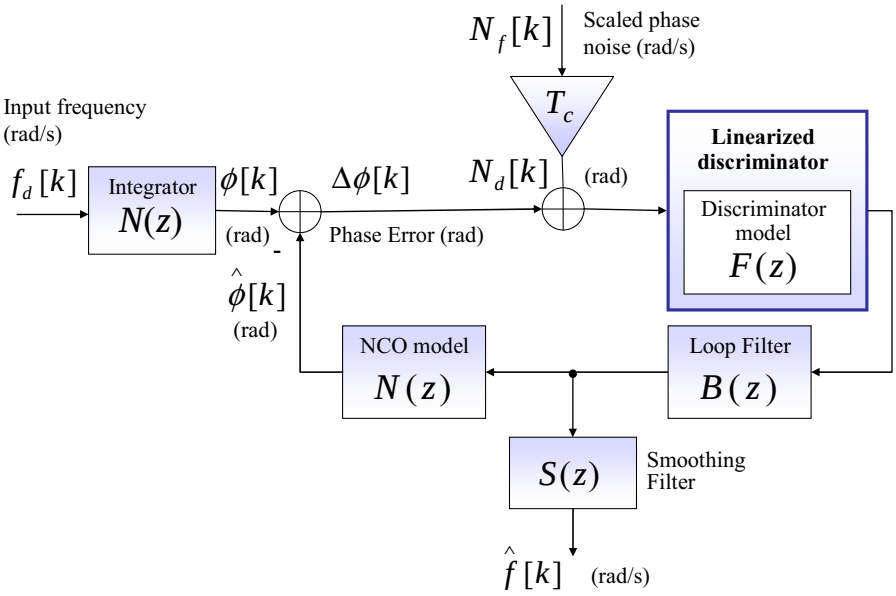

Figure 3-7: Frequency linear model of a PLL with discriminator with memory discriminator.

Similarly to the standard PLL, the memory discriminator based PLL can also be approximated as a linear frequency filter that computes the final Doppler frequency estimates as a linear combination of filtered noise and input signal frequency. The same approach for the derivation of the standard PLL frequency linear model has been used here as in *Section 3.1.2*, with the only difference, as it can be observed by comparing Figures 3-2 and 3-7, being the presence of the linear approximation of the memory discriminator. Thus, considering Eq. (2.32)and the PLL linear model defined in Figure 3-7, the signal and noise transfer functions for a PLL with memory discriminator can be evaluated as follows:

$$H_f(z) = \frac{S(z)F(z)B(z)N(z)}{1+F(z)B(z)N(z)}, \tag{3.41}$$

$$H_{nf}(z) = \frac{T_c S(z) F(z) B(z)}{1 + F(z) B(z) N(z)}, \tag{3.42}$$

where $F(z)$ is the transfer function of the memory discriminator.

Here the same models for the NCO and loop filter, as defined in Eqs. (3.24) and (3.22), are considered. As in the case with the standard loops, the effect of the smoothing filter, $S(z)$, is included in order to account for different methods for Doppler frequency determination. Having the expressions for the signal and noise transfer functions, the Doppler variance and jitter, and the Doppler bias given by Eqs. (3.28), (3.29) and (3.31) can be obtained.

Also in the case of an FLL with a memory discriminator the same approach as suggested for the standard FLL can be applied. Recall from **Chapter 2,** Figure 2-4 that a memory discriminator consists of three parts: squaring for removing the bit dependence from the correlator outputs, a low-pass filtering stage responsible to further extend the integration time and finally a memory-less discriminator that extracts the phase/frequency information. To derive the frequency linear loop model of an FLL with a memory discriminator the effect of the memory-less frequency discriminator can be modelled in the same way as described in *Section 3.1.3* - by replacing it by a phase discriminator followed by the differentiator defined in Eq.(3.37). In this way, the effects of the differentiator and the integrator placed after the FLL filter cancel out, and the remaining combination of the squaring stage, the low-pass filter and the memory-less phase discriminator can be approximated by its linear filter (Eq.) as in the case of the memory discriminator based PLL. This means that the Doppler variance, jitter and bias of an FLL with a memory discriminator can be evaluated using Eqs. (3.28), (3.29) and (3.31), where the signal and noise transfer functions are defined by Eqs. (3.41) and(3.42), respectively.

The derivation of the frequency linear loop model of a memory discriminator based common-rate FLL-assisted-PLL is very similar to the procedure described in *Section 3.1.4***,** therefore, in order to avoid repetition, only a brief discussion is given here. First, the frequency memory discriminator in the FLL path of the loop structure can be modelled in

the same way as described above for the case of the memory discriminator based FLL. Also here the effects of the differentiator and the integrator cancel out, so that the effect of joint loop structure can be modeled by using a loop filter with the transfer function, $B_{eq}(z)$, defined in Eq.(3.38) and the final expressions of the signal and noise transfer functions can be defined as follows:

$$H_f(z) = \frac{S(z)F(z)B_{eq}(z)N(z)}{1+F(z)B_{eq}(z)N(z)}, \tag{3.43}$$

$$H_{nf}(z) = \frac{T_c S(z)F(z)B_{eq}(z)}{1+F(z)B_{eq}(z)N(z)}. \tag{3.44}$$

3.1.2 Block Processing Architecture

As detailed in the previous chapter, in a block processing approach, a massive number of correlators are used to perform a simultaneous search for all possible code delays and Doppler frequencies. The receiver locally generates several replicas of the incoming code and carrier and evaluates their correlation with the incoming signal, so that the parameters of the incoming signal are estimated as those of the local replica that maximize the correlation function. In other words, block processing approach evaluates the function defined in Eq.(3.2) over a finite and discrete frequency grid.

Due to the high non-linearity of the "$\arg\max(\cdot)$" component in the block processing architecture, the linear tracking loop theory is not applicable and a different approach for the Doppler frequency variance analysis is required. Block processing and FFT-based techniques for frequency estimation have been object of extensive research (Palmer 1974, Rife & Boorstyn 1974) and several asymptotic findings, based on the Cramer-Rao Lower Bound (CRLB) and simulation results are available. In particular, as it has been

summarized in (Borio et al 2010), a frequency estimator obtained implementing a frequency search over a finite grid is characterized by three different error regions:

- **granularity errors**: since the frequency search is performed over a finite grid, $\{f_0, f_1, f_2, .., f_{N-1}\}$, the estimated frequency can assume only one of the values tested during the search. This error, due to the finite granularity of the grid, is independent of the input C/N_0 and dominates for high Signal-to-Noise ratios (SNRs). Granularity errors lead to a floor in the frequency estimator variance;
- **above threshold region:** block processing techniques are non-linear frequency estimators and thus exhibit a SNR dependent behaviour (Rife & Boorstyn 1974). A threshold is defined as the C/N_0 value below which the estimator variance starts increasing significantly as the SNR drops. When the estimator is operating above threshold, its variance approximately follows the CRLB;
- **below threshold region:** below a certain SNR, block processing techniques are unable to detect the signal presence and determine a valid frequency estimate. This essentially corresponds to the loss-of-lock condition in sequential tracking loops. A GNSS receiver should be able to detect this condition and stop outputting Doppler estimates.

According to (Rife & Boorstyn 1974, Chan et al 1997), in the above threshold region, the variance of frequency estimates approximately follows the CRLB that is given by (Kay 1993):

$$\sigma^2_{CRLB} = \frac{12}{(2\pi)^2 SNR \cdot N\left(N^2-1\right)} \cdot \left[\frac{2\pi}{T_s}\right]^2 \qquad \left[\frac{\text{rad}^2}{\text{s}^2}\right], \tag{3.45}$$

where

$$SNR = 2 \cdot C / N_0 \cdot T_s, \tag{3.46}$$

and is the pre-integration SNR . Whereas the term $\left[\frac{2\pi}{T_s}\right]^2$ has been introduced in order to get the variance of the frequency estimates expressed in units of rad^2/s^2. By substituting the expression of the pre-integration SNR (Eq.(3.46)) into Eq.(3.45) and considering that $T_c = NT_s$, the following expression for the standard deviation of frequency estimates obtained using block processing techniques is obtained (Borio et al 2010):

$$\sigma_{CRLB} = \frac{1}{T_c}\sqrt{\frac{6/T_c}{C/N_0}\cdot\frac{N^2}{N^2-1}} \approx \frac{1}{T_c}\sqrt{\frac{6/T_c}{C/N_0}} \quad \left[\frac{\text{rad}}{\text{s}}\right]. \tag{3.47}$$

In Eq.(3.47) the condition, $N \gg 1$, is used. A more detailed description of the process of the derivation of Eq.(3.47) is provided in **Appendix A**.

If compared to the expression of the Doppler jitter given in Eq.(3.29) with the squaring loss term $\left(1+\frac{1}{2T_c C/N_0}\right)$ neglected, Eq.(3.47) has the same functional form. By identifying the different terms in both Eq.(3.29) and Eq.(3.47) a parameter similar to the Doppler bandwidth can be defined for the block processing approach:

$$B_d = \frac{6}{T_c}. \tag{3.48}$$

However, it is important to note that in this case B_d is not derived from an approximate linear model as it has been done in the case of the sequential tracking loop architecture, but determined from the CRLB exploiting the functional similarity between Eqs. (3.47) and (3.29).

3.2 Practical Verification

In order to evaluate the proposed theoretical models for Doppler estimation analysis, several static and dynamic pedestrian-based field tests in various GPS operating environments have been conducted. A number of simulations were carried out as well to test the model suggested for the Doppler bias analysis under a wider range of dynamics.
This section introduces the methodology used for the empirical determination of the Doppler jitter values and compares the obtained results with the theoretical models developed in the first part of this chapter.

3.2.1 Doppler Jitter Model Verification

3.2.1.1 Attenuated Line-Of-Sight (LOS) Test

In the first experiment, data sets were collected in an open sky environment using an antenna located on the roof of the CCIT building, University of Calgary. The antenna used was the NovAtel 702 antenna with 29 dB gain, and noise figure of 2 dB. Figure 3-8 illustrates the adopted experimental setup.

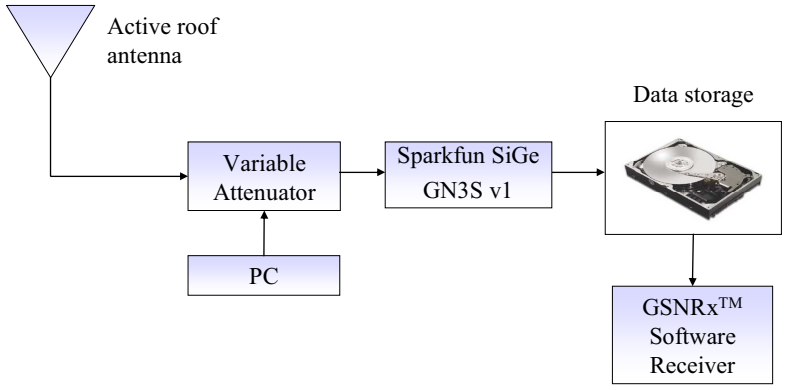

Figure 3-8: Experimental setup adopted for the attenuated LOS GPS data collection.

The received signal power was gradually decreased by means of a variable attenuator inserted prior to a Sparkfun SiGe GN3S v1 front-end, specifications of which are shown in Table 3-1. After a minute without attenuation the signal was progressively attenuated at a rate of 1 dB each 30 s for a total range of 40 dB. The collected data were stored in an external hard drive and processed in post mission using two versions of the University of Calgary's GNSS Software Navigation Receiver (GSNRx^{TM}), namely standard version (Petovello et al 2008) and a memory discriminator based architecture.

Table 3-1: Characteristics of the GPS signals collected using the SiGe GN3S v1 front-end.

Parameter	Value
Sampling frequency	$f_s = 16.367\ MHz$
Intermediate frequency	$f_{IF} = 4.1304\ MHz$
Sampling	Real
No. of bits	2

The collected data sets were processed several times using different values of the tracking loop parameters in order to analyze their impact on the quality of the Doppler estimates. The procedure adopted for the estimation of the Doppler jitter from the empirical data is illustrated in Figure 3-9.

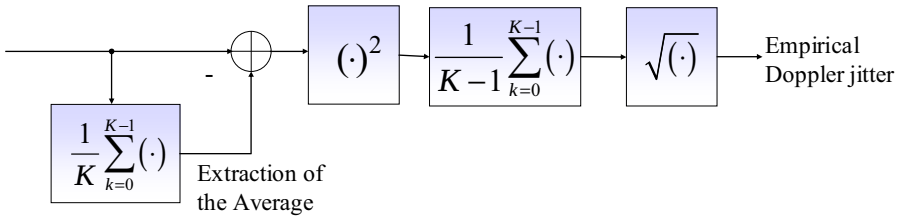

Figure 3-9: Doppler tracking jitter estimation procedure.

Following this procedure, the mean of the Doppler estimates provided by GSNRx^{TM} was obtained by implementing a moving average (MA) filter. The mean was then subtracted from the measurements which were further squared and filtered. Thus, the final estimate of the empirical Doppler jitter is obtained as follows:

$$\hat{\sigma}_f[n] = \sqrt{\frac{1}{K-1}\sum_{k=0}^{K-1}\left[\hat{f}[k-n] - \frac{1}{K}\sum_{k=0}^{K-1}\hat{f}[k-n]\right]^2} \quad . \tag{3.49}$$

Both in Figure 3-9 and Eq.(3.49), K represents the length of the analysis window of the MA filter. The use of a moving analysis window for the determination of the empirical Doppler jitter provides estimates as a function of time, and the length of the analysis window length, K. It is noted that all the results presented in this section were obtained using $K = 100$ ms. As GSNRx^{TM} provides C/N_0 estimates as a function of time, it was possible to associate a C/N_0 value to each empirical Doppler tracking jitter estimate obtained using Eq.(3.49). The C/N_0 estimates were also smoothed using a MA filter with the same length of the analysis window, $K = 100$ ms. In this way, it was possible to determine the empirical Doppler jitter as a function of the input C/N_0.

Attenuated LOS: Sequential Carrier Tracking – PLL

The validity of the models for the Doppler frequency variance (Eq.(3.28)) and the Doppler jitter (Eq.(3.29)) as applied to a standard 3rd order PLL was thoroughly investigated and verified by Sokolova (2009). The impact of the coherent integration time, as well as the effect of different implementations of the smoothing filter, $S(z)$, was studied and in all cases a good agreement between theoretical and empirical results was found. Therefore, only a brief illustration of performance of the above-mentioned theoretical models as applied to a PLL is provided here. Figure 3-10 shows the Doppler jitter obtained using a

fixed coherent integration time of 20 ms, but different loop bandwidth values for a third order PLL.

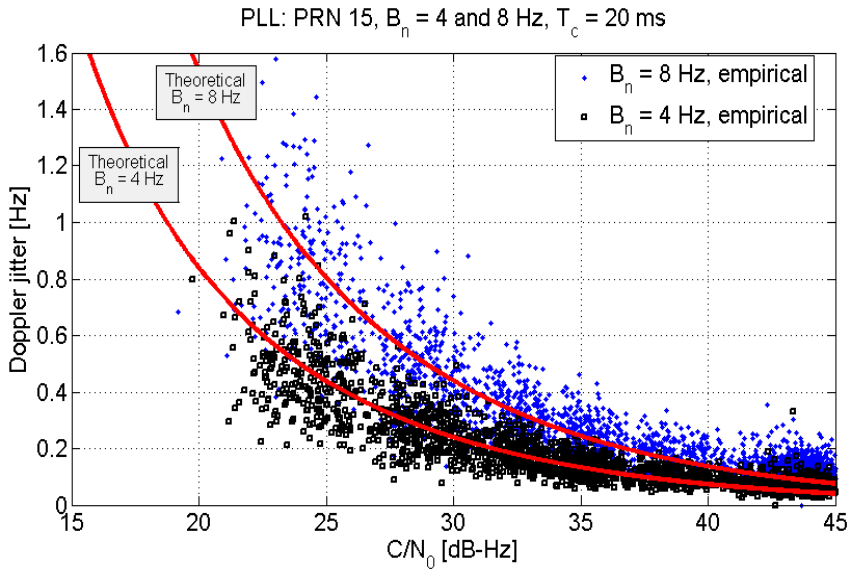

Figure 3-10: Empirical and theoretical jitter of the raw Doppler measurements as a function of C/N_0 and loop bandwidth, 3rd order PLL.

Empirical data are compared to the theoretical Doppler jitter defined in Eq.(3.29) showing a good agreement between theoretical and empirical results. Figure 3-10 also illustrates the fact that narrow bandwidths shield the tracking loop from excessive noise power, and give better Doppler estimates with lower variance in the measurements. It is noted that similar decreasing jitter behaviour is observed when investigating the effect of reduced loop noise bandwidth.

Table 3-2 compares the values of the loop and Doppler bandwidths for the cases considered in Figure 3-10 highlighting the relationship between the two parameters. The Doppler bandwidth values in Table 3-2 have been obtained by numerically integrating Eq.(3.27).

Table 3-2: Loop and Doppler bandwidth for raw Doppler estimation; 3rd order PLL, T_c = 20 ms.

Parameter	Value	
Loop bandwidth B_n [Hz]	4.00	8.00
Doppler bandwidth B_d [Hz]	0.89	2.99

Attenuated LOS: Sequential Carrier Tracking – FLL

In order to test the proposed model for the FLL case, GSNRx™ was constrained to operate in FLL-only mode. Figure 3-11 shows the results generated by a second order FLL using a 2 Hz loop bandwidth and a 10 ms coherent integration time. The value of the Doppler bandwidth found in this case was 0.138 Hz. Here the empirical Doppler jitter is compared against the proposed theoretical Doppler jitter (Eq.(3.29)) and the expression for the frequency jitter (Eq.(3.33)) suggested by Ward et al (2005).

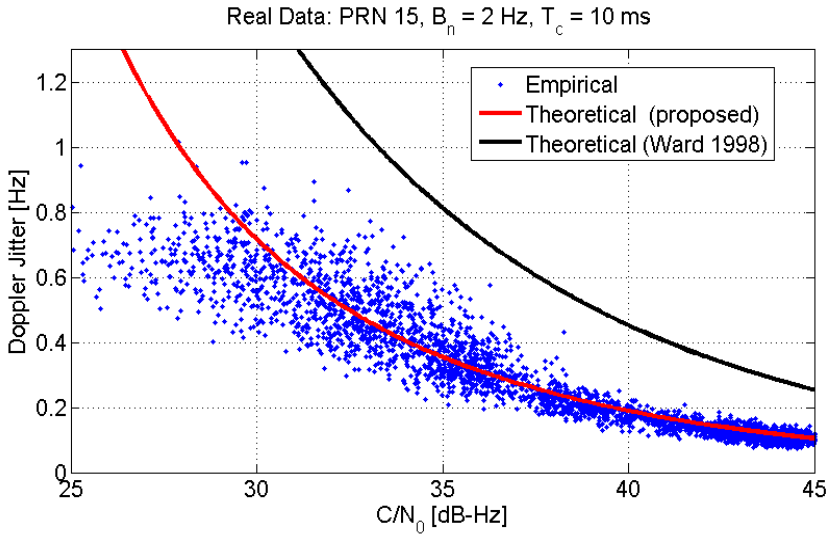

Figure 3-11: Empirical and theoretical Doppler jitter of raw Doppler measurements as a function of C/N_0. 2nd order FLL, B_n = 2 Hz, B_d = 0.138 Hz, T_c = 10 ms.

As it can be observed from Figure 3-11, the proposed model (Eq.(3.29)) is in good agreement with the empirical results, whereas Eq. (3.33) overestimates the Doppler jitter.

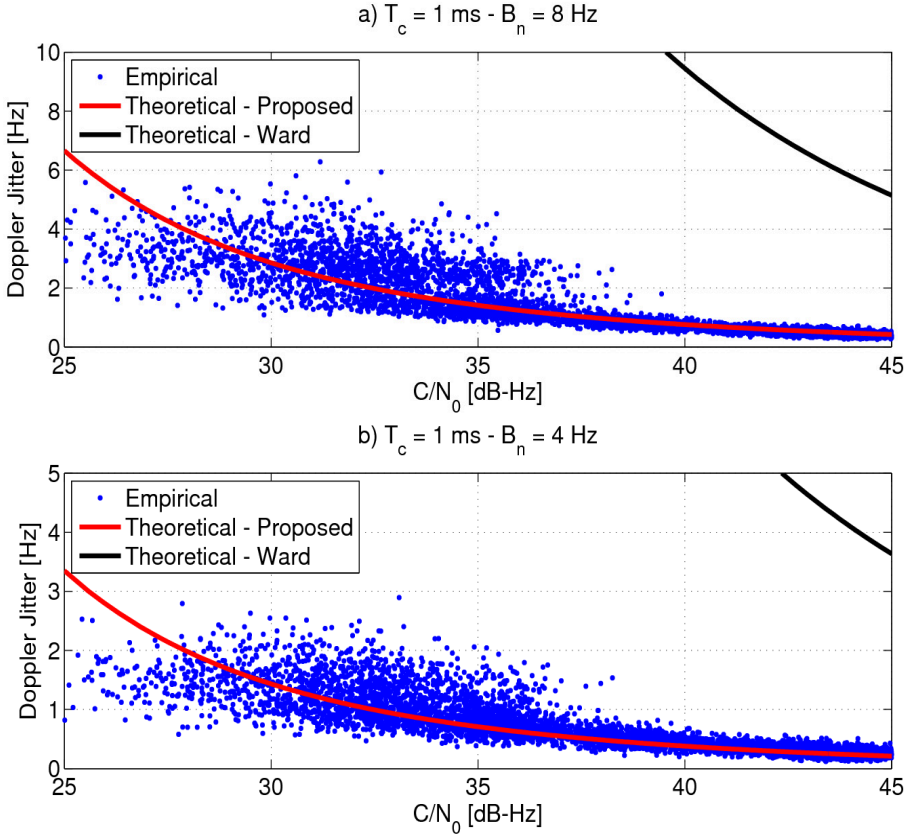

Figure 3-12: Empirical and theoretical Doppler jitter of raw Doppler measurements as a function of C/N_0. 2nd order FLL, T_c = 1 ms. a) B_n = 8 Hz, b) B_n = 4 Hz.

The difference between these two different models becomes even more significant when lower integration times and larger loop bandwidths are considered. This can be explained by the fact that the difference between the loop and Doppler bandwidth increases and model given by Eq.(3.33) becomes more and more inaccurate. This divergence can be

clearly seen in Figure 3-12 where the cases of fixed $T_c = 1$ ms, and $B_n =$ 4, and 8 Hz are considered. Thus, it can be concluded that the analytical approach used in this work is a better method for predicting the carrier tracking loop performance in terms of frequency jitter when compared to the approach involving interpolation of the Monte Carlo simulation results used by Ward (1998). In particular, the concept of Doppler bandwidth introduced in *Section 3.1.2*, Eq.(3.27), allows an accurate characterization of the noise propagation process in the loop considering the effects of the loop components including the smoothing filter, $S(z)$. By using this parameter, a more accurate evaluation of the carrier tracking loop performance in terms of the Doppler frequency jitter is achieved.

Table 3-3 shows the values of the loop and Doppler bandwidths for the cases considered in Figure 3-12 supporting the fact that for shorter coherent integration times and larger values of the loop bandwidth the difference between the loop and Doppler bandwidths becomes larger.

Table 3-3: Loop and Doppler bandwidth for raw Doppler estimation; 2nd order FLL, T_c = 1 ms.

Parameter	Value	
Loop bandwidth B_n [Hz]	4.00	8.00
Doppler bandwidth B_d [Hz]	0.06	0.21

Attenuated LOS Data: Sequential Carrier Tracking - FLL-assisted-PLL

To be able to evaluate the model developed for the common rate FLL-assisted-PLL, GSNRx™ was constrained to operate in an FLL-assisted-PLL mode only. The empirical data were processed as defined by Eq.(3.49). The theoretical Doppler jitter values were obtained using the model given in Eq.(3.29) , where the effect of coupling the PLL and FLL loops in a single structure was accounted for as described by Eq.(3.38). Results obtained using a common rate FLL-assisted-PLL are shown in Figure 3-13, where cases

with 4 Hz and 8 Hz loop bandwidth in both the PLL and FLL branches and 1 ms coherent integration time are considered, whereas Table 3-4 shows the values of the common loop and Doppler bandwidth for the cases considered in Figure 3-13.

As it can be observed from Figure 3-13 and Table 3-4, coupling the PLL and FLL in a single loop structure results in a higher level of noise transferred from the input signal to the final Doppler estimate. To be more specific, a common-rate FLL-assisted-PLL provides less accurate Doppler estimates compared to PLL- and FLL-only designs. This is due to the fact that noise is transferred to the final Doppler estimate by both PLL and FLL branches, the result of which is a loop with a higher Doppler bandwidth. However, as indicated by Ward (1998), an FLL-assisted-PLL design should provide better lock performance since it combines the features of both PLL and FLL tracking techniques. For this reason FLL-assisted-PLL should be used only during acquisition. Therefore, due to its higher robustness to high dynamics when compared to a pure PLL design, it is still beneficial to use this type of tracking loop for the improvement of the overall receiver performance. Figure 3-13 demonstrates as well that the theoretical values of the Doppler jitter match the empirical results in the case of a common-rate FLL-assisted-PLL, providing further confirmation of the validity of the developed theoretical model.

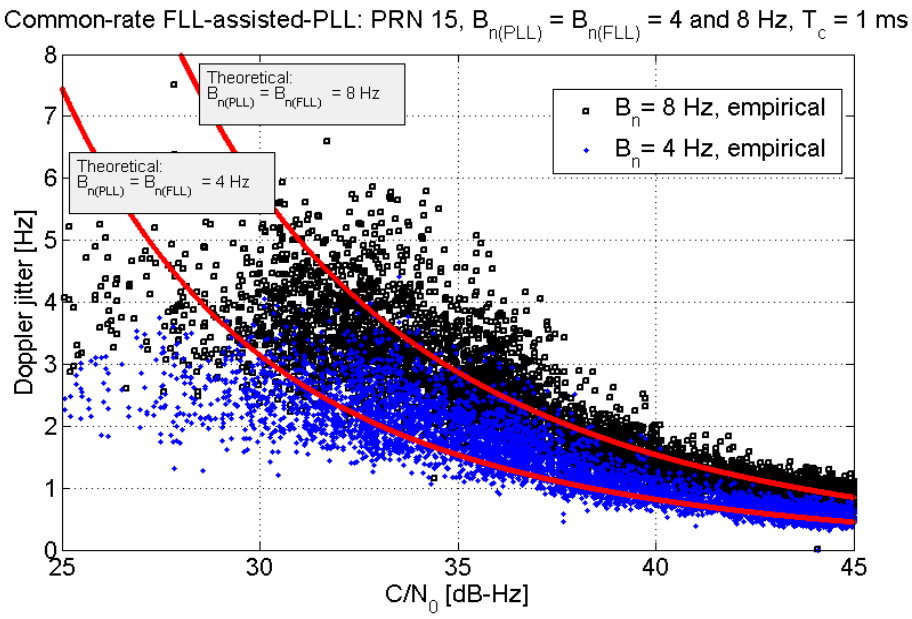

Figure 3-13: Empirical and theoretical Doppler jitter of raw Doppler measurements as a function of C/N_0 obtained using a common rate FLL-assisted-PLL. Cases considered: loop bandwidths, $B_{n(PLL)} = B_{n(FLL)}$ 4 Hz and = 8 Hz and T_c = 1 ms.

Table 3-4: Common loop and Doppler bandwidth for raw Doppler estimation; Common-rate FLL-assisted-PLL T_c = 1 ms.

Parameter	Value	
Loop bandwidth B_n [Hz]	4.00	8.00
Doppler bandwidth B_d [Hz]	0.22	0.89

Attenuated LOS: Sequential Carrier Tracking - Memory Discriminator Based Tracking Loops

As discussed in *Section 3.1.5* the same approach can be applied for the analysis of memory discriminator based tracking loops. Figure 3-14 illustrates the theoretical Doppler jitter

obtained using a 3rd order memory discriminator based PLL using 1 ms coherent integration time, 5 Hz loop bandwidth and the forgetting factor, α, equal to 0 and 0.8, where $\alpha = 0$ represents the case of a standard tracking loop. Such a short coherent integration time was chosen in order to allow usage of a higher value of the forgetting factor α, (Borio et al 2009a, Sokolova 2009). The theoretical Doppler jitter in this case was determined as defined by Eq.(3.29), where the effect of the memory discriminator was accounted for by using the expression of the noise transfer function found in Eq.(3.42) when evaluating the Doppler bandwidth. The empirical data were processed as described in Figure 3-9 and Eq.(3.49).

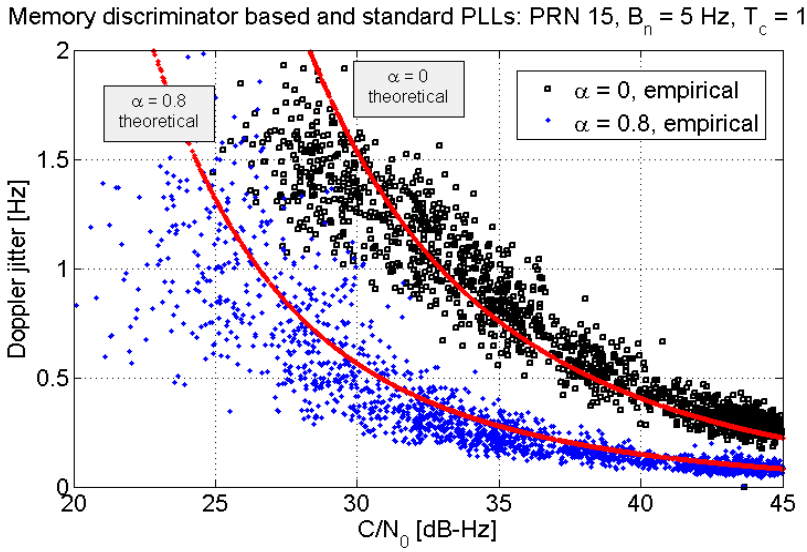

Figure 3-14: Empirical and theoretical Doppler jitter of raw Doppler measurements as a function of C/N_0 and forgetting factor, α, obtained using a memory discriminator based 3rd order PLL, T_c = 1 ms, B_n = 5 Hz.

Values of the Doppler bandwidth obtained in the cases considered in Figure 3-14 are compared in Table 3-5, illustrating the performance of a PLL with a memory discriminator

compared to a standard loop in terms of the amount of noise transferred by the loop to the final Doppler estimate.

Table 3-5: Doppler bandwidth for raw Doppler estimation in the cases of a standard and a memory discriminator based PLL. B_n = 5 Hz, T_c = 1 ms.

Parameter	Value	
Forgetting factor α	0 (standard loop)	0.8
Doppler bandwidth B_d [Hz]	0.08	0.01

Figure 3-15 shows the case considering a memory discriminator based 2nd order FLL.

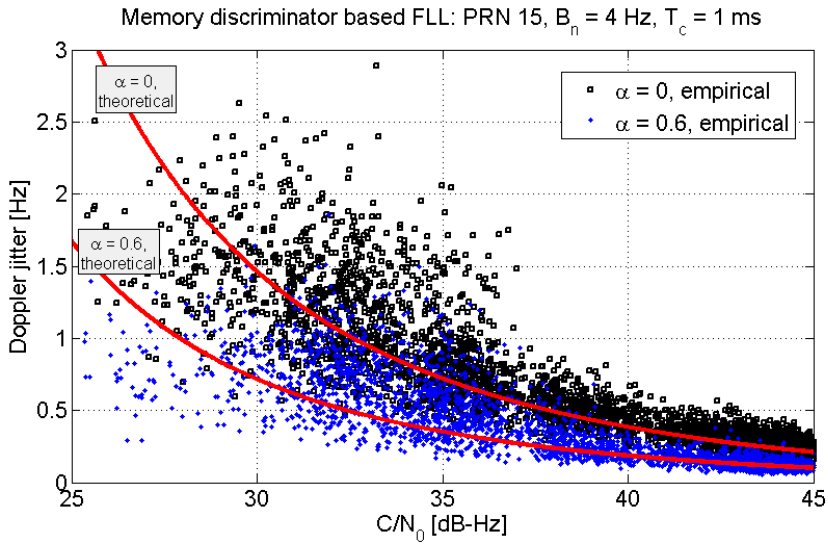

Figure 3-15: Empirical and theoretical Doppler jitter of raw Doppler measurements as a function of C/N_0 and forgetting factor, α, obtained using a memory discriminator based 2nd order FLL, T_c = 1 ms, B_n = 4 Hz.

Following the procedure used for the analysis of the results above, the theoretical Doppler jitter was determined by applying Eq.(3.42) to the model defined in Eq.(3.29) and

compared with the Doppler jitter values computed from the empirical data. The coherent integration time used in this case was 1 ms and the loop bandwidth 4 Hz allowing the use of α up to 0.6.

As Figures 3-14 and 3-15 are showing, memory discriminators improve the quality of Doppler estimates by reducing the variance of the measurements. Using the extended theoretical model including the effect of memory discriminators allows one to effectively predict the quality of Doppler measurements obtained from memory discriminator based carrier tracking loops.

Attenuated LOS: Block Processing

For the practical verification of the theoretical model proposed for the block processing approach a modified version of GSNRx^{TM} implementing block processing techniques, namely the GSNRx™-rr (GSNRx^{TM} - reference rover), has been used. To achieve higher tracking sensitivity, the software receiver was designed to be capable of simultaneously processing test and reference data in order to remove the navigation data bits and extend the coherent integration time possible for the test data set beyond 20 ms (Satyanarayana et al 2010). Figure 3-16 illustrates the test setup used for collecting the data used in this case.

In this configuration the received signal was split between two channels of the National Instruments (NI) *PXI-5661* signal analyzer. The signal on the first channel (RF chain 1) was progressively attenuated with a step of 1 dB each 30 s for a total range of 40 dB after a minute without attenuation, whereas the signal on the second channel (RF chain 2) was not attenuated and used as a reference signal.

Both data sets were stored in an external hard drive and processed in post mission using GSNRx^{TM}-rr. The reason there has been used a second LNA at the input of the NI system is that from experience it is known that absent a second LNA, the C/N_0 level of captured GNSS signals is too degraded for acquisition to work reliably.

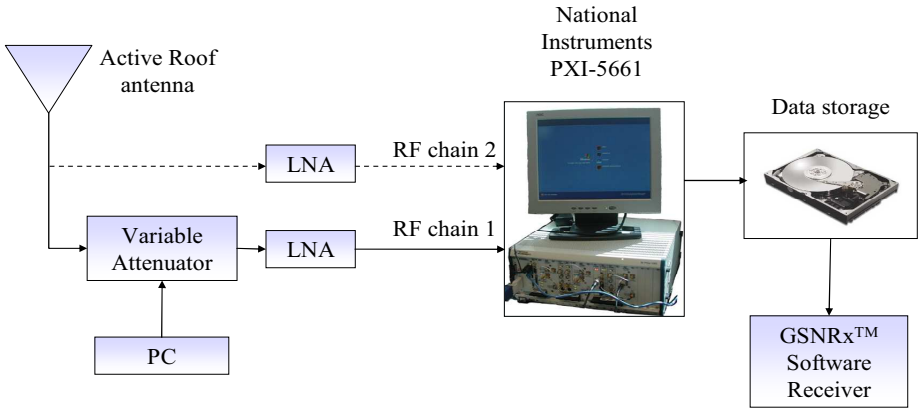

Figure 3-16: Experimental setup for the attenuated LOS GPS data collection adopted for the case of block processing approach.

Results obtained using this approach are presented in Figure 3-17, where the values representing the CRLB (Eq.(3.47)) and empirical Doppler jitter values determined using different integration times are compared. In all cases a step equal to 0.2 Hz was used to perform the search for the correlation peak in the frequency domain.

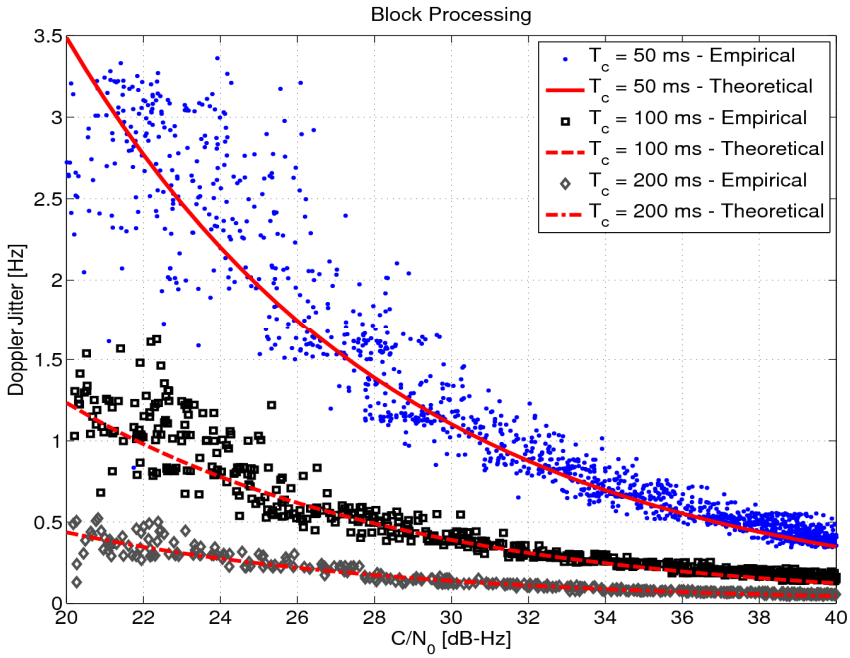

Figure 3-17: Empirical and theoretical Doppler jitter of raw Doppler measurements as a function of C/N_0, PRN 20. The measurements used to evaluate the empirical Doppler jitter were obtained using a modified version of GSNRx™ implementing block processing techniques.

Also in this case a good agreement between empirical and theoretical results is found supporting previous results on frequency estimation using batch/block processing (Chan et al 1997) and showing that a parameter, playing the same role as the Doppler bandwidth, can also be defined for block processing approach.

3.2.1.2 Moderate Urban Canyon Environment: Sequential Architecture

Further analysis of the Doppler jitter was performed by studying data collected in more realistic conditions and in the presence of different signal impairments. Several static and

pedestrian-based tests were performed in various real world operating environments such as under forest canopy, in urban canyon environment and indoors. Although all the tests were successfully performed, only two of them, are detailed here in order to avoid repetition of similar results.

The first test has been performed in a moderate urban canyon environment on the University of Calgary campus (51° latitude). This particular scenario has been chosen because it represents a realistic situation with a steep elevation mask present in moderate urban canyons. Buildings obscured the signals on the east and west sides of the location at elevation angles up to 50° and 30°, respectively. In addition, a walled walkway obscured signals arriving from the north below about 25° in elevation (MacGougan 2003). The southern direction was relatively unhindered with some trees contributing to signal masking from the southwest side of the test site. Moreover, the buildings surrounding the test location have glass and metallic surfaces that act as signal blockers and reflectors creating strong multipath.

Photos of the test location and results obtained using a standard version of the software receiver compared to the ones obtained using the memory discriminator based architecture using α = 0.3 are shown in Figure 3-18. Coherent integration time in this case was set to 20 ms and loop bandwidth to 8 Hz. An urban canyon is a type of environment where the measured C/N_0 is significantly affected by slow fades that degrade the signal quality, directly translating the reduced received power into increased Doppler tracking jitter. This trend can be seen in Figure 3-18.

Although the proposed theoretical model for Doppler jitter analysis only considers the thermal noise introduced by the carrier tracking loops, due to the fact that both the C/N_0 estimates and the Doppler values provided by the GSNRx^{TM} receiver are evaluated from the same correlator outputs, they are both affected by the same impairments. Therefore, such phenomena as multipath and fading which are not accounted for in the model are partially compensated by the use of the C/N_0 provided by the receiver.

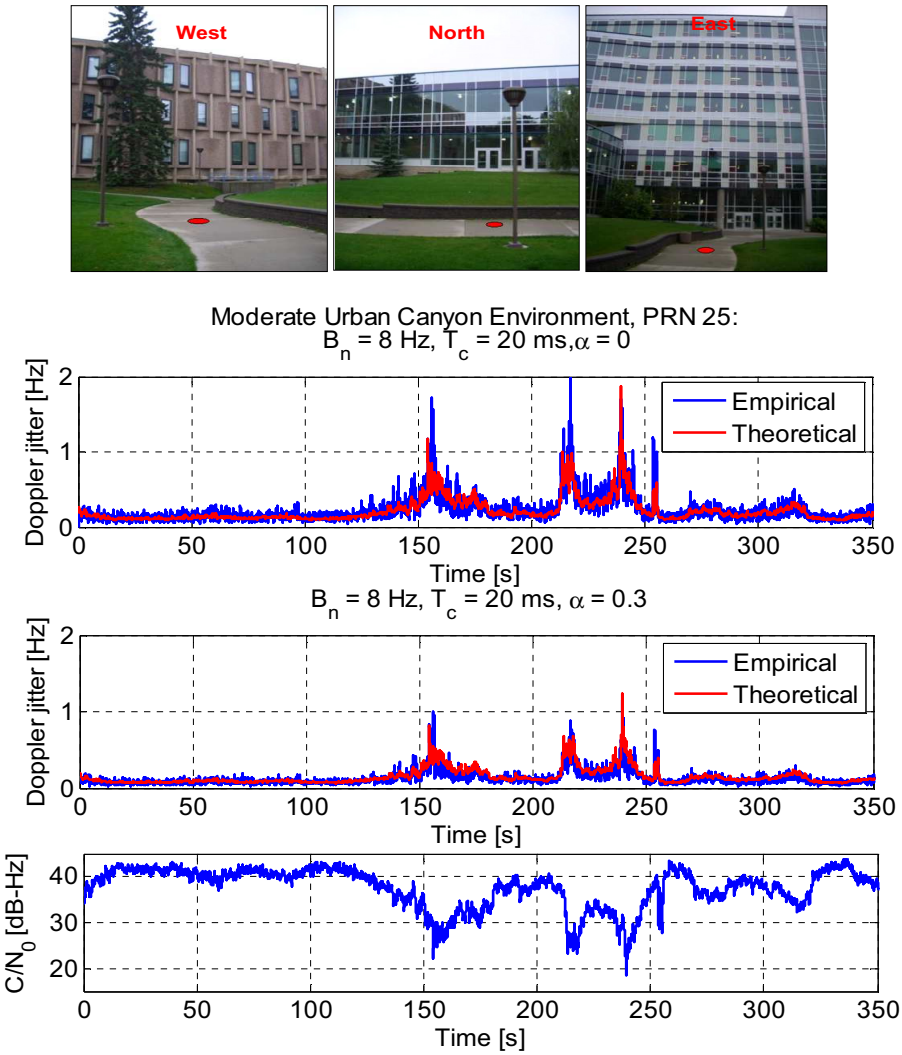

Figure 3-18: Environment view and Doppler jitter analysis of raw Doppler measurements obtained using standard and memory discriminator based tracking loop architectures.

It is noted that during the entire test, sample results of which are presented in Figure 3-18, the receiver maintained phase lock, and therefore operated in the PLL tracking mode.

However, when constraining the receiver to operate in FLL-assisted-PLL or FLL modes, similar results were obtained verifying that the proposed theoretical framework is valid in each case considered. Figure 3-18 also illustrates the ability of the memory discriminator based architecture to provide better Doppler estimates in the presence of multipath and fading compared to the standard receiver architecture.

3.2.1.3 Indoor Environment/Wooden Residential House: Block Processing Architecture

The second experiment represents a pedestrian-based test performed in a typical North American wooden residential house. The house contains an upper level with wooden walls and large windows, and a basement with a concrete wall structure and small windows located at ceiling level. As wooden walls attenuate the received GPS signal much less than concrete ones, the upper floor represents a less challenging environment while the basement area produced very low power signals with C/N_0 ranging as low as 17 dB-Hz.
The test was initialized and ended outside the house where the user stayed stationary for 60 seconds in both cases. After that, the test trajectory illustrated in Figure 3-19, including several loops on the main level of the house at the start, and then several loops in the basement area was followed. To be able to track the signals in such challenging environments, the GSNRx^{TM}-rr version implementing block processing techniques was used. In this case the reference antenna was placed on the roof of a shed outside the house while the rover antenna was continuously carried along the trajectory indoors as described above. Data were collected using two channels of the *NI PXI-5661* signal analyzer and processed in post-mission.

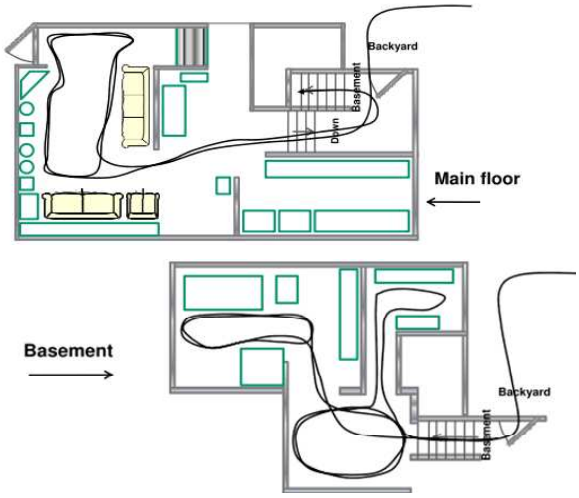

Figure 3-19: Schematic map of the building and test trajectory used for the pedestrian-based indoor data collection, (Satyanarayana et al 2010).

Figure 3-20 shows the results obtained using 100 ms integration time and a 0.2 Hz search step used to perform the search for the correlation peak in the frequency domain. The theoretical Doppler jitter was determined using Eq.(3.47), whereas the empirical data were processed according to Eq.(3.49). Also in this case a good match between empirical and predicted Doppler jitter is observed showing the validity of the proposed model for the block processing approach.

In this experiment the length of the moving average filter for the empirical estimation of the Doppler jitter, *K*, (Eq.(3.49)), has been limited to 200 ms in order to preserve possible effects in the Doppler measurements caused by the user gait. Long integrations would remove the effects of the user gait from the Doppler mean, leading to biased estimates of the Doppler jitter. Slower variations in the Doppler measurements during the section of the test trajectory indoors can be the result of the user motion along the trajectory. As it can be seen from Figure 3-19, on both the main floor and in the basement several minor loops

were made. Another possible reason for this type of behavior can be due to effects of Rayleigh fading.

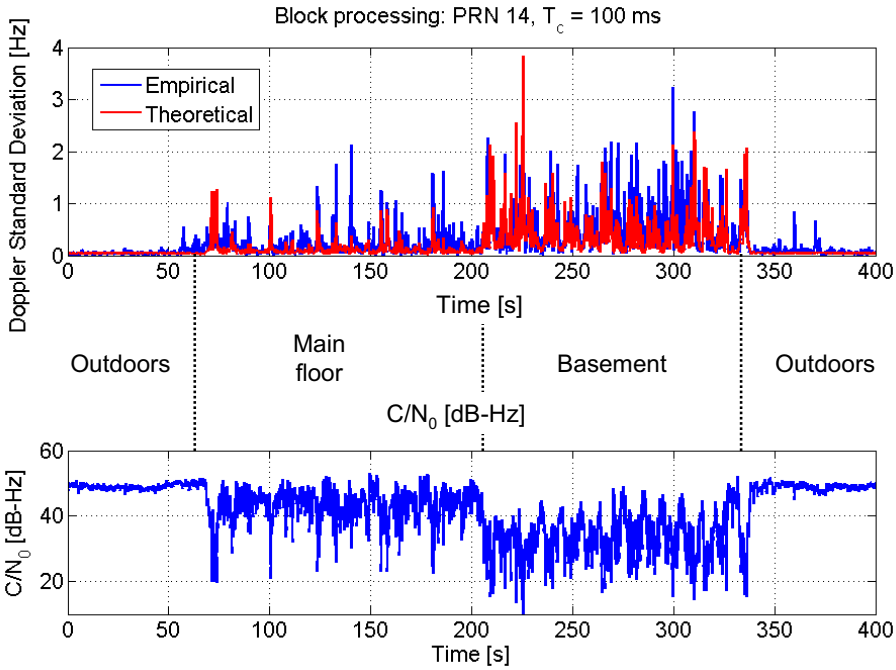

Figure 3-20: Doppler jitter analysis for a pedestrian-based test in an indoor environment. Doppler measurements were obtained using a block processing approach.

3.2.2 Doppler Bias Model Verification

This section gives a brief overview of the test methodology adopted for the Doppler bias analysis using the model given in Eq.(3.31) As defined previously, Doppler bias is a measure of the systematic error in Doppler estimates introduced by the transient response of the loop to changes in the input frequency.

To be able to determine the Doppler bias a reference solution is required. Therefore, a GPS hardware simulator, the GSS 7700 from Spirent capable of providing an accurate reference Doppler solution and generating various scenarios, was used. The adopted setup is shown in Figure 3-21. In the case of hardware simulations, there is no antenna, and the source (antenna) temperature is actually room temperature rather than antenna temperature. This means that the noise level in a simulated environment in general is higher than in the real case. To simulate the effect of an active antenna, a high gain must be applied at the first processing stage. Thus, in all tests discussed herein where a hardware simulator is used, a 30 dB LNA with a noise figure of 1.5 dB is applied to the output of the simulator.

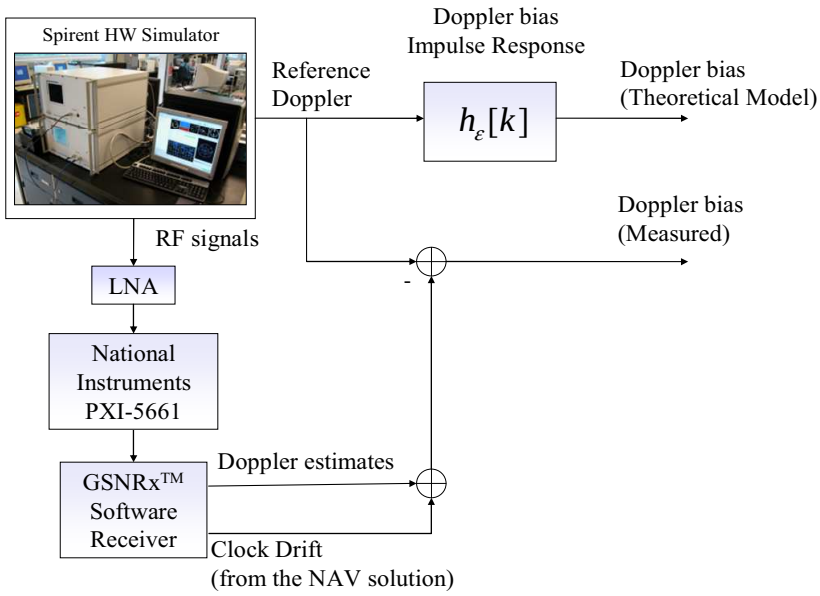

Figure 3-21: Experimental setup adopted for the evaluation of the Doppler bias.

As Figure 3-21 illustrates, the Spirent GSS 7700 hardware simulator was used for generating RF signals and reference Doppler values. The RF signals were collected using

the *NI PXI-5661* front-end and the collected data were processed by GSNRx^{TM} to estimate the Doppler and clock drift and evaluate the Doppler bias. Several experiments were performed simulating different trajectories and different levels of dynamics. Since findings were similar using each of these experimental data sets, only one scenario is considered in this section, namely a scenario simulating the dynamics of a road bound vehicle moving along the rectangular trajectory illustrated in Figure 3-22. For this test a maximum constant velocity of 17 m/s was simulated. In all, there were seven 90 degrees turns: each turn, starting from the second one, exhibiting increasing magnitudes of acceleration from 0.5 g to 3 g in 0.5 g increments per turn.

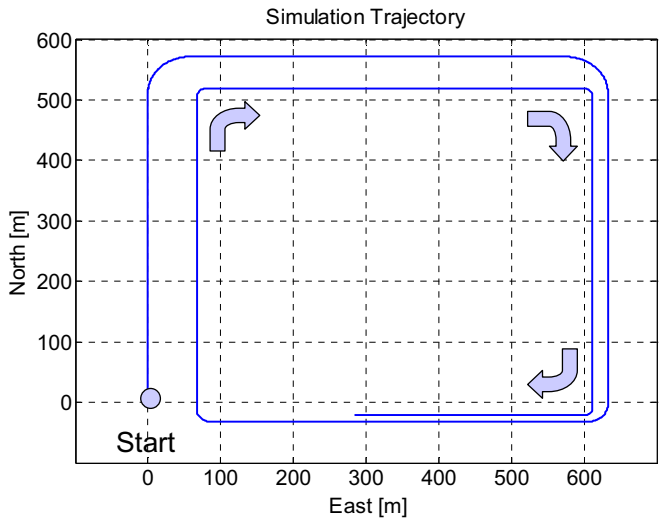

Figure 3-22: Simulated test trajectory.

In order to better observe the biases that could have been completely hidden by noise in the presence of strong attenuation, clear-sky conditions were simulated. In total, there were 10 satellites in view during the simulation, all with a relative channel power of 10 dB (-150 dBW).

At each turn of the trajectory the receiver experiences a sharp jerk at the start and end of the turn. Figure 3-23 shows the dynamics (acceleration and jerk) during a 1 g turn section of the simulation trajectory. For this 1 g turn, similarly as with the other consecutive turns, there are a sharp north and east jerk values at the start and end of the turn.

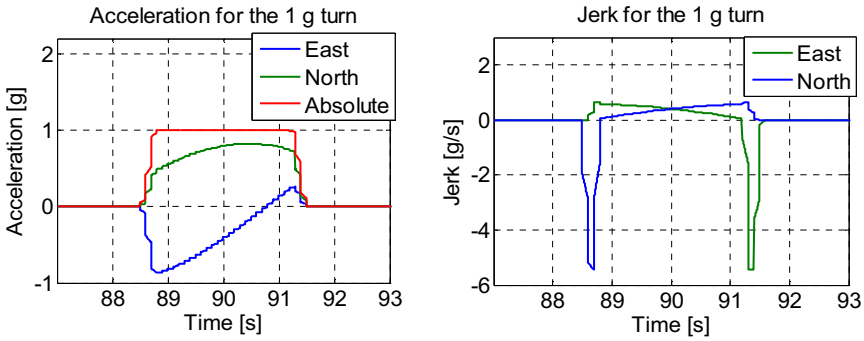

Figure 3-23: Acceleration and jerk experienced by the receiver during a 1 g turn.

The tracking loops of the receiver are not able to instantaneously follow the rapid Doppler variations thereby a bias is introduced at each turn. The Doppler bias was measured and compared against the theoretical Doppler bias obtained by filtering the true Doppler provided by the simulator with the bias impulse response given by Eq.(3.32). Both standard and memory discriminator based tracking loops were used for data processing using different values of tracking loop parameters.

It should be considered that the GSS 7700 hardware simulator is not able to generate a continuous reference Doppler which is approximated by a piece-wise linear function resulting in Doppler frequency values linearly changing over 100 ms intervals. Therefore, the generated reference Doppler looks like a sawtooth wave. This behaviour is directly transferred to the theoretical Doppler rate bias.

3.2.2.1 Standard Tracking Loops

The observed and theoretically predicted biases for a 2 g turn in the simulated trajectory obtained using a third order PLL are compared in Figure 3-24. To assure the receiver to maintain phase lock during high dynamic sections of the trajectory a 10 Hz loop bandwidth and 1 ms coherent integration time were used. The obtained raw Doppler measurements were smoothed with a MA filter with a 100 ms analysis window. For the determination of the theoretical bias values, the effect of the MA filter was accounted for in the theoretical model by setting the smoothing filter, $S(z)$, as defined in Eq.(2.13) in the signal frequency transfer function (Eq.(3.20)). As it can be seen from Figure 3-25 the proposed theoretical model effectively predicts the Doppler bias introduced by a third order PLL.

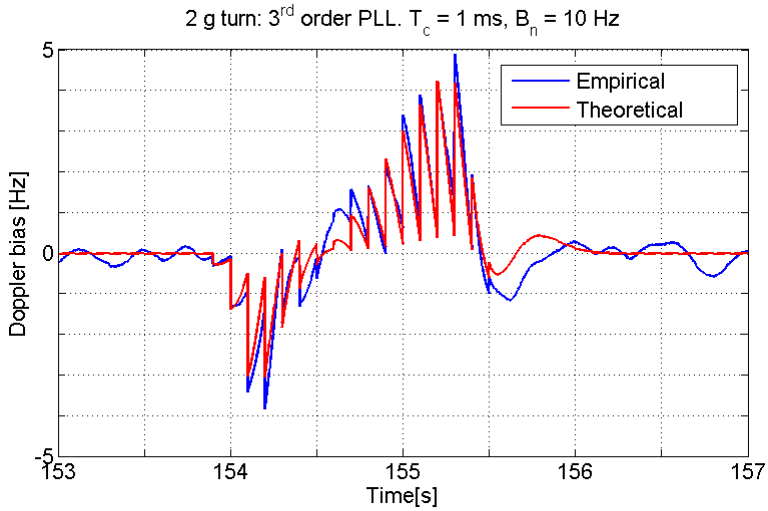

Figure 3-24: Observed and predicted Doppler bias of a 3rd order PLL, 2 g turn. The raw Doppler measurements were filtered using a MA filter with a 100 ms analysis window. (PRN 18).

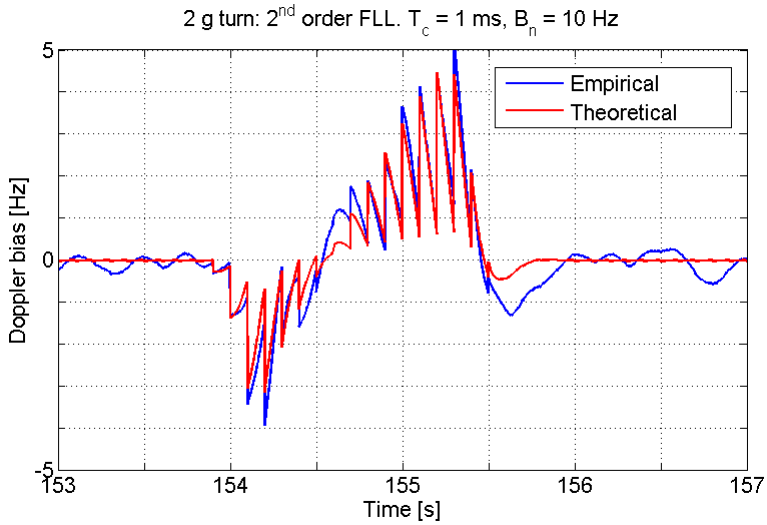

Figure 3-25: Observed and predicted Doppler bias of a 2nd order FLL, 2 g turn. The raw Doppler measurements were filtered using a MA filter with a 100 ms analysis window. (PRN 18).

The same dataset was used to test the FLL model. The software receiver was constrained to operate in the FLL mode and the theoretical Doppler bias was determined using Eq.(3.31). Also in this case the obtained raw Doppler measurements were smoothed with a MA filter with a 100 ms analysis window. A 10 Hz loop bandwidth and 1 ms coherent integration time were used. As shown in *Section 3.1.3*, the behaviour of an FLL, when considering the linear model approximation, is equivalent to the one of a PLL. This fact can be observed from the results presented in Figures 3-24 and 3-25 showing empirical and theoretically predicted biases for a 2 g turn for PLL and FLL. The two loops react in the same way to the same type of dynamics.

To test the model proposed for the evaluation of the Doppler bias in the case of the common-rate FLL-assisted-PLL, GSNRx™ was constrained to operate in the FLL-assisted-PLL mode and the theoretical Doppler bias was determined using Eq. (3.31), in this case accounting for the coupled loop structure by using the relation given in Eq.(3.38). Figure 3-

26 shows the observed and theoretically predicted biases for a 2.5 g turn in the simulated trajectory. Here as well the obtained raw Doppler measurements were smoothed with a MA filter with a 100 ms analysis window in order to reduce the noise in the measurements. 1 ms coherent integration time and loop bandwidth of 10 Hz in both the PLL and FLL branches were used.

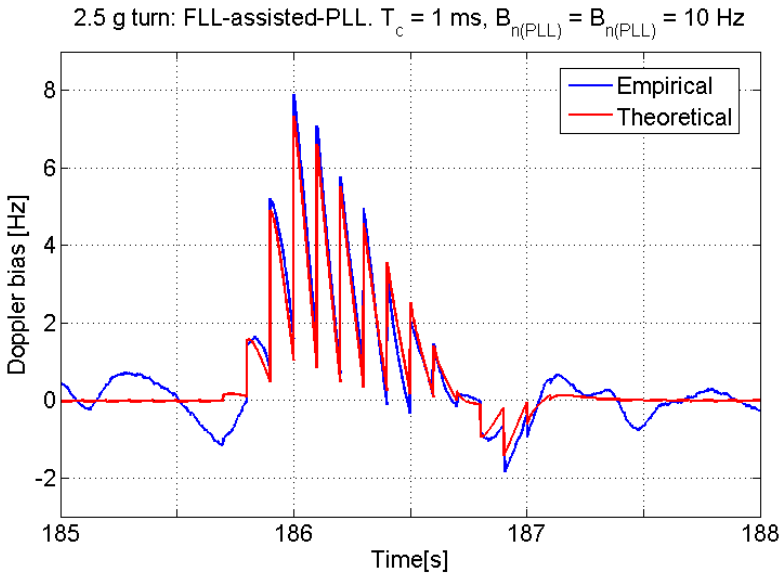

Figure 3-26: Observed and predicted Doppler bias of a common-rate FLL-assisted-PLL, 2.5 g turn. The raw Doppler measurements were filtered using a MA filter with a 100 ms analysis window. (PRN 29).

Results presented in this subsection indicate that the proposed theoretical model Eq. (3.31), is able to effectively predict the Doppler bias caused by changes in the input Doppler frequency. It has been shown that the developed model can also include the effect of the smoothing filter, $S(z)$. The model has been evaluated for different levels of dynamics, and in all cases a good agreement between the measured and predicted Doppler bias was

observed. More results on the models performance applied to a 3rd order PLL can be found in (Sokolova 2009).

3.2.2.2 Memory Discriminator Based Tracking Loops

As it has been discussed in **Chapter 2** and demonstrated previously by Borio et al (2009a) and Sokolova (2009), the memory discriminator based tracking loop architecture is capable to provide more accurate Doppler estimates by rejecting a larger quantity of noise with respect to the standard tracking loop architecture. Introduction of a low-pass filter prior to the memory-less phase/frequency discriminator reduces the amount of noise transferred to the discriminator, allowing it to stay in its linear region and the tracking loop to maintain lock. This, in its turn, allows the memory discriminator based architecture to bear higher dynamics without loosing phase lock when compared to the standard PLL architecture. This fact can be illustrated by the results obtained from this simulation. The same data set was processed using the standard and memory discriminator based tracking loop architectures. In both cases an 8 Hz loop bandwidth and 1 ms coherent integration time was used and the forgetting factor parameter, α, was set equal to 0.8 for the memory discriminator based architecture. Figure 3-27 illustrates the absolute acceleration and the tracking mode indicating which state the given receiver channel is operating at.

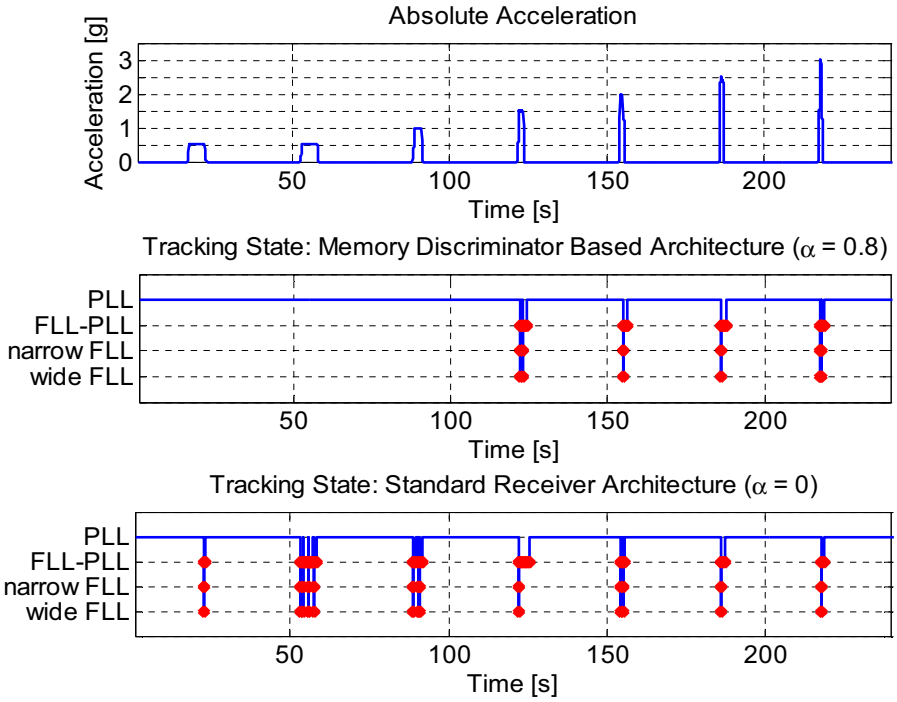

Figure 3-27: Absolute acceleration experienced by the receiver during the simulation and the tracking state of the standard and memory discriminator based receiver architectures. PRN 18, B_n = 8 Hz, T_c = 1 ms.

Table 3-6 lists the tracking modes specified for the GSNRx™ software (Petovello & O'Driscoll 2007) which are valid for both receiver architectures used in this thesis and the abbreviations that will be used herein for these modes. The tracking modes are regulated by the Phase and Frequency Lock Indicators (PLI/FLI) (van Dierendonck 1996) that determine the quality of the frequency and phase estimations.

Table 3-6: Abbreviations of tracking modes of the GSNRx^{TM} software receiver.

Abbreviation used herein	GSNRx^{TM} tracking mode
PLL	PLL
FLL-PLL	FLL-assisted-PLL
narrow FLL	Narrow pull-in FLL
wide FLL	wide pull-in FLL
Initializing	Initializing

While the standard receiver was losing phase lock and therefore transiting to the FLL-assisted-PLL and FLL modes during all the turns in the trajectory, the memory discriminator based receiver architecture was capable to maintain phase lock and remain in the PLL-only mode during the first 3 turns (from 0.5 g to 1 g). It should be noted though that for higher values of the loop bandwidth higher level of dynamics can be resisted by both standard and memory discriminator tracking loops architectures, but the same relative improved performance of the memory discriminator based architecture is observed. In this regard, it is important to consider that the major advantage of the memory discriminator based architecture is the noise rejection capability. Its increased resilience against thermal noise allows a memory discriminator based tracking loop to maintain lock under higher dynamics. Whereas the joint impact of noise and dynamics makes standard loop lose lock. This also means that the values of the Doppler bias measured by a standard and memory discriminator based tracking loop of the same order using equal values of the loop bandwidth and coherent integration time will be similar.

To give a better overview of how the developed model for Doppler bias analysis performs when applied to memory discriminator based tracking loops, analysis of the results for a 2.5 g turn for a 2nd order memory discriminator based FLL are presented. Figure 3-28 compares the measured and predicted Doppler bias values obtained using a 10 Hz loop bandwidth, 1

ms coherent integration time and $\alpha = 0.4$. Raw Doppler measurements were smoothed with a MA filter with a 100 ms analysis window.

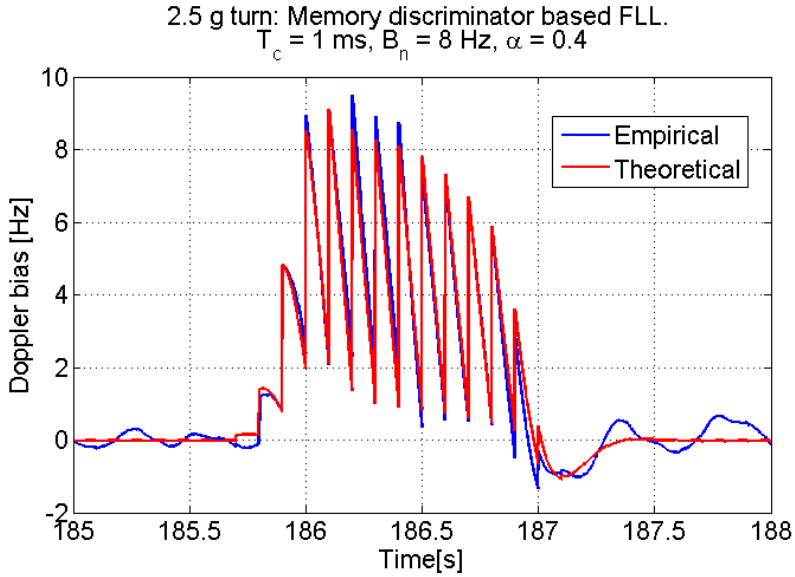

Figure 3-28: Observed and predicted Doppler bias for a 2nd order memory discriminator based FLL, 2.5 g turn, PRN 18. The raw Doppler measurements were filtered using a MA filter with a 100 ms analysis window.

The results presented in Figure 3-28 are consistent with the ones obtained for the case of the standard receiver architecture. A good match between empirical and predicted Doppler bias is found, showing the validity and applicability of the proposed theoretical framework for quantifying the effect of dynamics on the Doppler estimates for the memory discriminator based tracking loops.

CHAPTER 4: LOOP FILTER DESIGN BASED ON THE DOPPLER BANDWIDTH

This chapter presents a new approach to designing the loop filter based on the Doppler bandwidth. The proposed approach provides control over the noise variance of the Doppler frequency measurements. Both standard and memory discriminator based PLLs are considered.

In the first part of the chapter, a review of the general principle of the controlled-root formulation for the digital loop filter design is provided. First the standard approach, as proposed by Stephens & Thomas (1995) is described. Then the special case of memory discriminator based tracking loops is considered.

To be able to design the PLL loop filter based on the Doppler bandwidth, the original controlled-root formulation was modified. A discussion of the motivation behind this design and a detailed description of the algorithm for the design of the loop filter based on the Doppler bandwidth is given in the second part of the chapter. In order to apply the proposed design approach to the memory discriminator based PLL, similar modifications were applied to the controlled-root formulation extended to account for the additional pole introduced by exponential filtering.

In the last part of the chapter a short discussion on the choice of the Doppler bandwidth value to be used in the design is given and the effectiveness of the proposed approach is tested using live GPS L1 C/A data.

4.1 Controlled-root Formulation: General Principle

Most of the current approaches for the design of digital tracking loop filters are based on the transformation of a continuous-time system into the discrete-time domain. The filter is first designed in the analogue domain and its digital counterpart is then obtained by means of mapping functions, such as for example the bilinear or impulse invariant transforms. The necessary condition for the digital filter to be equivalent to its analogue counterpart is to

have the product between the loop noise bandwidth, B_n, and the integration time, T_c, (B_nT_c) be close to zero (Lindsey & Chie 1981, Stephens & Thomas 1995). In particular, it has been shown experimentally that the third order loop can remain stable for B_nT_c less than 0.55. As this product increases the loop roots are displaced with respect to the original position designed in the analogue domain. Also changes in the open loop gain can be observed and the actual loop noise bandwidth increases more rapidly than the desired bandwidth (Stephens & Thomas 1995). The error in the actual loop noise bandwidth becomes more prominent with increased B_nT_c, for example it exceeds 10% when B_nT_c>0.1 (Curran et al 2011).

In this way, the B_nT_c constraint required for having a stable loop significantly limits the maximum integration time and/or loop noise bandwidth. The controlled-root formulation (Stephens & Thomas 1995) is one of the approaches proposed in order to overcome these shortcomings.

According to the controlled-root formulation, the poles of the loop filter are constrained to lie on specific positions depending on design parameters, such as the decay-rate and the damping factor. In this way, the poles are positioned in order to ensure a stable loop and the design parameters are adjusted in order to meet the bandwidth requirements. More specifically, according to (Stephens & Thomas 1995), the system poles are parameterized as follows:

$$\begin{aligned}&\{z_1, z_2; z_3, z_4; z_5, z_6; \ldots\}\\ &\quad = \left\{e^{-\beta(1\pm\eta_1)T_c}; e^{-\beta\lambda_2(1\pm\eta_2)T_c}; e^{-\beta\lambda_3(1\pm\eta_3)T_c}; \ldots\right\}\end{aligned} \tag{4.1}$$

where $\{z_i\}_{i=1}^{L}$ are the poles of the transfer function of the loop, β is the control parameter that is adjusted to meet the bandwidth requirements and determines the decay rate of the loop impulse response, whereas $\{\lambda_i\}$ and $\{\eta_i\}$ are the $N-1$ constants determining the damping characteristics of the loop with $\lambda_1 = 1$. The choice of all $\lambda_i = 1$ and $\eta_i = 0$

corresponds to a super-critically damped response, whereas $\lambda_i = 1$ and $\eta_i = j = \sqrt{-1}$ to the standard underdamped response. In both cases the L poles are constrained to lie on a segment parallel to the imaginary axis, the distance to which from the Z-plane origin is controlled by β. This relationship is illustrated in Figure 4-1.

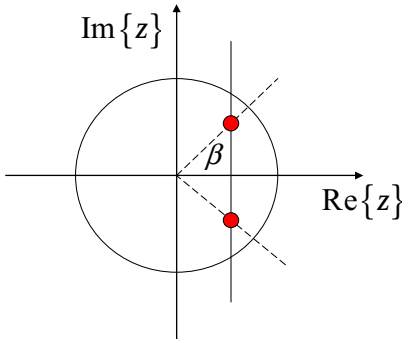

Figure 4-1: Root-locus diagram illustrating the relationship between the pole placement and the control parameter, β, (Borio & O'Driscoll 2008).

In this regard, it is important to consider that the controlled-root formulation allows constraining only L poles, corresponding to L free parameters – the integrator gains, whereas the position of the remaining poles is determined by the type of NCO (Stephens & Thomas 1995) and memory discriminator (Borio et al 2009a).

The procedure of determining the control parameter, β, is summarized in Figure 4-2, where the control parameter, β, is progressively adjusted in order to meet the bandwidth requirements and used for fixing the position of L poles.

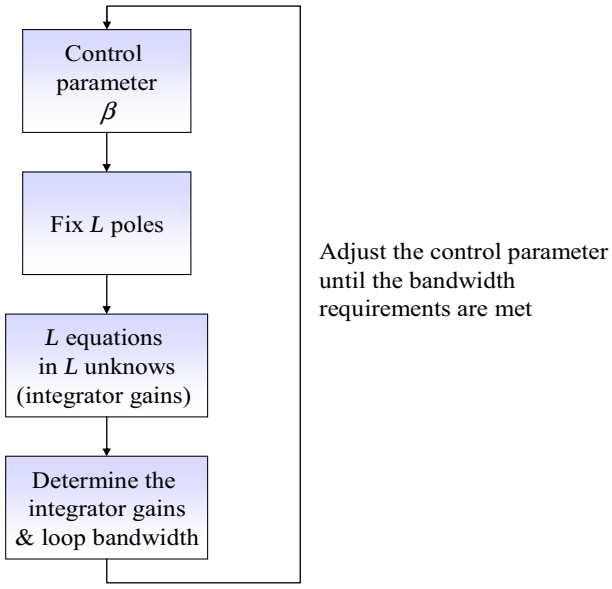

Figure 4-2: Iterative algorithm for determining the control parameter, β, used for loop filter design according to the controlled-root formulation (Borio et al 2009a).

As it can be seen from Figure 4-2, first L poles are fixed according to an initial value of the control parameter, β. The values of these L poles are then substituted into the expression of the loop transfer function, so that a system of L equations with L unknowns is defined. Recall the expression of the transfer function of the standard PLL derived in the previous chapter (Eq.(3.8)), which takes the following form after substituting the expression of the NCO transfer function (Eq.(3.24)):

$$H(z) = \frac{\frac{1}{2}(z+1)T_c B(z)}{z(z-1) + \frac{1}{2}(z+1)T_c B(z)}. \tag{4.2}$$

Each pole is converted into an equation of the type:

$$D(z_i) = z_i(z_i - 1) + \frac{1}{2}(z_i + 1)T_c B(z_i) = 0, \tag{4.3}$$

where $D(\cdot)$ is the denominator of the transfer function given in Eq.(4.2), z_i is the i^{th} pole of the system and the unknowns are the integrator gains in $B(z_i)$. Also, when multiple poles are present, the following condition for the derivative of $D(z)$ has to be verified

$$\left.\frac{d^h D(z)}{dz^h}\right|_{z=z_i} = 0 \qquad h = 1, \ldots, H-1, \tag{4.4}$$

where H is the order of the pole. Eqs. (4.3) and (4.4) form a linear system of L equations containing L unknowns. By solving this system of equations, the integrator gains $\{K_i\}_{i=0}^{L-1}$ can be determined, and finally, the loop noise bandwidth (Eq.(3.11)) can be evaluated. The control parameter, β, is then iteratively adjusted until the required bandwidth is obtained. Since the integrator gains are derived specifically for a given $B_n T_c$ value, this approach effectively solves the problem of deviation between the actual loop noise bandwidth and the desired design bandwidth. However, as it has been shown by Stephens & Thomas (1995), when using this method the $B_n T_c$ product should be kept lower than 0.4 for third order loops with rate-only feedback NCOs. Beyond this limit it is not possible to obtain stable loops.

4.1.1 Controlled-root Formulation: Memory Discriminator Based Carrier Tracking Loops

The general structure of memory discriminator based tracking loops adopting exponential filtering was described in **Chapter 2**. This section will provide a brief overview of the approach used for designing the loop filter in this type of tracking loops. Exponential filtering used in the memory discriminators introduces an additional pole into the system which has to be accounted for when designing the loop filter. In this case, it is impossible to use the direct transformation of the analog filters (Lindsey & Chie 1981). The controlled-

root formulation discussed in the previous section can be applied, but it allows one to fix the positions of only L poles, as only L free parameters are available. Thus, to be able to account for that additional pole, the controlled-root formulation has to be modified. Position of the L poles can be fixed as in the original approach, whereas the position of the remaining pole can be determined exploiting the constraints imposed by the structure of the loop transfer function, which is expressed as follows:

$$\begin{aligned} H(z) &= \frac{N(z)B(z)F(z)}{1+N(z)B(z)F(z)} = \\ &= \frac{\frac{1-\alpha}{2}(z+1)\sum_{i=0}^{L-1} K_i z^i (z-1)^{L-1-i}}{(z-1)^L(z-\alpha)+\frac{1-\alpha}{2}(z+1)\sum_{i=0}^{L-1} K_i z^i (z-1)^{L-1-i}} = \\ &= \frac{D_\alpha(z)-(z-1)^L(z-\alpha)}{D_\alpha(z)}. \end{aligned} \tag{4.5}$$

In Eq.(4.5)

$$D_\alpha(z) = (z-1)^L(z-\alpha)+\frac{1-\alpha}{2}(z+1)\sum_{i=0}^{L-1} K_i z^i (z-1)^{L-1-i} \tag{4.6}$$

is the denominator of $H(z)$ that determines the poles of the system, and the transfer functions $N(z)$, $B(z)$ and $F(z)$ are defined in Eqs. (3.24), (3.22) and (2.32), respectively. Having determined position of all poles, the integrator gains, $\{K_i\}_{i=0}^{L-1}$, can be computed and the loop noise bandwidth evaluated. Similarly to the original approach, the process is repeated until the loop noise bandwidth requirements are met by adjusting the control parameter, β. In the case of a third order PLL, the system is characterized by four poles, three of which are fixed according to the controlled-root formulation, whereas the position of the fourth pole essentially depends on the forgetting factor parameter, α. A

detailed discussion on the loop filter design in the case of exponential discriminators and the impact of the forgetting factor, α, on the stability of the loop is given in (Borio et al 2009a, Sokolova 2009). It has been shown that the loop becomes unstable for α greater than a threshold value α_T. Figure 4-3 shows the magnitude of the pole controlled by α as a function of the forgetting factor considering several bandwidths and coherent integration times of 20 and 10 ms. The pole magnitude increases almost linearly as a function of α until the threshold value, α_T, is reached. It is important to emphasize that the threshold is different for each combination of loop bandwidth and coherent integration time.

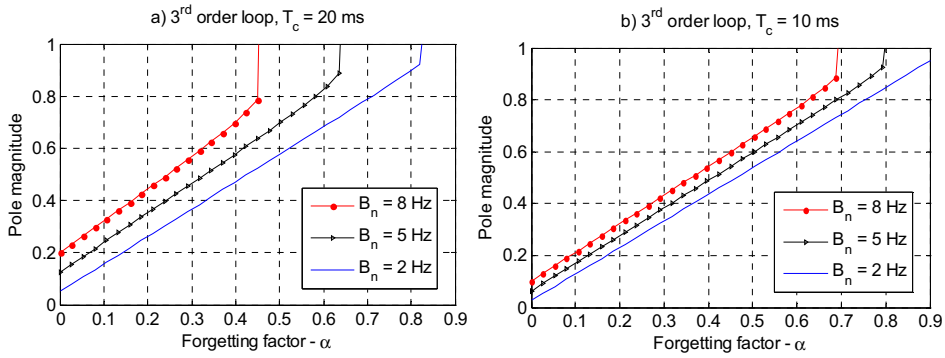

Figure 4-3: Pole magnitude as a function of the forgetting factor, α, and loop noise bandwidth B_n. a) T_c = 20 ms, b) T_c = 10 ms.

4.2 Loop Filter Design Based on the Doppler Bandwidth

4.2.1 Standard Carrier Tracking Loops

Compared to the approaches for digital filter design based on the transformation of a continuous-time system into a discrete-time one, the controlled-root formulation offers a higher flexibility. The introduction of the Doppler bandwidth (Eq. (3.27)) and the flexibility of the controlled-root formulation allows one to design the loop filter in a way which

provides control over the noise variance of the Doppler frequency measurements. As detailed in **Chapter 3**, the Doppler bandwidth, B_d, was derived as a counterpart of the loop noise bandwidth, B_n, to quantify the amount of noise transferred from the input frequency noise to the final Doppler frequency estimate, considering the overall frequency linear model of the tracking loop (Figure 3-2). Together with the coherent integration time, T_c, and C/N_0, the Doppler bandwidth is used to determine the Doppler jitter (Eq.(3.29)). Designing the loop filter based on Doppler bandwidth instead of loop noise bandwidth, as it is done in the controlled-root formulation discussed above, allows one to configure the tracking loop to output Doppler measurements with a desired level of Doppler jitter. To be more specific, recall the expression of the Doppler jitter given in Eq.(3.28). As it follows from this expression, if the values of the Doppler jitter, σ_f, and C/N_0 are specified, the corresponding value of the Doppler bandwidth can be determined. If the loop filter is designed based on this value of the Doppler bandwidth, the tracking loop would be capable of producing Doppler frequency measurements with the specified Doppler jitter at a specified level of C/N_0. A practical example using GPS L1 C/A signals will be considered later in this chapter to clarify the algorithm and verify the proposed approach. To be able to design the loop filter based on Doppler bandwidth, it is necessary to modify the original controlled-root formulation. As shown in Figure 4-4, the adopted algorithm is similar to the original formulation but the control parameter is adjusted in order to obtain a desired Doppler bandwidth.

Following the original approach, first, poles are fixed according to an initial value of β. The values of these L poles are substituted into the expression of the loop transfer function, each pole of which can be converted into an equation of the type defined in Eq.(4.3), so that a system of L equations containing L unknowns is obtained. This system of equations is then solved for the integrator gains, $\{K_i\}_{i=0}^{L-1}$. This allows one to determine the frequency noise transfer function, which in the case of a PLL, is given by Eq.(3.20) and evaluate the Doppler bandwidth, B_d, (Eq.(3.27)).

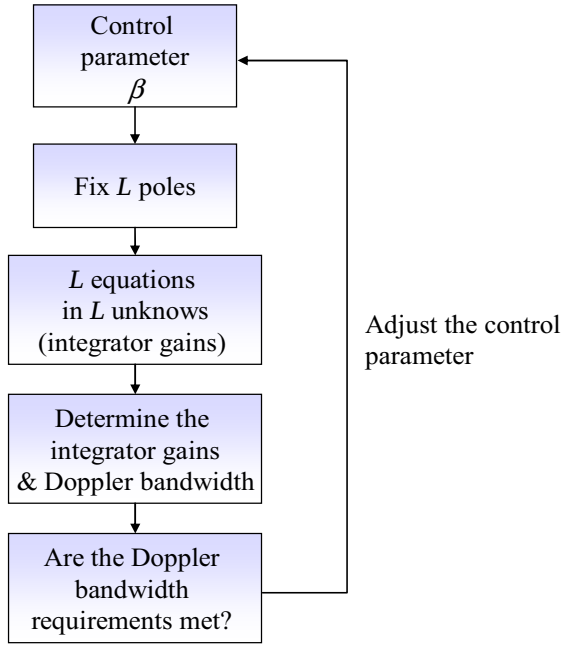

Figure 4-4: Iterative algorithm used for loop filter design based on Doppler bandwidth.

Similar to the original formulation, the control parameter, β, is iteratively adjusted until the required Doppler bandwidth is obtained. It is important to emphasize that similarly to the original formulation, in this case as well the stability of the tracking loop is limited by the product of the coherent integration time and the Doppler bandwidth, B_d. By studying the root location of the system it has been found that the maximum achievable value of $B_d T_c$ providing a stable loop is 0.27. As it has been shown in the previous chapter, B_d differs from the loop noise bandwidth and further investigation is required to characterise the exact relationship between these two parameters. However, in the design algorithm illustrated in Figure 4-4, when the required value of the Doppler bandwidth is finally achieved, the corresponding loop noise bandwidth, B_n, can also be computed by using the final values of

the integrator gains $\{K_i\}_{i=0}^{L-1}$ to determine the loop transfer function defined in Eq.(4.2), and then numerically integrating Eq.(3.12). Figure 4-5 illustrates the relationship between the Doppler bandwidth and corresponding loop noise bandwidth for a standard 3rd order PLL considering 10 and 20 ms coherent integration times.

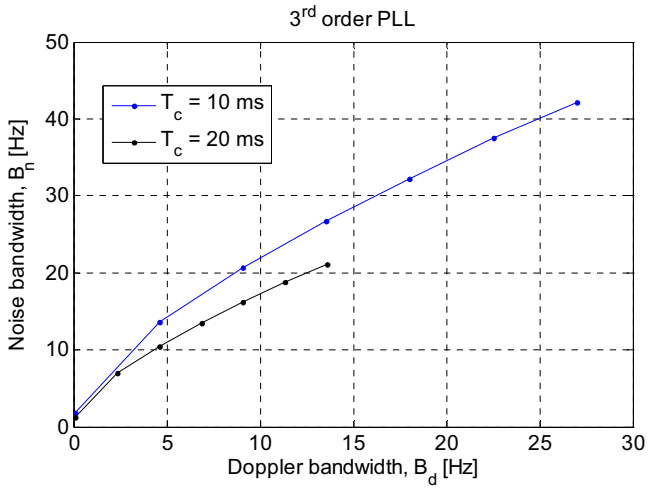

Figure 4-5: Doppler bandwidth as a function of the loop noise bandwidth for a third order PLL designed based on Doppler bandwidth parameter. T_c = 20 and 10 ms.

4.2.2 Memory Discriminator Based Carrier Tracking Loops

A similar design algorithm can be applied to memory discriminator based tracking loops. But, as it has been explained previously, due to the use of exponential filtering in the memory discriminator, an additional pole is introduced into the system. The procedure shown in Figure 4-4 can be modified in the same way as described in *Section 4.1.1*, where the original controlled-root formulation was altered to account for the effect of an additional pole. In particular, after initializing the control parameter, first the position of the L poles can be fixed, whereas the position of the remaining pole can be determined

according to the constraints imposed by the structure of the loop transfer function defined in Eq.(4.5). Then the same procedure as described in the previous section can be followed.

Figure 4-6 shows the root position as a function of α for a 3rd order memory discriminator based PLL designed based on the Doppler bandwidth, considering the case of 0.3 Hz Doppler bandwidth and 20 ms coherent integration time. It also highlights the relationship between Doppler bandwidth and the loop noise bandwidth. In *Section 4.1.1* it has been shown that the magnitude of the pole controlled by the forgetting factor, α, increases as a function of α until a certain threshold value, α_T, is reached. This is also valid in the case of the loops designed based on the Doppler bandwidth. In particular, Figure 4-3 shows that for the case of a 5 Hz loop noise bandwidth and 20 ms coherent integration time, this threshold value is about 0.6.

As it can be observed from Figure 4-6, this threshold is reached when the Doppler bandwidth is equal to 0.3 Hz, and the corresponding loop noise bandwidth is equal to 5.2 Hz. Also in this case, the loop noise bandwidth was evaluated by performing numerical integration of Eq.(3.12), where the loop transfer function (Eq.(4.2)) was determined by using the final values of the integrator gains $\{K_i\}_{i=0}^{L-1}$ computed in the design procedure. As the value of the forgetting factor, α, increases, the pole controlled by α is progressively pushed outside the unit circle resulting in an unstable system. It is possible to use higher values of Doppler bandwidth for designing the loop, by either choosing a smaller value of α, or shorter coherent integration time.

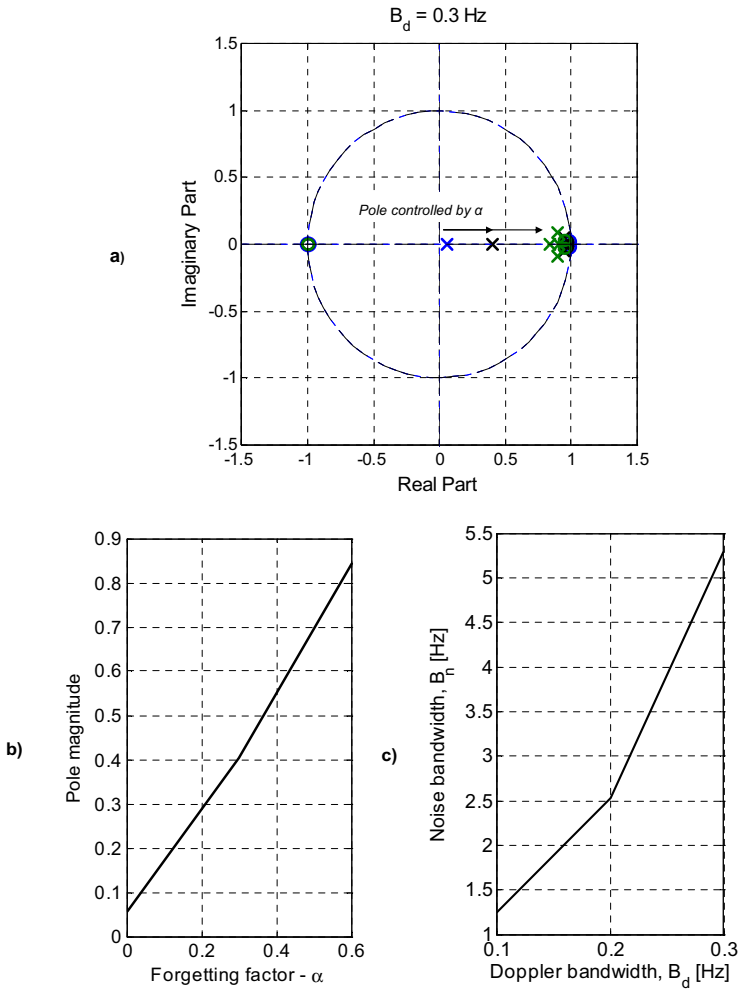

Figure 4-6: a) Zero/pole placement as a function of the forgetting factor, α. Third order loop designed based on B_d = 0.3 Hz using 20 ms coherent integration time. b) Pole magnitude as a function of the forgetting factor, α. c) Doppler bandwidth as a function of loop noise bandwidth.

4.3 Practical Verification of the Design

The fact that the Doppler bandwidth, B_d, is used as a design parameter in the proposed approach makes it possible to specify a threshold value of the Doppler jitter to be expected at a given level of C/N_0 – for example, the tracking sensitivity limit. By substituting the desired threshold value of the Doppler jitter and the specified value of C/N_0 into the theoretical model of the Doppler jitter defined in Eq.(3.29), the corresponding value of the Doppler bandwidth can be determined and used for design of the loop filter. This allows one to design the tracking loop in such a way that the jitter of the obtained Doppler frequency measurements will stay under the desired Doppler jitter until the specified level of C/N_0 is reached. Alternatively, one can simply select the value of B_d to be used for loop filter design. Then, by using this value in the theoretical model of the Doppler jitter (Eq.(3.29)), an accurate prediction of the expected Doppler jitter as a function of C/N_0 can be obtained.

An important consideration in this approach is the choice of the Doppler bandwidth value. Typically, one would choose the lowest possible Doppler jitter when designing the loop, however one must select a Doppler bandwidth which is commensurate with the expected value of user dynamics. If a very narrow Doppler bandwidth is selected, the receiver might simply lose lock due to the experienced user-satellite motion.

The reasoning behind the choice of this parameter is the same as in the case of choosing the loop noise bandwidth in traditional tracking loops. As it has been mentioned previously, the Doppler bandwidth has been derived as a related design parameter to the loop noise bandwidth. The major difference between these two parameters is that Doppler bandwidth provides a more faithful interpretation of the bandwidth required to track particular system dynamics. Thus, assuming that the change in Doppler frequency due to the motion of the satellite is negligible (Tsui 2005), the following relationship

$$\delta f_d = a \cdot \frac{f_r}{c}, \tag{4.7}$$

where δf_d is the Doppler rate, a is the user acceleration, f_r is the GPS L1 centre frequency and c is the speed of light, can be used to determine the corresponding change in the Doppler frequency. In Eq.(4.7) it has been assumed that the user is accelerating along the direction parallel to the user-to-satellite unit vector. This assumption corresponds to the worst case scenario, where the Doppler frequency change is maximum. The computed change in the Doppler frequency will provide approximate information about the value of the Doppler bandwidth to be used for designing the tracking loop. Consider a simple example of a standard road bound vehicle capable of accelerating from 0 to 100 km/h in 10 seconds $\left(a = 2.8\, m/s^2\right)$. The corresponding change in the Doppler frequency in this case is 14.6 Hz, meaning that the value of the Doppler bandwidth to be used should be at least 14.6 Hz or higher.

In addition to this, as it has been mentioned in the previous chapter, in the case of pedestrian motion higher frequency components are introduced by the users' gait. These frequency components also depend on the type of users' motion - running or walking. In order to determine the appropriate Doppler bandwidth to track this type of dynamics, these components also have to be included. In this regard, it is also noted that in theory, one can use the spectral content of the Doppler observations to determine the Doppler bandwidth, but in practice this does not yield any easily usable information. Also, since the use of the inertial sensors co-located with GNSS receivers is becoming more and more common in consumer devices such as for example smart-phones and Personal Digital Assistants (PDA) it is, as well, worth considering the use of the inertial sensor data for on-line determination of the Doppler bandwidth.

To assess the effectiveness of the proposed approach for loop filter design, data collected in the attenuated LOS test was used. A detailed description of the equipment setup used in this data collection and the methodology adopted to process the data, as well as to determine empirical Doppler jitter values is given *Section 3.2.1.1*.

As the data in this test were collected in stationary mode, a fairly low (0.5 Hz) Doppler jitter threshold at C/N_0 equal to 25 dB-Hz was selected. Substituting the specified Doppler

jitter threshold and C/N_0 values into the theoretical model of the Doppler jitter (Eq.(3.29)), the corresponding value of Doppler bandwidth is found to be equal to 1.3 Hz. The loop filter of a standard PLL was then designed based on the obtained value of B_d using the approach proposed in *Section 4.2.1* and following the procedure detailed in Figure 4-4. In this particular case, a 20 ms coherent integration time was used. The attenuated LOS data set was then processed using the PLL designed based on the specified parameters.

Figure 4-7 compares the expected Doppler jitter values determined using the specified parameters in the theoretical model (Eq.(3.29)) with the Doppler jitter computed using the empirical data. The empirical data were processed according to the procedure detailed in Figure 3-9 and Eq.(3.49). As it can be seen from Figure 4-7, the empirical data closely follow the expected Doppler jitter values and the specified Doppler jitter threshold is not exceeded confirming the validity of the proposed design algorithm.

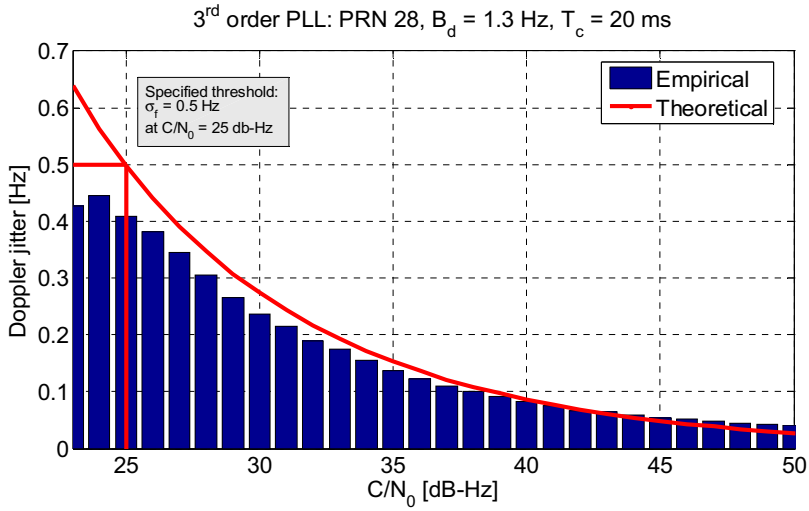

Figure 4-7: Empirical and theoretical jitter of the raw Doppler measurements as a function of C/N_0, obtained using a standard 3rd order PLL designed based on the Doppler bandwidth.

To demonstrate the validity of the proposed design algorithm developed for the case of the memory discriminator based PLL, an $\alpha = 0.2$ was considered. Because of the higher noise rejection capability of this type of tracking loop a lower Doppler jitter threshold of 0.3 Hz at C/N_0 equal to 25 dB-Hz was selected. Using the same theoretical model of Doppler jitter (Eq.(3.29)), and substituting the specified values of σ_f and C/N_0, the corresponding Doppler bandwidth was found to be equal to 0.5 Hz. The loop filter was then designed based on $B_d = 0.5$ Hz using the approach described in *Section 4.2.2.* In this case as well a 20 ms coherent integration time was used. Figure 4-8 shows the results obtained by processing the attenuated LOS data set with the memory discriminator based PLL designed using the specified parameters.

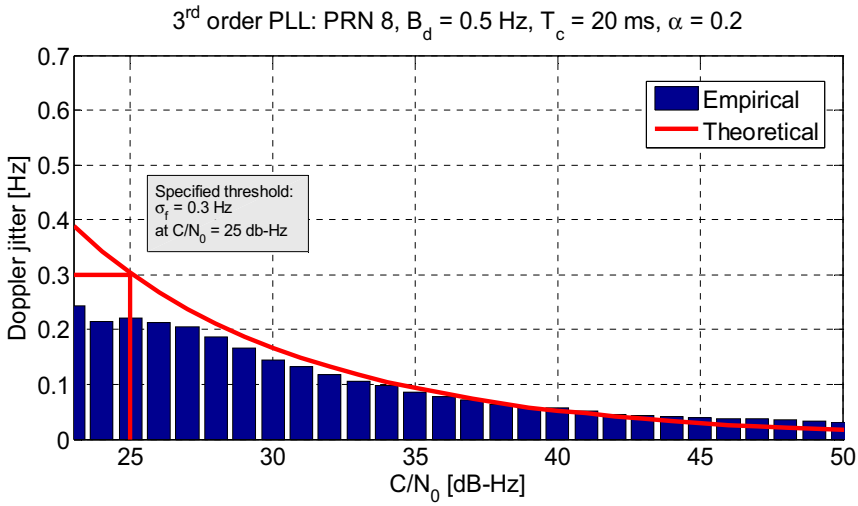

Figure 4-8: Empirical and theoretical jitter of the raw Doppler measurements as a function of C/N_0, obtained using a 3rd order memory discriminator based PLL designed based on the Doppler bandwidth.

The empirical data were processed as defined in Eq.(3.49) and compared to the expected Doppler jitter values determined by using the theoretical model (Eq.(3.29)).

As it can be seen from Figure 4-8, also in this case a good agreement between the expected and empirical Doppler jitter is observed and the specified Doppler jitter threshold is not exceeded.

Results shown in Figures 4-7 and 4-8 confirm the validity of the proposed design algorithm as applied to standard and memory discriminator based PLLs, and also the fact that by designing the loop filter based on the Doppler bandwidth, a loop capable to provide the Doppler measurements with the desired level of jitter is obtained. Finally, it is important to consider that the beneficial feature of this approach is not in the capability of the tracking loop to provide more accurate Doppler measurements, but in the capability to provide control over the noise variance of the measurements.

CHAPTER 5: THEORETICAL FRAMEWORK FOR DOPPLER FREQUENCY RATE ESTIMATION: SEQUENTIAL AND BLOCK PROCESSING ARCHITECTURES

In this chapter the analytic approaches used in **Chapter 3** with respect to the process of Doppler estimation are extended and applied to the process of Doppler rate estimation. Both sequential carrier tracking, including the standard and memory discriminator based approaches, and block processing techniques are considered. In a similar way, a theoretical framework for Doppler rate estimation relating the variance and biases of the Doppler rate estimates to the C/N_0, user dynamics and algorithm parameters is introduced for each of the mentioned approaches. In the case of sequential carrier tracking, the standard tracking loop linear theory is now reformulated with respect to the signal Doppler frequency rate, the frequency rate noise and the final Doppler rate measurement provided by the loop. For the block processing approach, an expression of the variance of the Doppler rate estimates is derived based on the CRLB for the Doppler frequency measurements (Eq.(3.47)).
The proposed theoretical framework for Doppler rate estimation analysis is validated in the second half of this chapter using simulated and actual GPS L1 C/A signals. Test methodology and equipment setup used for the performed experiments are described, and the results obtained using the proposed theoretical models for the Doppler variance and bias are compared against empirical data.

5.1 Doppler Rate: Theoretical Analysis

5.1.1 Doppler Rate Estimation in GNSS

Consider the analytic representation of the signal at the input of the processing block given in Eq.(3.1)

$$r[n] = A\exp\{j2\pi f_{IF} nT_s\}\exp\{j\varphi[n]\} + \tilde{w}[n]. \quad (5.1)$$

In Eq.(5.1), the navigation message $d(\cdot)$ is assumed to be constant over the observation time used by the receiver to generate a correlator output. Since the intermediate frequency, f_{IF}, is known to the receiver, only the time varying phase, $\varphi[n]$, has to be estimated. This phase can be approximated using a polynomial expansion

$$\varphi[n] = \varphi_0 + f_d nT_s + \frac{1}{2}\dot{f}_d n^2 T_s^2, \quad (5.2)$$

where φ_0 is a constant phase term, f_d is the Doppler frequency in rad/s and $\dot{f}_d$ is Doppler frequency rate in rad/s^2. The estimation of the coefficients, φ_0, f_d and $\dot{f}_d$ in Eq.(5.2) corresponds to the problem of estimation of the parameters of a chirp signal, i.e., a signal with a polynomial phase of second order (Abatzoglou 1986, Djurić & Kay 1990, Peleg & Porat 1991). This problem has been extensively studied with respect to various applications other than GNSS based navigation, such as, for example, radar technology. In particular, the CRLB for the variances of the estimated parameters of complex signals with polynomial phase has been derived by Peleg & Porat (1991), whereas algorithms attaining these bounds have been proposed by Abatzoglou (1986).

In GNSS, Doppler rate measurements are obtained by considering several measurement epochs. During each measurement epoch, N samples of the input signal (Eq.(5.1)) are used to produce a new frequency estimate, $\hat{f}$, which is then used to update previous Doppler rate measurements. The basic assumption made in GNSS receivers is that the impact of Doppler rate is negligible over a single measurement epoch, $\dot{f}\,NT_s = \dot{f}\,T_c \ll \frac{1}{T_c}$, meaning that the maximum change in the signal Doppler frequency is small compared to the inverse of the integration time $T_c = NT_s$. For this reason, the different techniques implemented in GNSS receivers, such as PLL and block processing, simply neglect Doppler rate during a

single processing epoch. As mentioned in the previous chapter, the rate of change of the Doppler frequency caused by the satellite motion is very low (Tsui 2005) and for this reason has a negligible effect. Therefore, the dominant factor contributing to the change of the Doppler frequency is the acceleration of the receiver. Consider a simple example of pedestrian motion. Levels of dynamics typical to this type of motion are low, with the average walking speed of 1.35 m/s. Sudden turns or stops can be expected to induce accelerations of the order of 1.4 m/s^2 (Fugger 2000). By substituting this value, $a = 1.4 \quad m/s^2$, into Eq.(4.7), the corresponding change in the Doppler frequency for $T_c = 20\ ms$, the longest coherent integration time achievable with no external assistance, is equal to only 0.15 Hz. In Eq.(4.7), it has been assumed that the user is accelerating along the direction parallel to the user-to-satellite unit vector. This example supports the assumptions adopted by a GNSS receiver for computing Doppler rate measurements.

Doppler rate is then estimated, as detailed in **Chapter 2**, by differentiating Doppler measurements over multiple epochs. This assumption corresponds to approximating the time varying Doppler frequency of a GNSS signal by a staircase function as illustrated in Figure 5-1.

This assumption leads to suboptimal algorithms for the estimation of Doppler rate and, consequently, to estimator variances greater than the CRLB provided in (Djurić & Kay 1990, Peleg & Porat 1991):

$$\sigma^2_{\dot{f},CRLB} = \frac{720}{2C/N_0 T_s^5 M(M^2-1)(M^2-4)} \approx \frac{360}{C/N_0 k^5 T_c^5}. \tag{5.3}$$

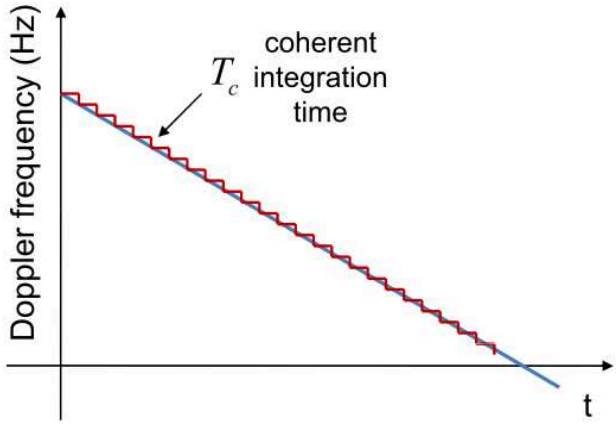

Figure 5-1: In GNSS receivers, the Doppler frequency is assumed constant during each processing epoch, i.e., the impact of Doppler rate is neglected during the integration time $T_c = NT_s$.

In Eq.(5.3), M is the total number of samples used for estimating the Doppler rate, $\dot{f}$, and $M = kN$ is a multiple of the number of samples used during a single processing epoch. This means that if Doppler rate is estimated by differentiating two consecutive Doppler frequency measurements, $M = 2N$ and

$$\sigma^2_{\dot{f},CRLB} = \frac{11.25}{C/N_0 T_c^5} = \frac{1}{T_c^4}\frac{11.25/T_c}{C/N_0}. \tag{5.4}$$

In regard to Eq.(5.1), the expression given in Eq.(5.3) refers to the case where time index is assumed to be $n = 0,1,\ldots,M-1$. More specifically, it is possible to show that the Doppler rate variance also depends on the time interval used for obtaining the measurements (Djurić & Kay 1990). If the time instants at which the correlator outputs are chosen are symmetric with respect to zero, a better operability is achieved. The zero instant refers to the time at which the Doppler rate is estimated. Due to the real-time nature of GPS, only a causal interval, $n = 0,1,\ldots,M-1$, can be used. Appendix A will provide more details on the derivation of Eqs. (5.3) and (5.4).

In the following sections, Eq.(5.4) will be used as a comparison term for the algorithms used in GNSS receivers.

5.1.2 Doppler Rate Variance and Bias Analysis: Sequential Carrier Tracking Loops

5.1.2.1 PLL

In a standard PLL, the input signal, $r[n]$, is at first correlated with a local carrier replica which is generated on the basis of a previous estimate of the signal Doppler frequency. As detailed above, the local carrier does not include any Doppler rate terms since the input signal frequency is assumed constant over the integration time, T_c. Each correlation is computed over *N* samples and the correlator output is then used to compute an estimate of the average phase error between incoming and local signals. This phase estimate is obtained using a phase discriminator. The phase error is filtered and a new estimate of the Doppler frequency, $f_{raw}[k]$, is obtained. Raw Doppler measurements are then used to drive the NCO for the local carrier generation. Finally, as discussed in **Chapter 2,** Doppler rate observables are obtained by differentiating the Doppler measurements, $\hat{f}[k]$.

To be able to evaluate the quality of Doppler rate measurements, the same approach based on the linear tracking loop theory described in **Chapter 3** can also be used here. The PLL linear analysis can be further extended to characterize the noise propagation process from the input signal to the final Doppler rate estimate. Figure 5-2 illustrates the PLL model as a frequency rate filter also detailing the process of Doppler rate derivation in a PLL.

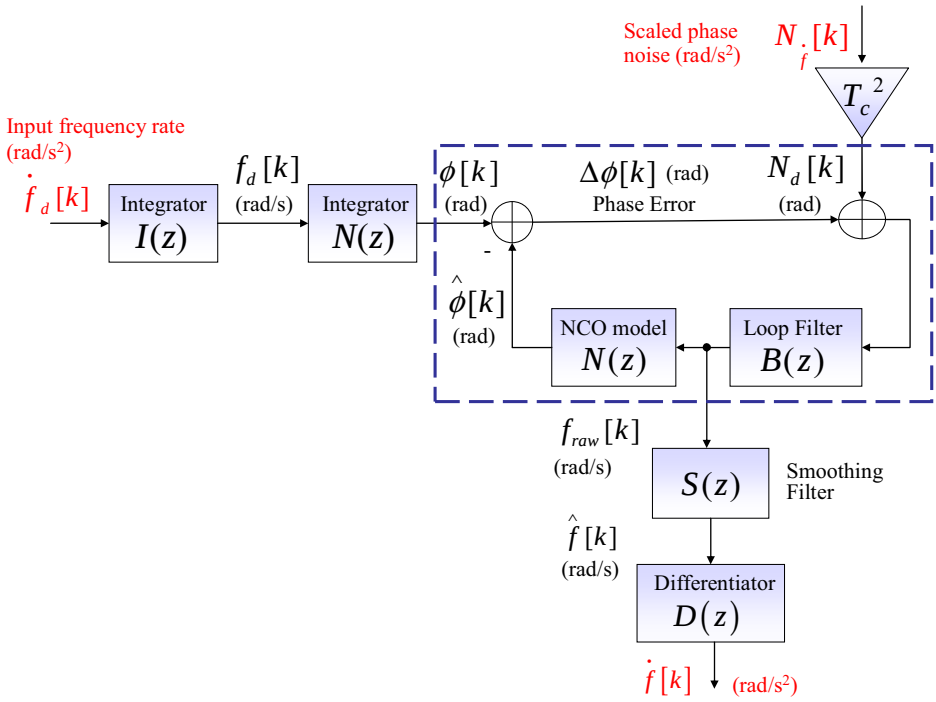

Figure 5-2: PLL as a frequency rate filter. The final Doppler rate estimates are formed as a combination of filtered input signal frequency rate and noise.

With respect to the linear model of the PLL as a frequency filter derived in **Chapter 3** (Figure 3-2), the following modifications have been introduced:

- the true input frequency rate, $\dot{f}_d[k]$, has been explicitly modeled by introducing an additional integrator , $I(z)=\frac{T_c}{1-z^{-1}}$, so that the phase, $\phi[k]$, is obtained by performing double integration of $\dot{f}_d[k]$;

- a scaled phase noise, $N_{\dot{f}}[k]$, has been introduced by normalizing $N_d[k]$ by T_c^2, the coherent integration time squared. This normalization was required in order to have all quantities at the inputs and output of the PLL model in units of radians per second squared;
- a first order differentiator, $D(z)$, is used to model the derivation of the Doppler rate measurements.

As illustrated in Figure 5-2, in a PLL, the final Doppler rate estimate is obtained as:

$$\dot{\hat{f}}[k] = d[k] * \hat{f}[k] = d[k] * s[k] * f_{raw}[k], \tag{5.5}$$

where $d[k] = Z^{-1}\{D(z)\}$ is the impulse response of the differentiator used for obtaining Doppler rate measurements, characterised by the following transfer function:

$$D(z) = \frac{1}{T_c}\left[1 - z^{-1}\right]. \tag{5.6}$$

Although different types of differentiators can be used to derive the Doppler rate measurements, for simplicity reasons, only the case of the first order differentiator (Eq.(5.6)) will be considered in this thesis.

$s[k]$ in Eq.(5.5) is the impulse response of the smoothing filter added to incorporate both raw and carrier phase derived Doppler measurements. This smoothing filter is defined by the transfer function, $S(z)$, given in Eqs. (2.13) and (3.17). Exactly as in the previous chapters, in the simplest case when raw Doppler measurements are used directly, $S(z) = 1$, whereas for carrier phase derived Doppler measurements, $S(z) = I(z)\Delta(z)$, where $I(z)$ and $\Delta(z)$ are the transfer functions of an integrator and a differentiator defined by Eqs. (2.11) and (2.12)

Considering the model introduced in Figure 5-2, and following the same procedure that was used in the case of the Doppler measurements in **Chapter 3**, it is possible to show that the final Doppler rate estimate, $\dot{f}[k]$, is also obtained as a linear combination of filtered input signal frequency rate and noise:

$$\dot{f}[k] = h_{\dot{f}_d}[k] * \dot{f}_d[k] + h_{n\dot{f}}[k] * N_{\dot{f}}[k], \tag{5.7}$$

where $h_{\dot{f}_d}[k]$ and $h_{n\dot{f}}[k]$ are the frequency rate and frequency rate noise impulse responses. In the Z-domain, Eq.(5.7) can be written as:

$$\dot{f}(z) = \underbrace{\frac{S(z)B(z)N(z)}{1+B(z)N(z)}}_{H_{\dot{f}_d}(z)} \cdot \dot{f}_d(z) + \underbrace{\frac{T_c^2 D(z)S(z)B(z)}{1+B(z)N(z)}}_{H_{n\dot{f}}(z)} \cdot N_{\dot{f}}(z), \tag{5.8}$$

where $H_{\dot{f}_d}(z)$ and $H_{n\dot{f}}(z)$ represent the transfer functions that characterise the signal frequency rate and noise impulse responses and are derived from the model given in Figure 5-2. In Eq.(5.8), $B(z)$ and $N(z)$ are the loop filter and NCO model transfer functions respectively. The variance of Doppler rate estimates is then obtained as

$$\sigma_{\dot{f}}^2 = Var\left\{\dot{f}[k]\right\} = T_c \int_{-0.5/T_c}^{0.5/T_c} \left| H_{n\dot{f}}\left(e^{j2\pi fT_c}\right)\right|^2 df \, Var\left\{N_{\dot{f}}[k]\right\}. \tag{5.9}$$

In Eq.(5.9), it has been assumed that the term $\left(h_{\dot{f}_d}[k] * \dot{f}_d[k]\right)$ in Eq.(5.7) is deterministic and therefore does not contribute to the variance of the final Doppler rate estimates. It can however introduce a bias in $\dot{f}[k]$ as discussed in the second part of this section. In a similar way as in the case of Doppler frequency and phase measurements discussed in **Chapter 3**, it is possible to define a single parameter, the **Doppler rate bandwidth** that

determines the amount of noise transferred from the phase discriminator output to the final Doppler rate estimates. The Doppler rate bandwidth is defined as follows:

$$B_{\dot{f}} = \frac{1}{2}\int_{-0.5/T_c}^{0.5/T_c} \left| H_{n\dot{f}}\left(e^{j2\pi f T_c}\right)\right|^2 df \qquad [Hz]. \tag{5.10}$$

Aside from characterising the ability of the tracking loop to produce accurate Doppler rate estimates, the Doppler rate bandwidth parameter also accounts for the impact of different differentiators/filters $\left(D(z)S(z)\right)$ used for producing the final Doppler rate measurements.

Since the frequency rate noise, $N_{\dot{f}}[k]$, at the input of the extended PLL linear model is a normalized version of the input phase noise, $N_{\dot{f}}[k] = \frac{N_d[k]}{T_c^2}$, $N_{\dot{f}}[k]$ is a zero mean white sequence with variance

$$\begin{aligned} Var\left\{N_{\dot{f}}[k]\right\} &= \frac{1}{T_c^4} Var\left\{N_d[k]\right\} \\ &= \frac{1}{T_c^4}\frac{1}{2T_c C/N_0}\left(1+\frac{1}{2T_c C/N_0}\right) \qquad \left[\left(\frac{rad^2}{s^2}\right)\right]. \end{aligned} \tag{5.11}$$

In this way, the variance of Doppler rate measurements in a standard PLL becomes

$$\sigma_{\dot{f}}^2 = \frac{1}{T_c^4}\frac{B_{\dot{f}}}{C/N_0}\left(1+\frac{1}{2T_c C/N_0}\right) \qquad \left[\frac{rad^2}{s^4}\right]. \tag{5.12}$$

Using the previous result, the Doppler rate jitter for a standard PLL assumes the following expression:

$$\sigma_{\dot{f}} = \frac{1}{T_c^2}\sqrt{\frac{B_{\dot{f}}}{C/N_0}\left(1+\frac{1}{2T_c C/N_0}\right)} \qquad \left[\frac{rad}{s^2}\right]. \tag{5.13}$$

Eq.(5.13) has a similar functional form as the expression given in Eq.(5.4) when the term $\left(1+\frac{1}{2T_c C/N_0}\right)$ is neglected. However it not possible to compare directly the performance of a sequential tracking loop with the CRLB. In sequential tracking loops, computation of a single Doppler/Doppler rate estimate is based on evaluation of a number of samples, *M*.. This is due to the presence of a reaction block and a filter that in sequential tracking loops introduce memory in the system, i.e., past information is retained for the computation of a single Doppler/Doppler rate estimate. This makes *M* difficult to determine.

Doppler Rate Bias Analysis

Similarly to the case of the Doppler measurements, due to the transient response of the tracking loop to rapid changes in the input signal frequency rate and latencies caused by the smoothing filter, $S(z)$, a bias is introduced in the Doppler rate estimates. The same analysis approach, as introduced in **Chapter 3**, can also be used here, thus, systemic errors in the Doppler rate measurements can be defined as

$$\varepsilon_{\dot{f}} = E\left[\dot{f}_d[k] - \dot{\hat{f}}[k]\right]. \tag{5.14}$$

Then, using the relationship introduced in Eq.(5.7), and considering the fact that $N_{\dot{f}}[k]$ is also zero mean, the systemic error, Eq.(5.14) can be formulated as follows:

$$\varepsilon_{\dot{f}}[k] = \dot{f}_d[k] - h_{\dot{f}_d}[k] * \dot{f}_d[k] = \left(\delta[k] - h_{\dot{f}_d}[k]\right) * \dot{f}_d[k] = h_{\varepsilon_{\dot{f}}}[k] * \dot{f}_d[k], \tag{5.15}$$

where

$$h_{\varepsilon_{\dot{f}}}[k] = \delta[k] - h_{\dot{f}_d}[k] \tag{5.16}$$

is the bias impulse response, and $\delta[k]$ is the Kronecker delta. As defined in the previous section, $\dot{f}_d[k]$ and $h_{\dot{f}_d}[k]$ denote the input signal frequency rate and the loop frequency rate impulse response, respectively. The model defined in Eq.(5.15) allows one to quantify the bias introduced by the loop due to the variations in the input Doppler rate. However, it should be noted that as in the case of the bias in the Doppler estimates, a reference for Doppler rate measurements is required to be able to perform an experimental comparative analysis.

5.1.2.2 FLL

The adopted analysis can then be applied to the FLL. As it has been discussed in detail in **Chapter 3**, an FLL operates in a similar way as the PLL. In an FLL, the frequency discriminator implicitly performs a phase differentiation using two subsequent correlator outputs $\left(P[k] \text{ and } P[k-1]\right)$, as shown in Figure 3-3. Thus, the output of the loop filter is a raw estimate of the Doppler rate, $\dot{f}_{raw}[k]$. The additional integrator is used to obtain a new estimate of the Doppler frequency used by the NCO to generate the local carrier. As the raw Doppler rate estimate, $\dot{f}_{raw}[k]$, is very noisy, the use of a smoothing filter is desirable, so that the final Doppler rate estimate is obtained as

$$\dot{f}[k] = s[k] * \dot{f}_{raw}[k], \tag{5.17}$$

where $s[k]$ is the impulse response of a smoothing filter with transfer function $S(z)$, (Eq.(2.13)). In **Chapter 3** it was shown that PLL and FLL are characterized by the same linear model with respect to the Doppler frequency, and that the advantage of the FLL is due to the phase unwrapping implicitly implemented when a frequency discriminator followed by an integrator are used. By replacing the frequency discriminator by a phase

discriminator followed by the differentiator, $\Delta_f(z)$, (Eq.(3.37)) and using the same approach for the derivation of the linear tracking loop model as in the case of the PLL analysis discussed above, it can be shown that a similar result holds for the Doppler rate. However, in the case of the FLL, the final Doppler rate estimate is given as:

$$\dot{f}(z) = \underbrace{\frac{S(z)B(z)N(z)}{1+B(z)N(z)}}_{H_{\dot{f}_d}(z)} \cdot \dot{f}_d(z) + \underbrace{\frac{T_c^2 \Delta_f(z) S(z) B(z)}{1+B(z)N(z)}}_{H_{n\dot{f}}(z)} \cdot N_{\dot{f}}(z), \tag{5.18}$$

where $\Delta_f(z) = \frac{1}{T_c}\left[1 - z^{-1}\right]$ is a first order differentiator which, as explained in the previous chapter, is fully determined by the frequency discriminator. This implies that although the general expression of the final frequency rate estimate provided by the PLL and FLL is the same, performance of these two tracking loops with respect to Doppler rate estimation is equivalent only in the case when a first order differentiator $\left(D(z) = \frac{1}{T_c}\left[1 - z^{-1}\right]\right)$ is used in the PLL for the computation of the Doppler rate observables.

The Doppler rate variance, jitter and bias of the measurements obtained from the FLL can then be determined by applying the expressions of the signal frequency rate and noise transfer functions, $H_{\dot{f}_d}(z)$ and $H_{n\dot{f}}(z)$ (Eq.(5.18)), to the models defined in Eqs. (5.11), (5.13) and (5.15).

5.1.2.3 FLL-assisted-PLL

The procedure used for derivation of the approximated linear loop model of a common-rate FLL-assisted-PLL was discussed in detail in the previous chapter in regard to Doppler estimation. It has been shown that the effect of coupling the PLL and FLL loops in a single

structure can be modeled by using a loop filter with the transfer function, $B_{eq}(z)$, given by the sum of the FLL and PLL loop filter transfer functions, (Eq.(3.38)). In an FLL-assisted-PLL the Doppler rate observations are obtained in the same way as shown in Eq.(5.5), namely by time differentiating the Doppler measurements. Thus, considering the relationship given in Eq.(3.38), and using the same approach as described above, it can be shown that the final Doppler rate estimate produced by a common-rate FLL-assisted-PLL is given by a linear combination of filtered input signal frequency rate and noise, and thus can be expressed as:

$$\dot{f}(z) = \underbrace{\frac{S(z)B_{eq}(z)N(z)}{1+B_{eq}(z)N(z)}}_{H_{\dot{f}_d}(z)} \cdot \dot{f}_d(z) + \underbrace{\frac{T_c^2 D(z)S(z)B_{eq}(z)}{1+B_{eq}(z)N(z)}}_{H_{n\dot{f}}(z)} \cdot N_{\dot{f}}(z), \tag{5.19}$$

where $H_{\dot{f}_d}(z)$ and $H_{n\dot{f}}(z)$ represent the signal frequency rate and noise transfer functions for this type of a tracking loop. Due to the generality of the theoretical models for the Doppler rate variance, jitter and bias analysis, Eqs. (5.11), (5.13) and (5.15) can also be applied to the common-rate FLL-assisted-PLL tracking loop. First, using the expression of the frequency rate noise transfer function, $H_{n\dot{f}}(z)$, the Doppler rate bandwidth can be determined as defined in Eq.(5.10). This allows one to determine the Doppler rate variance and jitter. The Doppler bias can be evaluated by analysing the signal frequency rate transfer function, $H_{\dot{f}_d}(z)$, as shown in Eq.(5.15).

5.1.2.4 Memory Discriminator Based Tracking Loops

Because of the similarity in the basic structure of the standard and memory discriminator based carrier tracking loops, the approach used to determine the variance and bias of

Doppler rate measurements obtained from the standard tracking loops can be easily applied to the memory discriminator based tracking loops. As discussed in the previous chapter, in the case of the memory discriminator based tracking loops (PLL, FLL and FLL-assisted-PLL) it is necessary to account for the presence of an additional low-pass filtering stage, which in this thesis has been chosen to be represented by an exponential filter. Thus, following the approach used in **Chapter 3**, a memory discriminator can be approximated by a linear filter (Eq.(2.32)) which can be adapted into the linear models of the standard tracking loops. Moreover, determination of Doppler rate measurements in the memory discriminator based tracking loops is performed in the same way as it is done in the standard tracking loops. Thus, in the case of the memory discriminator based PLL the signal frequency rate and noise transfer functions are given by:

$$H_{\dot{f}_d}(z) = \frac{S(z)F(z)B(z)N(z)}{1+B(z)N(z)}, \tag{5.20}$$

$$H_{n\dot{f}}(z) = \frac{T_c^2 D(z)S(z)F(z)B(z)}{1+F(z)B(z)N(z)}. \tag{5.21}$$

The same approach as suggested for the standard FLL can be applied in the case of the memory discriminator based FLL. Thus, when $D(z) = \Delta_f(z) = \frac{1}{T_c}\left[1 - z^{-1}\right]$, Eq.(5.21) can be directly applied to characterise the frequency rate noise transfer function of the memory discriminator based FLL. Otherwise, the transfer function of the differentiator, $D(z)$, in Eq.(5.21) can be simply replaced by $\Delta_f(z)$.

Eqs. (5.20) and (5.21) also apply to the common-rate FLL-assisted-PLL where the loop filter transfer function, $B(z)$, is replaced by $B_{eq}(z)$ (Eq.(3.38)) and can be used for evaluation of the Doppler variance, jitter and bias as defined in Eqs. (5.11), (5.13) and (5.15), respectively.

5.1.3 Block Processing Architecture

In *Section 3.1.2*, it has been shown that, under the assumption of negligible Doppler rate, the variance of the Doppler measurements produced by block processing approach approximately follows the CRLB (Eq.(3.47)). Considering this, and accounting for the effect of the differentiator used for computing Doppler rate measurements it is possible to derive an expression for the variance of the Doppler rate and define the concept of Doppler rate bandwidth for block processing architectures.

In the block processing approach the frequency measurements, $f_{raw}[k]$ (Figure 2-7), form a white sequence since each frequency estimate is obtained using a different block of disjoint input samples, $r[n]$. As explained in **Chapter 2**, in the block processing approach, Doppler rate measurements are obtained by applying a differentiator, $D(z)$, on the estimated Doppler frequencies. Exploiting the fact that, in this case, $f_{raw}[k]$ is a white sequence, it is possible to express the power spectral density of the Doppler rate measurements as

$$P_{\dot{f}}(f) = \frac{1}{T_c^2}\sigma_{CRLB}^2 \left|\widetilde{D}\left(\exp\{j2\pi f T_c\}\right)\right|^2, \tag{5.22}$$

where

$$\widetilde{D}(z) = T_c D(z), \tag{5.23}$$

which is a normalized version of $D(z)$. This normalization has been performed in order to better highlight the different quantities in Eq.(5.22), and also in the following equations. To be more specific, $\widetilde{D}(z)$ is unitless. The variance of the Doppler rate measurements can then be expressed as follows:

$$\sigma_{\dot{f}}^2 = Var\left\{\dot{f}[k]\right\} = \frac{1}{T_c^2}\sigma_{CRLB}^2\left[T_c\int_{-0.5/T_c}^{0.5/T_c}\left|\widetilde{D}\left(e^{j2\pi fT_c}\right)\right|^2 df\right] =$$
$$= \frac{1}{T_c^2}\sigma_{CRLB}^2\left[\int_{-0.5}^{0.5}\left|\widetilde{D}\left(e^{j2\pi\phi}\right)\right|^2 d\phi\right] \qquad \left[\frac{rad^2}{s^4}\right]. \tag{5.24}$$

In Eq.(5.24) the integral in the last line is a unitless quantity and the variance of $\dot{f}[k]$ is thus expressed in $\left[\frac{rad^2}{s^4}\right]$. As it has been mentioned previously, only the case of a first order differentiator used for computation of the Doppler rate measurements will be considered in this thesis. In this case, $\widetilde{D}(z) = 1 - z^{-1}$, and

$$\int_{-0.5}^{0.5}\left|\widetilde{D}\left(e^{j2\pi\phi}\right)\right|^2 d\phi = 2. \tag{5.25}$$

By substituting the expression for the for the standard deviation of frequency estimates obtained using block processing techniques, σ_{CRLB}, given in Eq.(3.47) into Eq.(5.24), the following expression for the standard deviation of Doppler rate estimates can be found:

$$\sigma_{\dot{f}} = \frac{1}{T_c^2}\sqrt{\frac{\frac{6}{T_c}\left[\int_{-0.5}^{0.5}\left|\widetilde{D}\left(e^{j2\pi\phi}\right)\right|^2 d\phi\right]}{C/N_0}} = \frac{1}{T_c^2}\sqrt{\frac{B_{\dot{f}}}{C/N_0}} \qquad \left[\frac{rad}{s^2}\right], \tag{5.26}$$

where the part

$$B_{\dot{f}} = \frac{6}{T_c}\left[\int_{-0.5}^{0.5}\left|\widetilde{D}\left(e^{j2\pi\phi}\right)\right|^2 d\phi\right] \qquad [Hz] \tag{5.27}$$

defines the Doppler rate bandwidth parameter for the block processing approach. For the specific case of $D(z)$ being a first order differentiator, Eq.(5.27) assumes the following form:

$$B_{\dot{f}} = \frac{12}{T_c}. \tag{5.28}$$

In this way the variance of Doppler rate estimates can be formulated as follows:

$$\sigma^2_{\dot{f}} = \frac{1}{T_c^4}\frac{12/T_c}{C/N_0} \qquad \left[\frac{rad^2}{s^4}\right]. \tag{5.29}$$

Eq.(5.29) has the same functional form as Eq.(5.4) providing the CRLB of the Doppler rate estimates.

By comparing Eqs. (5.4) and (5.29), it can be concluded that block processing algorithms are not able to reach the CRLB showing that this technique is suboptimal with respect to other methods (Abatzoglou 1986) that attain this lower bound. The increase in variance is however small and is justified by a reduced computational load with respect to the algorithm described in (Abatzoglou 1986).

5.2 Practical Verification

The theoretical expressions of the Doppler rate jitter (Eqs. (5.13) and (5.29)) and bias (Eq.(5.15)) have been validated through the use of data simulated by means of a hardware GPS simulator in addition to using actual GPS L1 signals. Several static and dynamic pedestrian-based field tests in various GPS operating environments have been conducted, some of these experiments have been described in **Chapter 3**, where they were used for the evaluation of the theoretical model for the Doppler frequency estimation analysis. Also in this case, the tests presented in this section represent only sample results and several additional experiments have been performed with similar findings.

5.2.1 Doppler Rate Jitter Model Verification

The validity of the proposed theoretical models of Doppler rate jitter is verified by comparing the Doppler rate jitter values predicted using the expressions defined in Eqs. (5.13) and (5.29) with the measurements of the actual Doppler rate jitter. The empirical Doppler jitter has been determined by first calculating the mean of the Doppler rate measurements provided by the GSNRx^{TM} receiver using a moving average (MA) filter. The mean was then subtracted from the measurements which were further squared and filtered. In this way, the final estimate of the empirical Doppler rate jitter can be expressed as follows:

$$\hat{\sigma}_{\dot{f}}[n] = \sqrt{\frac{1}{K-1}\sum_{k=0}^{K-1}\left[\dot{f}[k-n] - \frac{1}{K}\sum_{k=0}^{K-1}\dot{f}[k-n]\right]^2}, \tag{5.30}$$

where K represents the length of the MA filter analysis window.

5.2.1.1 Attenuated Line-Of-Sight (LOS) Test

In this experiment, the LOS RF data were recorded using a stationary rooftop-mounted antenna. The equipment setup and procedure used to perform this data collection are described in detail in *Section 3.2.1.1* (in particular, Figure 3-8 and Table 3-1). The signals were acquired, providing Doppler frequency rate and C/N_0 estimates. Thus, using the C/N_0 values estimated by the receiver and knowing the length of the integration period, T_c, it was possible to determine the empirical Doppler rate jitter as a function of the input C/N_0.

Attenuated LOS: Sequential Carrier Tracking – PLL

Figure 5-3 shows the jitter of Doppler rate measurements obtained by time differentiating raw Doppler observables using a 200 ms period compared to the ones determined by performing double time differentiation of the carrier phase measurements. In this particular case a Savitsky-Golay type of smoothing filter/differentiator (Savitzky & Golay 1964) with a 10 ms analysis window was used to generate the carrier phase derived Doppler measurements. The obtained carrier phase derived Doppler measurements were further differentiated using a 200 ms period in order to get the Doppler rate estimates.

In both cases, 1 ms coherent integration time and 8 Hz loop bandwidth were used. Empirical Doppler rate jitter values were determined as defined in Eq.(5.30), whereas the theoretical Doppler rate jitter was calculated using Eq.(5.13), where in the case of Doppler rate measurements derived from carrier phase observations the effect of the smoothing filter $S(z)$ was included through the use of $S(z) = I(z)\Delta(z)$.

As it can be observed in Figure 5-3, Doppler rate jitter results predicted using the theoretical model (Eq.(5.13)) are in good agreement with the measurements of the actual Doppler rate jitter, showing the ability of the proposed theoretical model to predict the quality of Doppler rate measurements determined from the raw Doppler measurements as well as the ones obtained from the carrier phase observations.

In order to evaluate the accuracy of the measurements, such factors as the loop bandwidth and coherent integration time, as well as the approach used to determine the Doppler rate (whether the measurements are derived by differentiating the filtered raw Doppler or by performing double differentiation of the carrier phase measurements) have to be considered. Also the size of the analysis window of the filters used in the process of derivation of the Doppler rate has to be taken into account.

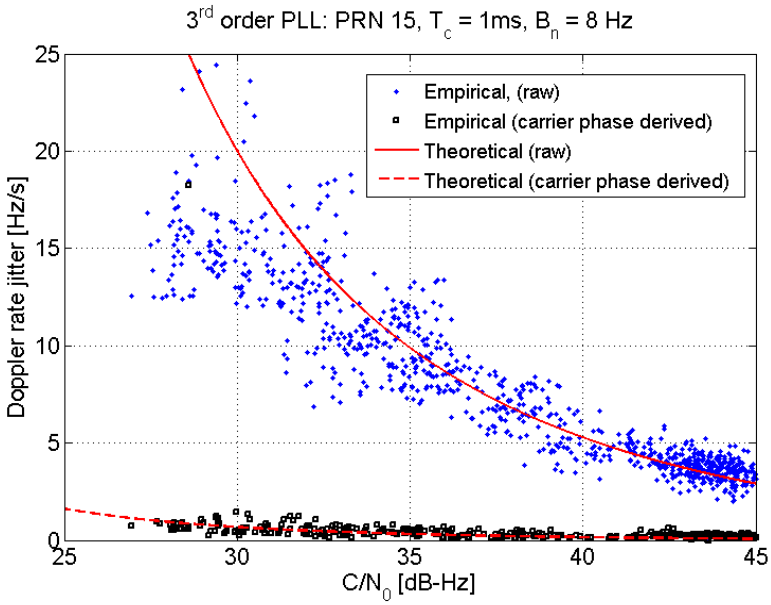

Figure 5-3: Empirical and theoretical jitter of Doppler rate estimates as a function of C/N_0. Doppler rate estimates obtained by differentiating raw Doppler measurements from a standard PLL and by performing a double differentiation of the carrier phase measurements. Differentiation is performed using a 200 ms period.

However, the main focus of this thesis is the development and verification of the theoretical model for Doppler rate analysis, while no effort has been made to achieve the best accuracy of the empirical results. Therefore, it is noted that by appropriate filtering a better measurement accuracy can be achieved in all the considered cases.

Attenuated LOS: Sequential Carrier Tracking – FLL

For testing of the proposed model in the case of the FLL, GSNRx™ was constrained to operate in FLL-only mode. Figure 5-4 shows the jitter of the Doppler rate measurements obtained directly from the output of the FLL loop filter and subsequently filtered using a

Moving Average filter with a 200 ms analysis window. A fixed coherent integration time of 1 ms was used by the FLL and different loop bandwidths were tested. The empirical Doppler rate jitter was determined as defined in Eq. (5.30) and compared to the results predicted using the theoretical model given in Eq.(5.13). A good agreement between the theoretical and empirical results can be observed from the plots presented in Figure 5-4, confirming the applicability of the model given in Eq.(5.13) to the FLL.

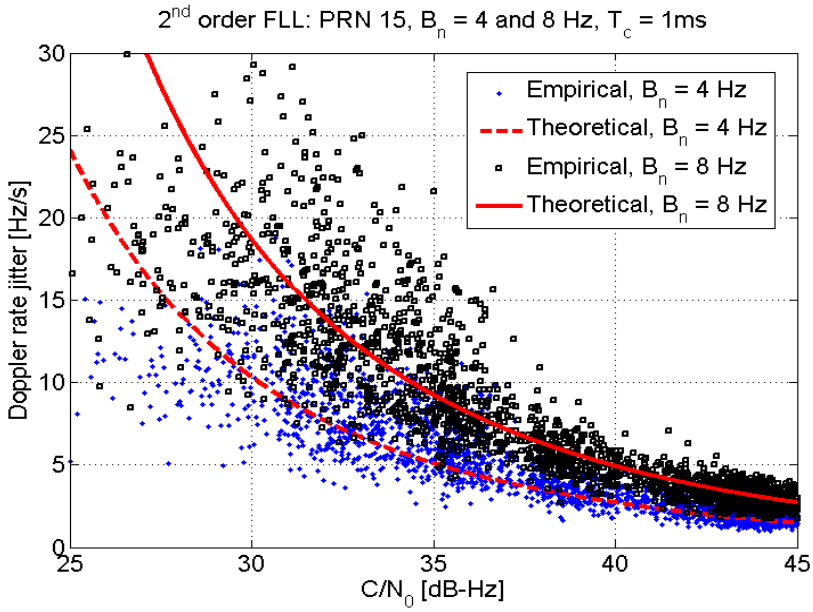

Figure 5-4: Empirical and theoretical jitter of the Doppler rate estimates as a function of C/N$_0$ and loop noise bandwidth B_n. Doppler rate estimates were obtained directly from the output of the FLL loop filter and subsequently filtered using a MA filter with a 200 ms analysis window.

Attenuated LOS: Sequential Carrier Tracking – FLL-assisted-PLL

The effectiveness of the theoretical model for the analysis of the Doppler rate jitter of the measurements provided by a standard common-rate FLL-assisted-PLL has been tested using the data obtained by processing the data set collected in this experiment in the FLL-assisted-PLL mode only. Here as well, the empirical data were processed as described in Eq. (5.30), whereas the theoretical Doppler rate jitter values were determined by using the relationship defined in Eq.(3.38) to account for the effect of coupling the PLL and FLL loops in a single structure, and applying it to the theoretical model given in Eq.(5.13).

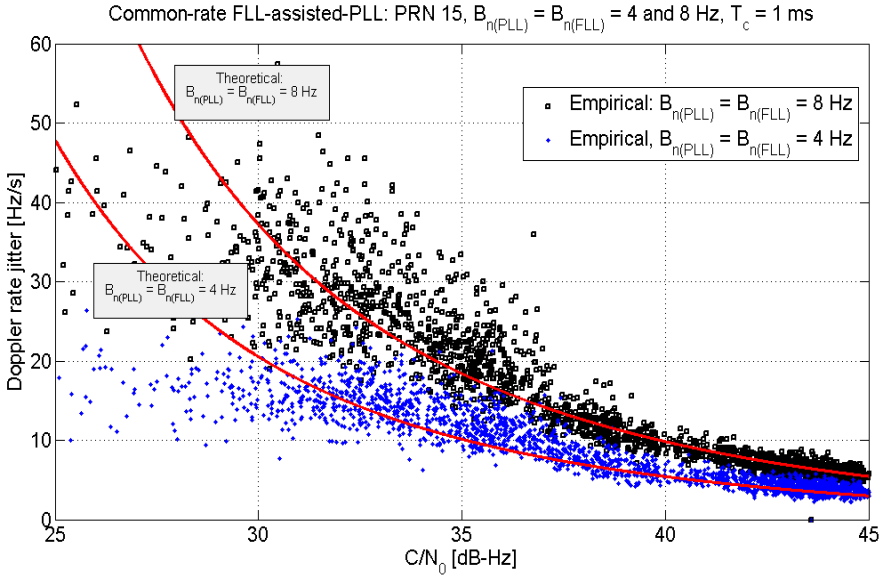

Figure 5-5: Empirical and theoretical Doppler rate jitter of raw Doppler rate measurements as a function of C/N_0 obtained using a common rate FLL-assisted-PLL. Cases considered: loop bandwidths, $B_{n(PLL)} = B_{n(FLL)}$ 4 Hz and 8 Hz and T_c = 1 ms.

Results obtained using a common-rate FLL-assisted-PLL are shown in Figure 5-5, where cases with 4 Hz and 8 Hz loop bandwidth in both the PLL and FLL branches and 1 ms coherent integration time are considered. In both cases considered in Figure 5-5, the Doppler rate measurements were obtained by time differentiating the raw Doppler observables using a 200 ms period.

From the results presented in Figure 5-5, a similar conclusion as in the case of Doppler estimation analysis in this type of a carrier tracking loop can be made. To be more specific, coupling the PLL and FLL in a single loop structure results in a higher level of noise transferred from the input signal to the final Doppler rate estimate resulting in less accurate measurements. Figure 5-5 also demonstrates that the theoretical values of the Doppler rate jitter match the empirical results indicating that the approach used for deriving the equivalent linear model of a common-rate FLL-assisted-PLL with regard to the Doppler rate estimate is correct, and that the theoretical model is also valid when applied to this type of a tracking loop structure.

Attenuated LOS: Sequential Carrier Tracking - Memory Discriminator Based Tracking Loops

In order to validate the proposed model for Doppler rate estimation in memory discriminator based tracking loops the collected data set has been processed by constraining the software receiver to operate in specified modes, namely PLL, FLL-assisted-PLL and FLL modes. In all the cases it has been observed that when compared to the standard loops, the memory discriminator based architecture provides more accurate Doppler rate estimates. The results have also shown good agreement between the Doppler rate jitter values predicted using the model defined in Eq.(5.13) and the actual Doppler rate jitter. It is noted, that to determine the theoretical Doppler rate jitter values, the model given in Eq.(5.13) has been extended to include the effect of memory discriminators by using the expression of the noise transfer function given in Eq.(5.21), where in the case of the

common-rate FLL-assisted-PLL the loop filter transfer function, $B(z)$, was replaced by $B_{eq}(z)$ (Eq.(3.38)). To avoid the repetition of similar findings, only the case of a memory discriminator based PLL will be presented here.

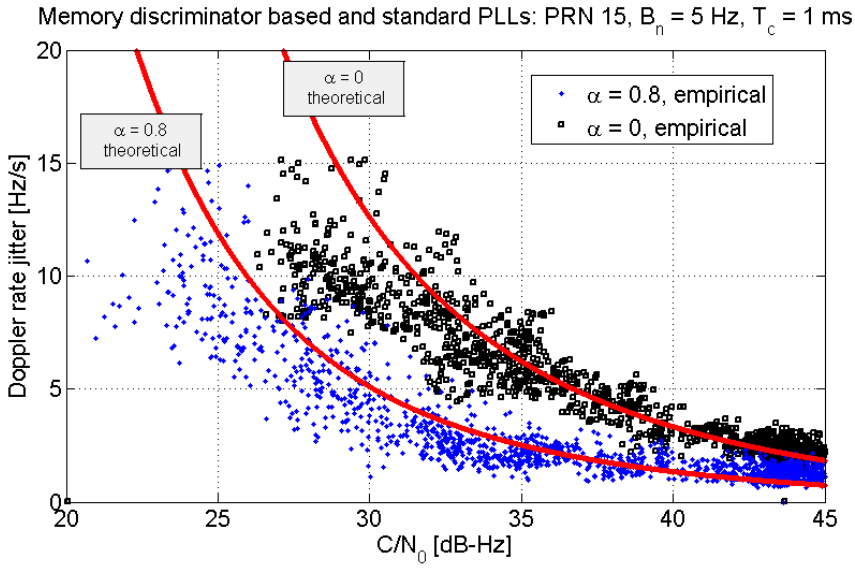

Figure 5-6: Comparison of empirical and theoretical Doppler rate jitter as a function of C/N_0 and forgetting factor, α, obtained using a memory discriminator based 3rd order PLL, T_c = 1 ms, B_n = 5 Hz. The Doppler rate estimates were obtained by differentiation of the raw Doppler measurements using a 200 ms period.

Figure 5-6 compares the theoretical Doppler rate jitter obtained using a 3rd order memory discriminator based PLL using 1 ms coherent integration time, 5 Hz loop bandwidth and a forgetting factor, α, equal to 0 and 0.8, where α = 0 represents the case of a standard tracking loop. In this particular case Doppler rate measurements were computed by time differentiating the raw Doppler observables using a 200 ms period.

Attenuated LOS: Block Processing

The equipment setup used to collect the data for practical verification of the model proposed for Doppler rate estimation in the block processing approach is illustrated in Figure 3-16. The procedure adopted to perform this data collection and general details about the GSNRx™-rr are provided in *Section 3.2.1*.

Results obtained using the block processing approach are presented in Figure 5-7 where the theoretical and empirical Doppler rate jitter values determined using different integration times are compared.

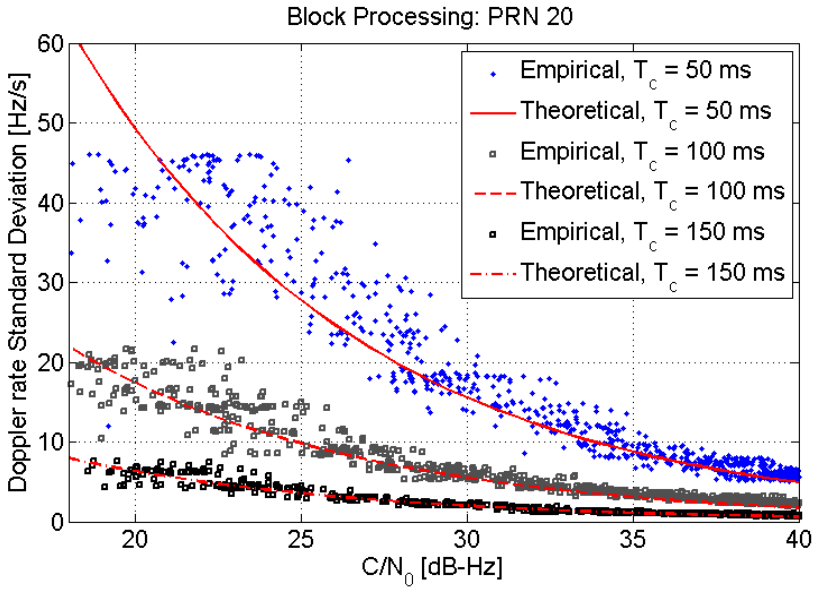

Figure 5-7: Empirical Doppler rate jitter compared to the proposed theoretical model as a function of C/N_0 and integration time. Doppler rate measurements obtained by performing the correlation peak search with a step of 0.2 Hz. No additional filtering applied to the empirical data.

The theoretical Doppler rate jitter was determined using Eq.(5.26), whereas the measured Doppler rate jitter results were processed as specified in Eq.(5.30). In all cases a step in the

frequency domain equal to 0.2 Hz was used to perform the search for the correlation peak. The Doppler rate measurements were obtained by differentiating raw Doppler observables obtained using the search strategy described in *Section 2.3.4*. It is important to consider, that no additional filtering has been applied to the empirical data prior to the determination of the Doppler rate jitter. Again, a good agreement between the empirical and theoretical results can be observed confirming the fact that also for the block processing approach a parameter identical in function the Doppler bandwidth can be defined.

5.2.1.2 Negligible Doppler Rate Assumption Verification

It is important to consider that both Eqs. (5.13) and (5.26) are derived under the assumption of negligible Doppler rate during the integration period, T_c. To confirm the validity of this assumption in practice, and further support the developed theoretical models, additional tests were performed. To have a full control over the user motion profile, a hardware GPS simulator, the GSS 7700 from Spirent was used to simulate the GPS signals. A simple linear trajectory has been simulated wherein the user was moving along the trajectory with a constant acceleration. Accelerations in the range of 0.1 - 2 m/s^2 were simulated. At the same time the signal was progressively attenuated with a step of 1 dB each 6 s after 30 seconds without attenuation. Equipment setups similar to the ones illustrated in Figures 3-8 and 3-16 were used. But in this case the RF signals were generated by the GSS 7700 hardware GPS simulator and external LNAs were used to simulate the effect of the active antenna.

Figures 5-8 and 5-9 illustrate the results obtained in the case of a 1.5 m/s^2 receiver acceleration. In particular, Figure 5-8 considers the case of a 3rd order PLL, where the empirical Doppler rate jitter values are compared to the theoretical ones determined according to the model defined in Eq.(5.13), whereas the comparison between the empirical results obtained using the block processing approach and the values computed using the theoretical expression given in Eq.(5.26) is shown in Figure 5-9.

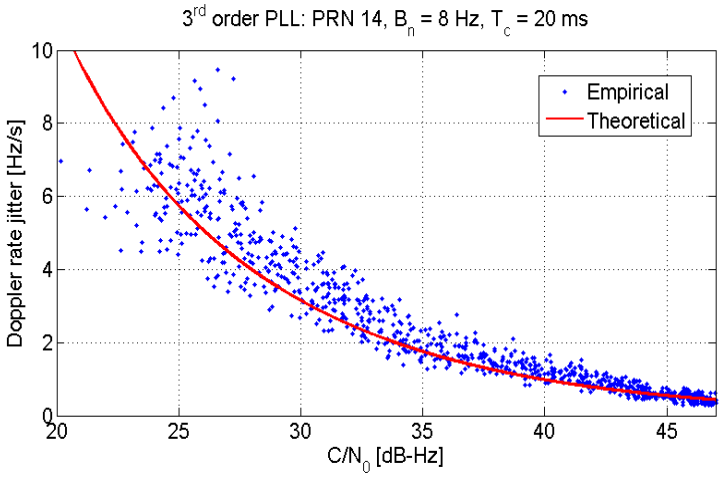

Figure 5-8: Empirical and theoretical Doppler rate jitter as a function of C/N_0. Doppler rate estimates obtained by differentiating the raw Doppler measurements with a 20 ms period and further filtered using a MA filter with 10 ms analysis window.

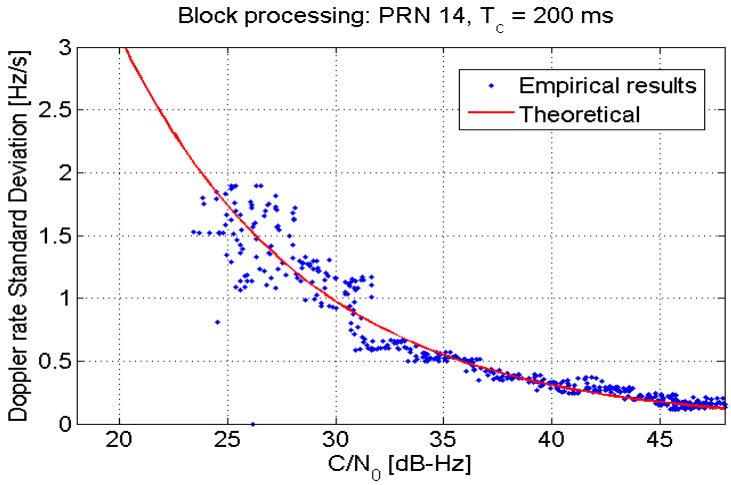

Figure 5-9: Predicted and measured Doppler rate jitter as a function of C/N_0. Doppler rate measurements were obtained by performing a search for the correlation peak with a step of 0.2 Hz. Constant user acceleration of 1.5 m/s^2 simulated during the entire data collection.

From the results in Figures 5-8 and 5-9, it is possible to conclude that the assumptions made by a GPS for measuring Doppler rate, i.e., Doppler rate has a negligible impact during the integration time, are still valid even when significant acceleration for a pedestrian user is present.

5.2.1.3 Moderate Urban Canyon Environment: Sequential Architecture

The theoretical model for the analysis of the Doppler rate measurement accuracy was further studied by using the GPS L1 C/A data collected in more realistic conditions and in the presence of different signal impairments. Results from a pedestrian-based test performed in a foliage obstructed environment will be presented in this section.

In this experiment, after staying stationary for one minute, a trajectory including areas with open-sky at the start and the end of the test, and a forested area in the middle of the trajectory was followed. Figure 5-9 summarizes the results for this test by comparing the measured and theoretical Doppler rate jitter. Because of large variations in the values of Doppler rate jitter, the logarithmic scale was used for better visualization of the results. In the case considered in Figure 5-9 the collected data set was processed using the standard GSNRx^{TM} receiver without any constrains. To be more specific, the choice of the tracking modes was regulated by the PLI and FLI of the software receiver (Petovello & O'Driscoll 2007). Based on the tracking status provided by the receiver at each measurement epoch, it was possible to determine the value of the Doppler rate bandwidth using the appropriate signal frequency rate transfer function, $H_{\dot{n}f}(z)$. Having determined the Doppler rate bandwidth, the theoretical value of the Doppler jitter could be computed by using the proposed model given in Eq.(5.13). Tracking loop parameters used for each tracking loop are specified in Table 5-1.

Table 5-1: Carrier tracking loop parameters used to process the data collected in the foliage obstructed environment.

Tracking State	Loop Bandwidth	Coherent integration time
PLL	$B_n = 8\ Hz$	$T_c = 1\ ms$
FLL-assisted-PLL	$B_{n_{(PLL)}} = 8\ Hz$ $B_{n_{(FLL)}} = 10\ Hz$	
Narrow pull-in FLL	$B_n = 10\ Hz$	
Wide pull-in FLL	$B_n = 10\ Hz$	

In the cases of the PLL and FLL-assisted-PLL the Doppler rate estimates were obtained by differentiating raw Doppler measurements using a 1 ms period and then filtering them using a MA filter with a 400 ms analysis window. Whereas in the case of the FLL (this includes both wide and narrow pull-in FLL modes) Doppler rate measurements were obtained directly from the output of the FLL loop filter and subsequently filtered using a MA filter with a 400 ms analysis window. The effect of the MA filter was accounted for in the theoretical model by setting $S(z)$ as defined in Eq.(2.13) in the expression of the frequency rate noise transfer function, $H_{\dot{n}f}(z)$. As in the case of the Doppler analysis detailed in **Chapter 3**, due to the fact that the C/N_0 estimates and the Doppler rate values provided by GSNRx^{TM} are evaluated from the same correlator outputs, they are both affected by the same impairments. Thus, also in the case of Doppler rate measurements multipath and fading phenomena, which are not accounted for in the theoretical model of the Doppler rate jitter, are partially compensated by the use of the C/N_0 provided by the receiver.

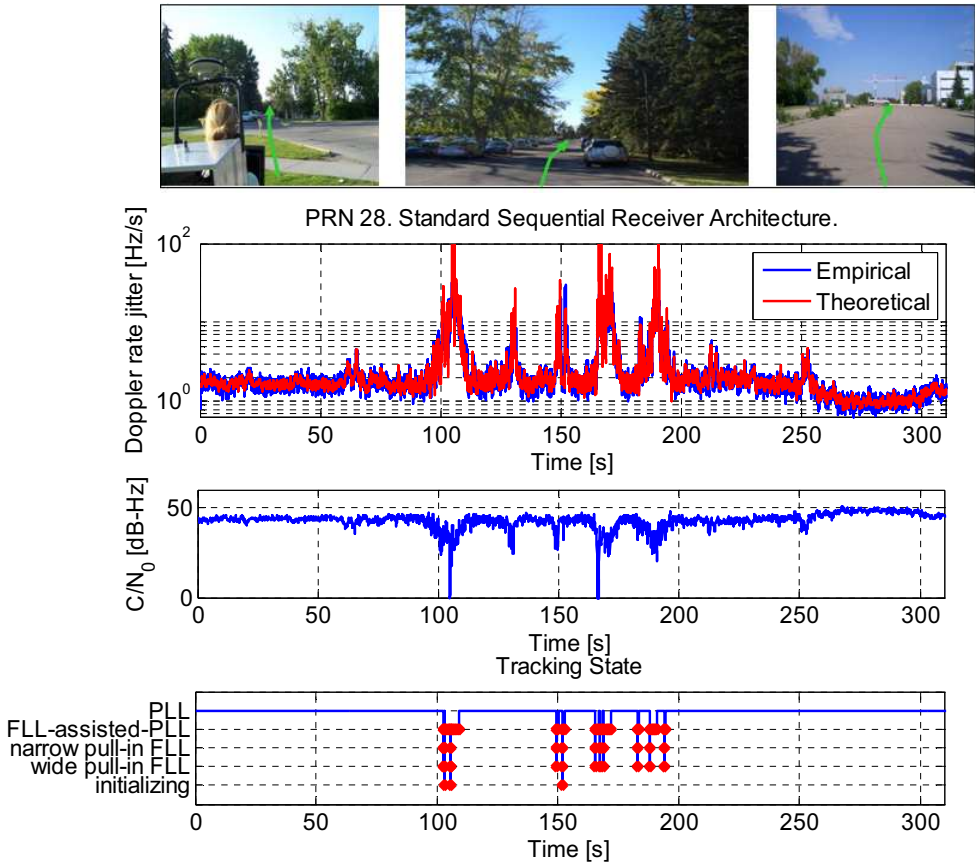

Figure 5-9: Environment view and Doppler rate jitter analysis for a pedestrian-based test in a foliage obstructed environment. Standard sequential architecture.

Results obtained in this test also demonstrate a good match between the Doppler rate jitter predicted using the theoretical model (Eq.(5.13)) and the empirical results, further confirming the validity of the proposed model. The collected data set has also been processed using the memory discriminator based architecture and results comparable to those obtained with the standard architecture were achieved.

5.2.1.4 Indoor Environment/Wooden Residential House: Block Processing Architecture

The procedure used to perform this data collection, test environment and equipment setup are described in detail in *Section 3.2.1.3*, where the test trajectory is explicitly described in Figure 3-19. About seven minutes of RF data were recorded in a pedestrian-based test performed in a typical North American wooden residential house, during which nine GPS satellites were tracked. The collected data set was processed using GSNRx^{TM}-rr version of the software receiver implementing block processing techniques. Following the data analysis methodology used in all the tests presented in this chapter, the empirical data were processed as specified in Eq.(5.30). The theoretical Doppler jitter, in its turn, was determined using the model defined in Eq.(5.26).

Figure 5-10 shows the results obtained in this test by using a 50 ms integration time, where a step equal to 0.2 Hz was used to perform the search for the correlation peak in the frequency domain.

The Doppler rate measurements in this case were obtained by differentiating the raw Doppler measurements using a 400 ms period. No additional filtering has been applied to either Doppler or Doppler rate measurements.

Change of the test environments from clear-sky/outdoors to main floor, then basement and back to clear-sky, experienced by the receiver resulted in different levels of signal attenuation, this can be observed from the C/N_0 plot at the bottom of Figure 5-10. In addition to this, since the user was in constant motion, making several loops on each level of the house, the effects of the user motion and gait caused variations in the Doppler rate measurements, effect of which was directly transferred to the Doppler rate jitter. Similar to the case of the sequential tracking loops, these effects are partially compensated for through the use of the C/N_0 provided by the receiver in the theoretical values of Doppler rate jitter determined using Eq.(5.26), leading to good agreement between the empirical and theoretical results.

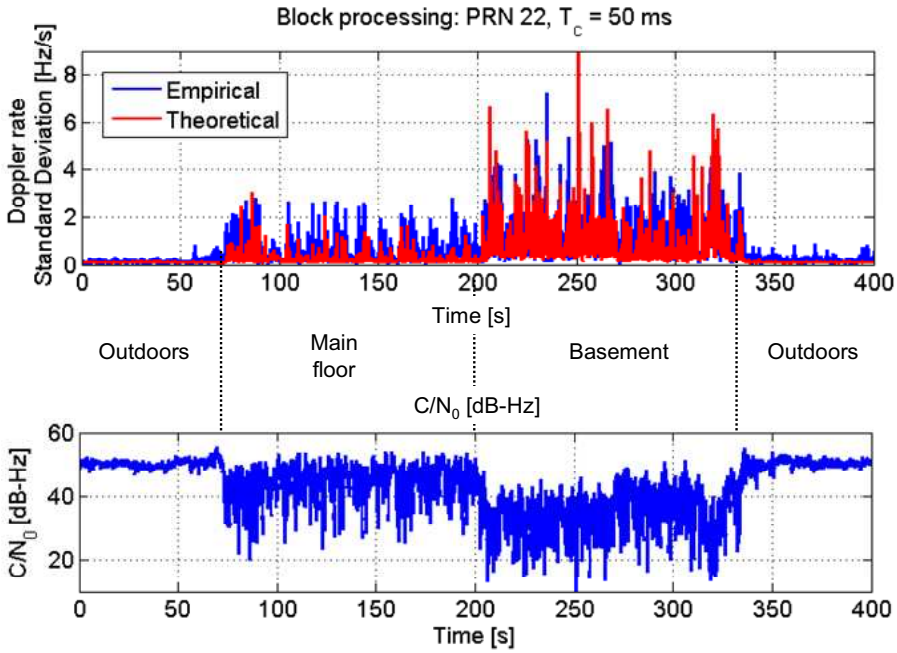

Figure 5-10: Doppler rate jitter analysis for a pedestrian-based test in an indoor environment, block processing approach. Doppler rate measurements were obtained by differentiating Doppler observables using a 400 ms period.

5.2.2 Doppler Rate Bias Model Verification

As in the case of Doppler bias considered in *Section 3.2.2*, to be able to validate the potential bias in the Doppler rate measurements, a reference Doppler rate solution is required. Therefore, the same experimental approach used in *Section 3.2.2* was applied here: a GPS hardware simulator, the GSS 7700 from Spirent was used for GPS signal generation and to provide an accurate reference. The same scenario, simulating the dynamics of a road bound vehicle moving along a rectangular trajectory, as used for the evaluation of the Doppler bias is considered. A detailed description of the simulated

platform dynamics, test methodology, equipment setup and specifications are provided in *Section 3.2.2*. In particular, Figures 3-22 and 3-25 (upper plot) illustrate the simulation trajectory and the absolute acceleration experienced by the receiver during the simulation. Because of higher levels of dynamics experienced by the receiver at each turn of the trajectory, the tracking loops of the receiver are not able to instantaneously follow the rapid variations in Doppler rate, leading to a bias introduced at each turn.

The Doppler rate bias was measured by taking the difference between the Doppler rate values estimated by the receiver and the reference Doppler rate provided by the hardware simulator. These measurements were then compared against the theoretical Doppler rate bias obtained by filtering the reference Doppler rate provided by the simulator with the bias impulse response given by Eq.(5.16).

Because of the way the hardware simulator generates the reference Doppler/Doppler rate, the theoretical Doppler rate bias looks like a sawtooth wave. Since the true Doppler rate is piece-wise linear, its derivative is discontinuous and these discontinuities are reflected in the predicted Doppler rate bias that assumes a sawtooth shape. It should be noted that this behaviour is observed in all the results presented in this section.

5.2.2.1 Doppler Rate Bias: Standard Tracking Loops

Figure 5-11 compares the measured and theoretically predicted biases for a 2 g turn in the simulated trajectory obtained using a third order PLL. The collected data set was processed using a 10 Hz loop bandwidth and 1 ms coherent integration time to assure that the receiver maintains phase lock during high dynamic sections of the trajectory. In order to obtain Doppler rate measurements, the raw Doppler estimates were filtered by a MA filter with 400 ms analysis window, and then subsequently differentiated using a 1 ms period. For the determination of the theoretical bias values, the effect of the MA filter was accounted for in the theoretical model by setting the smoothing filter, $S(z)$, as defined in Eq.(2.13) and substituting into the signal frequency transfer function (Eq.(3.19)). Figure 5-11 shows that

the proposed theoretical model is capable to effectively predict the Doppler rate bias introduced by a third order PLL.

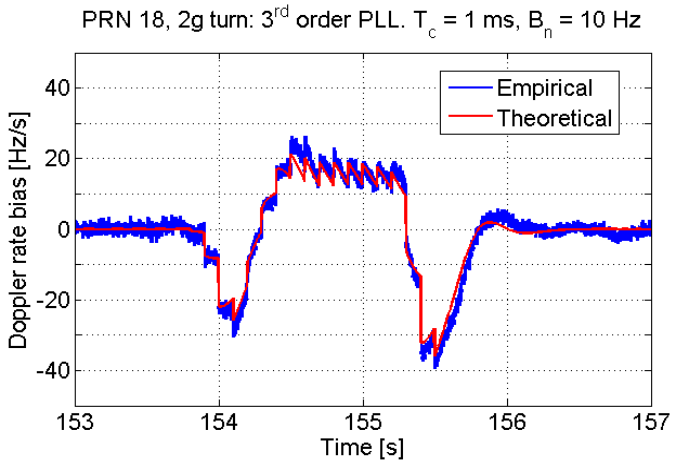

Figure 5-11: Observed and predicted Doppler rate bias of a 3rd order PLL, 2 g turn. The Doppler rate measurements were obtained by differentiating the raw Doppler measurements filtered using a MA filter with a 400 ms analysis window.

Good match between the theoretical and empirical Doppler rate biases also indicates that the developed model is capable to account for the effect of the smoothing filter, $S(z)$.

The same analysis has been performed with the data obtained by processing the collected data set in FLL mode. The theoretical Doppler rate bias was determined by filtering the reference Doppler rate with the bias impulse response given by Eq.(5.16), whereas the empirical one was computed as explained above, namely by taking a difference between the reference and measured Doppler rate values. Figure 5-12 illustrates the comparison of the predicted and measured Doppler rate bias values for a 2.5 g turn of the simulation trajectory.

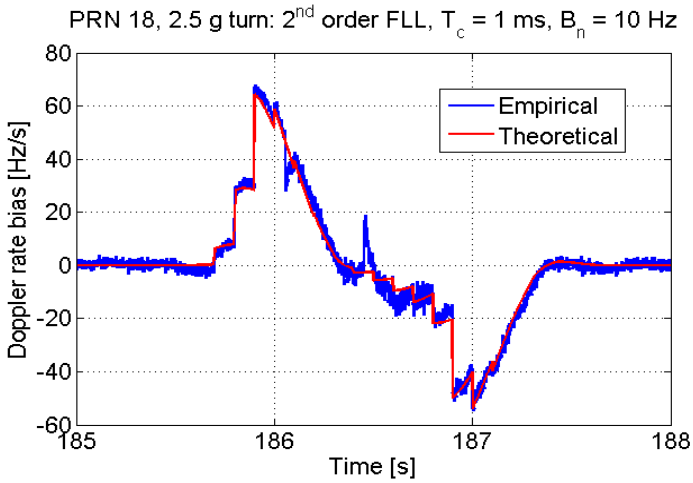

Figure 5-12: Observed and predicted Doppler rate bias of a 2nd order FLL, 2.5 g turn. Doppler rate measurements were obtained directly from the output of the FLL loop filter and subsequently filtered using a MA filter with a 400 ms analysis window.

The Doppler rate measurements were obtained directly from the output of the FLL loop filter and subsequently smoothed using a MA filter with a 400 ms analysis window. Also in this case a 10 Hz loop bandwidth and 1 ms coherent integration time were used.

Results for other turns of the simulated trajectory were analysed as well. As in the case of the Doppler bias analysis, it has been observed that when subjected to the same type of dynamics, PLL and FLL react in the same way. However, due to better lock performance of the FLL (Ward 1998) it can tolerate higher levels of platform dynamics when compared to PLL.

In the case of the common-rate FLL-assisted-PLL, the proposed theoretical model was validated by processing the collected data set with GSNRx™ constrained to operate in the FLL-assisted-PLL mode. As in the above, the theoretical values of the Doppler rate bias were determined by filtering the reference Doppler rate with the bias impulse response given by Eq.(5.16). To be able to apply Eq.(5.16) to this type of a tracking loop, the effect

of using PLL and FLL branches in a coupled mode was first modelled as defined in Eq.(3.38), and subsequently used to determine the transfer function of the input signal frequency rate, $H_{\dot{f}_d}(z)$, characterizing the signal frequency rate impulse response, $h_{\dot{f}_d}[k]$.

Figure 5-13 shows the observed and theoretically predicted Doppler rate biases for a 2.5 g turn. In this case as well, to obtain Doppler rate measurements, the raw Doppler estimates were filtered by a MA filter with 400 ms analysis window, and then subsequently differentiated using a 1 ms period. Loop bandwidth of 10 Hz in both the PLL and FLL branches, and 1 ms coherent integration time were used.

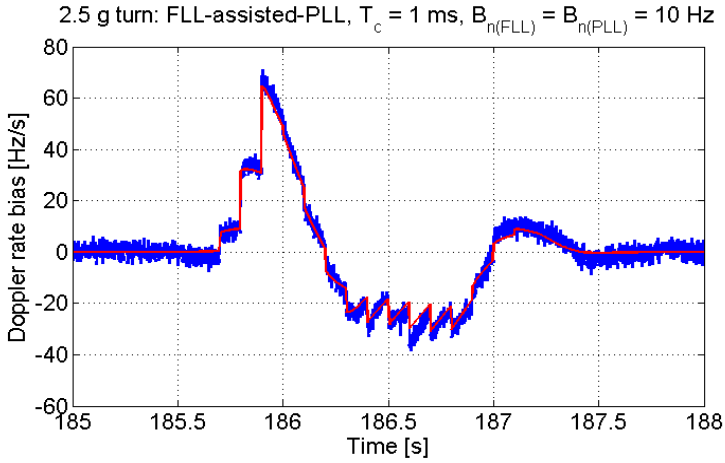

Figure 5-13: Measured and predicted Doppler rate bias of a common-rate FLL-assisted-PLL, 2.5 g turn. Loop bandwidth, $B_{n(PLL)} = B_{n(FLL)}$ 10 Hz and T_c = 1 ms.

Results presented in Figure 5-13 indicate that the proposed theoretical model for Doppler rate bias analysis is also able to effectively predict the Doppler rate bias of a common-rate FLL-assisted-PLL.

5.2.2.2 Doppler Rate Bias: Memory Discriminator Based Tracking Loops

Most of the material presented in *Section 3.2.2.2* on the performance of the memory discriminator based tracking loops in terms of Doppler tracking and Doppler bias estimation also apply to the case of Doppler rate estimation. Due to increased resilience against thermal noise, memory discriminator based tracking loops are capable to maintain lock under higher dynamics compared to the standard tracking loops which tend to loose lock under the joint impact of noise and dynamics. But, as it has been observed from the test results and as it is in fact expected in theory, the values of the Doppler rate bias measured by a standard and memory discriminator based tracking loop of the same order using equal values of the loop bandwidth and coherent integration time are similar.

To give an insight into how the developed theoretical model for Doppler rate bias analysis performs when applied to memory discriminator based tracking loops, this section will present the results for a 2.5 g turn for a 2^{nd} order memory discriminator based FLL. The measured and predicted Doppler rate bias values obtained using an 8 Hz loop bandwidth, 1 ms coherent integration time and $\alpha = 0.4$ are compared in Figure 5-14.

Since FLL provides direct access to Doppler rate information, the Doppler rate measurements were obtained directly at the output of the loop filter and then smoothed with a MA filter using a 400 ms analysis window.

The results presented in *Section 5.2.2* are consistent and show a good agreement between the Doppler rate bias values predicted using the theoretical model and the ones determined empirically. This leads to the conclusion that the proposed theoretical model for Doppler rate bias analysis is capable to effectively quantify the effect of dynamics on the Doppler rate estimates and is applicable to both standard and memory discriminator based tracking loops.

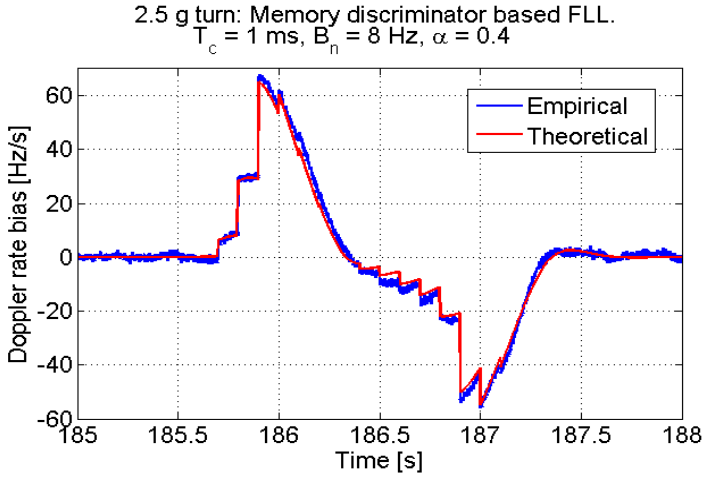

Figure 5-14: Measured and predicted Doppler bias for a 2nd order memory discriminator based FLL, 2.5 g turn, PRN 18. Doppler rate measurements were obtained directly from the output of the FLL loop filter and subsequently filtered using a MA filter with a 400 ms analysis window.

CHAPTER 6: CONCLUSIONS AND FUTURE WORK

The conclusions of the thesis are divided into two parts to reflect the two primary contributions of the performed research. The first being the theoretical framework for the analysis of the process of Doppler and Doppler rate estimation in GNSS receivers and other the approach to designing the loop filter based on the Doppler bandwidth parameter.

6.1 Conclusions

The major contribution of this thesis is the development of a complete theoretical framework for Doppler frequency and Doppler frequency rate estimation. In order to provide a comprehensive study of the noise propagation in the process of estimation of the above-mentioned parameters, two approaches commonly used in GNSS receivers were considered: the sequential carrier tracking, including the standard and the memory discriminator based approaches, and block processing techniques. The analysis of the sequential carrier tracking also explicitly considered three types of tracking loops: the PLL, common-rate FLL-assisted-PLL and FLL.

For each approach a theoretical model for predicting the quality of Doppler and Doppler rate measurements, relating their variance and bias to C/N_0, the user dynamics and the algorithm parameters was introduced. For the derivation of the theoretical models a different method for each of the approaches was used. In particular, in the case of the sequential carrier tracking loop architecture the standard tracking loop linear theory focusing on the propagation of the phase noise was reformulated with respect to the signal Doppler frequency and frequency rate, frequency and frequency rate noise and the final Doppler frequency and frequency rate measurements provided by the loop. The concepts of Doppler and Doppler rate bandwidths have been introduced and used for characterizing the quality of Doppler and Doppler rate measurements. As it has been shown in **Chapters 3**

and **4** when performing the analysis of the test results, both parameters can be used as metrics for comparative analysis.

For the block processing approach, the CRLB for frequency estimation was used to derive a tight approximation of the variance of the frequency estimates generated by block processing techniques. The derived expression was then subsequently used to determine the expression of the variance of the Doppler rate estimates.

The provided theoretical framework allows one not only to study and characterize the impact of different algorithm parameters such as the loop noise bandwidth and integration time, as well as the C/N_0 and the user dynamics on the accuracy of Doppler and Doppler rate measurements, but also to effectively predict the quality of the measurements.

The validity of the proposed theoretical framework has been proven using live GPS L1 C/A data collected in various GPS operating environments in both static and dynamic modes. Also a number of simulations were carried out to test the theoretical models under a wider range of dynamics. In all the experiments a thorough analysis of the results has been performed through comparison of the empirical results against the ones obtained using the developed theoretical models and in all cases a good agreement was observed.

The following conclusions have been made from the research presented on this particular topic throughout this thesis:

1. The concept of **Doppler bandwidth** was introduced to quantify the amount of noise transferred from the input of the tracking loop to the final frequency estimate. This concept represents a counterpart of the loop noise bandwidth for frequency estimation with the major difference being that Doppler bandwidth provides a closer interpretation of the bandwidth required to track particular system dynamics. Doppler bandwidth summarizes in a single parameter the ability of a tracking loop to produce smooth frequency estimates, including the effects of all loop components and the smoothing filter, $S(z)$. This quality makes it an effective

metric for comparing different receivers when the same input C/N_0 and coherent integration time are assumed.

2. To determine the amount of noise transferred from the input of the carrier tracking loop to the final Doppler frequency rate estimate the concept of **Doppler rate bandwidth** was introduced. Aside from characterising the ability of the tracking loop to produce accurate Doppler rate estimates, the Doppler rate bandwidth parameter also accounts for the impact of different differentiators/filters $\left(D(z)S(z)\right)$ used for producing the final Doppler rate measurements.
3. The developed theoretical models of the Doppler and Doppler rate jitter (Eqs. (3.29) and (5.13) can be effectively used for the assessment of the Doppler and Doppler rate measurement quality given the signal C/N_0 and the processing parameters used for their generation. The validity of both models as applied to standard and memory discriminator based PLL, FLL-assisted-PLL and FLL has been thoroughly verified by live and hardware simulated GPS data and in all cases a good agreement between empirical and theoretical results was observed.
4. The developed theoretical framework is general and applies to different methods for the derivation of Doppler measurements such as raw Doppler, carrier-phase derived and filtered raw Doppler measurements.
5. The proposed theoretical models for the Doppler and Doppler rate bias analysis (Eqs. (3.31) and (5.15)) are able to effectively predict the errors caused by changes in the input Doppler frequency Doppler frequency rate and the transient response of the tracking loops (PLL, FLL-assisted-PLL and FLL). The developed models can be used for quantifying the effect of dynamics on the Doppler and Doppler rate estimates for standard and memory discriminator based loops, including the effect of the smoothing filter, $S(z)$. The model has been evaluated for different levels of dynamics (acceleration levels up to 3 g) and in all cases a good agreement between values predicted using the theoretical model and the ones determined empirically was observed.

6. Under the assumption of negligible Doppler rate over a single measurement epoch, the variance of the Doppler frequency estimates generated by the block processing approach approximately follows the CRLB (Eq.(3.47)). Based on Eq.(3.47) a parameter playing the same role as the Doppler bandwidth, can also be defined for block processing approach. The validity and effectiveness of the model given in Eq.(3.47) have been confirmed by using live GPS data collected in stationary and pedestrian-based tests through comparison of the empirical results with the theoretical ones obtained by using the theoretical model (Eq.(3.47)).
7. Due to the assumption of negligible Doppler rate over a single measurement epoch made in block processing, block processing algorithms are not able to reach the CRLB in terms of Doppler frequency rate leading to suboptimal algorithms for the estimation of Doppler rate and, consequently, to estimator variances greater than the CRLB.
8. The proposed theoretical model for the variance of the Doppler rate measurements provided by the block processing approach (Eq.(5.26)) can also be effectively used for the assessment of the Doppler rate measurement quality as a function of the input C/N_0 and the coherent integration time. The validity of this model as well has been confirmed by live and hardware simulated GPS data.

The second contribution of this thesis is a new approach to designing the loop filter based on the Doppler bandwidth providing control over the noise variance of the Doppler frequency measurements. In order to implement this approach, the original controlled-root formulation approach to loop filter design proposed by Stephens & Thomas (1995) was modified. Both standard and memory discriminator based PLLs were considered. The design criteria behind this approach have been specified, and the effectiveness of proposed algorithm validated using real GPS L1 C/A data.

To sum up the research performed on this part of the thesis, the following conclusions can be drawn:

1. Designing the loop filter based on the Doppler bandwidth allows one to configure the tracking loop to output Doppler measurements with a desired level of Doppler jitter. The beneficial feature of this approach is not in the capability of the tracking loop to provide more accurate Doppler measurements, but in the capability to provide control over the noise variance of the measurements.
2. Similar to the standard approaches, the stability of the tracking loop designed based on Doppler bandwidth is limited by the product of the coherent integration time and the Doppler bandwidth, B_d. By studying the root location of the system it has been found that the maximum achievable value of $B_d T_c$ providing a stable loop in the case of a standard PLL is 0.27. In the case of the memory discriminator based PLL, in addition to being limited by the $B_d T_c$ product, system's stability also depends on the value of the forgetting factor parameter, α.

6.2 Future Work

Based on the results and conclusions of this research, the following recommendations can be made:

1. In this thesis the CRLB of the frequency rate measurements was used as a comparison term only for the block processing algorithms used in GNSS receivers. As it has been discussed in **Chapter 5**, the problem of using the CRLB as a comparison term for standard tracking loops is the evaluation of the number of samples used for the computation of a single Doppler estimate. The presence of a reaction block and a filter in standard tracking loops introduces memory in the system, i.e., past information is retained for the computation of a single Doppler estimate. This makes M, the number of samples used for the computation of a single Doppler estimate, quite complex. Thus, to be able to use CRLB as a

comparison term for standard tracking loops further investigation of different approaches for the determination of M is required.

2. Theoretical framework developed in this thesis does not include the analysis of the bias introduced due to the transient response of the block processing techniques to rapid changes in the input signal frequency/frequency rate. It is therefore desirable to extend the theoretical framework presented in this thesis to include this type of analysis as well.
3. Research presented in this thesis concentrates on noise propagation through the process of Doppler and Doppler rate estimation. To be able to extend the proposed theoretical framework to the final velocity/acceleration estimates further studies are required in order to include the effects of errors in the satellite ephemeris and the user position.

APPENDIX A: DETERMINATION OF THE CRLB FOR FREQUENCY AND FREQUENCY RATE PARAMETERS OF A CHIRP SIGNAL

The purpose of this appendix is to detail the procedure used for the determination of the CRLB for the frequency and frequency rate parameters of a chirp signal. The derivation is based on the material presented in (Djurić & Kay 1990, Peleg & Porat 1991) and general CRLB theory given in (Kay 1993).

The signal model is given as:

$$y[n] = \exp\{j\boldsymbol{\theta} \cdot v^T[n]\} + \eta[n] \qquad n = 1, 2, \ldots, N-1., \tag{A.1}$$

where

$$v[n] = \begin{bmatrix} 1 & n \cdot T_s & n^2 \cdot T_s^2 \end{bmatrix}, \tag{A.2}$$

and T_s is the sampling interval, $\boldsymbol{\theta} = [\varphi \quad f \quad \alpha]^T$ is the parameter vector and φ, f and α are the phase, frequency and frequency rate of the signal, respectively. All the parameters are expressed in units of rad/s^i, where $i = 0, 1 \, and \, 2$. It is also known that η is a zero mean complex Gaussian process

$$\eta[n] \sim \mathcal{N}_0\left(0, \sigma^2 I\right) \tag{A.3}$$

with variance σ^2. The real and imaginary parts of η are independent and white with equal variance (Djurić & Kay). The probability density function can be then written as follows:

$$p(y;\boldsymbol{\theta}) = \frac{1}{\left(2\pi\sigma^2\right)^N} \exp\left\{-\frac{1}{2\sigma^2}\sum_{n=0}^{N-1}\left|y[n] - \exp\{j\boldsymbol{\theta}\, v^T[n]\}\right|^2\right\}, \tag{A.4}$$

taking the logarithm of which yields

$$\log p(y;\boldsymbol{\theta}) = -N\log\left(2\pi\sigma^2\right) -$$
$$-\frac{1}{2\sigma^2}\left(\sum_{n=0}^{N-1}\left|y[n]\right|^2 + \sum_{n=0}^{N-1}\left|\exp\left\{j\boldsymbol{\theta}v^T[n]\right\}\right|^2 - 2\mathbb{R}e\left\{\sum_{n=0}^{N-1}y[n]\exp\left\{-j\boldsymbol{\theta}v^T[n]\right\}\right\}\right). \tag{A.5}$$

Differentiating once produces

$$\begin{aligned}\frac{\partial p(y;\boldsymbol{\theta})}{\partial\boldsymbol{\theta}} &= \frac{1}{\sigma^2}\frac{\partial}{\partial\boldsymbol{\theta}}\left[\mathbb{R}e\left\{\sum_{n=0}^{N-1}y[n]\exp\left\{-j\boldsymbol{\theta}v^T[n]\right\}\right\}\right] \\ &= \frac{1}{2\sigma^2}\left[\sum_{n=0}^{N-1}y[n]\frac{\partial}{\partial\boldsymbol{\theta}}\exp\left\{-j\boldsymbol{\theta}v^T[n]\right\} + \sum_{n=0}^{N-1}y*[n]\frac{\partial}{\partial\boldsymbol{\theta}}\exp\left\{j\boldsymbol{\theta}v^T[n]\right\}\right] \\ &= \frac{1}{2\sigma^2}\left[-j\sum_{n=0}^{N-1}v^T[n]y[n]\exp\left\{-j\boldsymbol{\theta}v^T[n]\right\} + j\sum_{n=0}^{N-1}v^T[n]y*[n]\exp\left\{j\boldsymbol{\theta}v^T[n]\right\}\right]\end{aligned} \tag{A.6}$$

After some manipulations Eq.(A.6) can be finally written as:

$$\frac{\partial p(y;\boldsymbol{\theta})}{\partial\boldsymbol{\theta}} = \sum_{n=0}^{N-1}\frac{v^T[n]}{\sigma^2}\mathbb{I}m\left\{y[n]\exp\left\{j\boldsymbol{\theta}v^T[n]\right\}\right\}. \tag{A.7}$$

The entries of the Fisher information matrix are given by

$$\begin{aligned}I(\boldsymbol{\theta}) &= \frac{1}{\sigma^4}\sum_{n=0}^{N-1}\sum_{m=0}^{N-1}E\left[\begin{array}{l}v^T[n]\mathbb{I}m\left\{y[n]\exp\left\{-j\boldsymbol{\theta}v^T[n]\right\}\right\}\cdot \\ \cdot\mathbb{I}m\left\{y[m]\exp\left\{-j\boldsymbol{\theta}v^T[m]\right\}\right\}\cdot v[m]\end{array}\right] \\ &= \frac{1}{\sigma^4}\sum_{n=0}^{N-1}\sum_{m=0}^{N-1}\underbrace{v^T[n]}_{3x1}\underbrace{a(m,n)}_{1x1}\underbrace{v[m]}_{1x3}\end{aligned} \tag{A.8}$$

where

$$a(m,n) = E\left[\mathbb{I}m\left\{y[n]\exp\left\{-j\boldsymbol{\theta}\, v^T[n]\right\}\right\}\cdot \mathbb{I}m\left\{y[m]\exp\left\{-j\boldsymbol{\theta}\, v^T[m]\right\}\right\}\right]$$
$$= \begin{cases} 0 & for \quad m \neq n \\ \sigma^2 & for \quad m = n \end{cases} \tag{A.9}$$

Thus, since

$$E\left[\mathbb{I}m^2\left\{y[n]\exp\left\{-j\boldsymbol{\theta}\, v^T[n]\right\}\right\}\right]$$
$$= Var\left[\mathbb{I}m\left\{y[n]\exp\left\{-j\boldsymbol{\theta}\, v^T[n]\right\}\right\}\right] = \sigma^2 \tag{A.10}$$

the Fisher information matrix can be written as follows

$$I(\boldsymbol{\theta}) = \frac{1}{\sigma^2}\sum_{n=0}^{N-1} v^T[n]\, v[n] =$$
$$= \frac{1}{\sigma^2}\cdot\begin{bmatrix} \sum_{n=0}^{N-1}1 & T_s\sum_{n=0}^{N-1}n & T_s^2\sum_{n=0}^{N-1}n^2 \\ T_s\sum_{n=0}^{N-1}n & T_s^2\sum_{n=0}^{N-1}n^2 & T_s^3\sum_{n=0}^{N-1}n^3 \\ T_s^2\sum_{n=0}^{N-1}n^2 & T_s^3\sum_{n=0}^{N-1}n^3 & T_s^4\sum_{n=0}^{N-1}n^4 \end{bmatrix}$$
$$= \frac{N}{\sigma^2}\cdot\begin{bmatrix} 1 & T_s\frac{N-1}{2} & \frac{T_s^2(N-1)(2N-1)}{6} \\ T_s\frac{N-1}{2} & \frac{T_s^2(N-1)(2N-1)}{6} & \frac{T_s^3N(N-1)^2}{4} \\ \frac{T_s^2(N-1)(2N-1)}{6} & \frac{T_s^3N(N-1)^2}{4} & \frac{T_s^4(N-1)(2N-1)(3N^2-3N-1)}{30} \end{bmatrix} \tag{A.11}$$

Following identities were used to derive Eq.(A.11):

$$\sum_{n=0}^{N-1} n = \frac{N(N-1)}{2}$$
$$\sum_{n=0}^{N-1} n^2 = \frac{N(N-1)(2N-1)}{6}$$
$$\sum_{n=0}^{N-1} n^3 = \frac{N^2(N-1)^2}{4} \qquad \text{(A.12)}$$
$$\sum_{n=0}^{N-1} n^4 = \frac{N(N-1)(2N-1)(3N^2-3N-1)}{30}$$

Exploiting the relationship

$$\frac{1}{\sigma^2} = 2 \cdot C / N_0 T_s , \qquad \text{(A.13)}$$

and the fact that $NT_s = T_c$, the CRLB for the wanted parameters can be finally defined from Eq.(A.11). Thus, for the frequency:

$$I(\boldsymbol{\theta})^{-1}_{2,2} = \sigma^2_{f_d,crlb} = \frac{12\sigma^2}{NT_s^2(N-1)(N+1)} \approx \frac{12}{2C / N_0 T_s^3 N^3} = \frac{6}{C / N_0 T_c^3} \qquad \left[\frac{rad^2}{s^2}\right]. \qquad \text{(A.14)}$$

It is noted that in Eq.(A.14) the condition $N \gg 1$ was used.

In the case of the frequency rate, due to the fact that Doppler frequency rate measurements are estimated by differentiating two consecutive Doppler frequency measurements, the relationship $M = 2N$ was used leading to the following expression:

$$I(\boldsymbol{\theta})^{-1}_{3,3} = \sigma^2_{\alpha,crlb} = \frac{720}{2C / N_0 T_s^5 M(M^2-1)(M^2-4)} \approx \frac{11.25}{C / N_0 \cdot T_c^5} \qquad \left[\frac{rad^2}{s^4}\right]. \qquad \text{(A.15)}$$

APPENDIX B: FROM SIGNAL MODEL TO LIKELIGHOOD FUNCTION

Presented below is a brief description of the derivation of the Maximum Likelihood (ML) function for a GNSS signal. A more detailed explanation of the computation procedure can be found in such references as for example (Rife 1974, Flower 2002, O'Driscoll 2007), whereas the basic concepts of the ML estimation approach are presented in (Kay 1993).
For a single signal, the model of the signal at the input of the signal processing blocks (acquisition and tracking) can be written as follows:

$$\begin{aligned} y[n] &= \sqrt{2C_i}\, d_i\left[n-\frac{\tau_i}{T_s}\right] c_i\left[n-\frac{\tau_i}{T_s}\right] \cos\left(2\pi\left(f_{IF}+f_{d,i}\right)\cdot nT_s+\varphi_i\right)+w[n] \\ &= s\left[n\middle|C_i,\varphi_i,\tau_i,f_{d,i}\right]+w[n]=s\left[n\middle|\boldsymbol{\theta}\right]+w[n] \end{aligned}, \tag{B.1}$$

where the subscript i refers to the i^{th} signal and

- C_i is the carrier power;
- $d_i(\cdot)$ is the bit sequence modeling the transmitted navigation message;
- $c_i(\cdot)$ is the signal spreading sequence;
- τ_i is the delay experienced by the received signal;
- $f_{d,i}$ and φ_i are the carrier Doppler frequency and phase;
- f_{IF} is the receiver intermediate frequency;

In Eq.(B.1), $w[n]$ is assumed to be a zero mean complex additive white Gaussian noise process with single sided power spectral density (PSD) N_0, whereas $\boldsymbol{\theta}$ denotes the vector of the signal parameters and is defined as:

$$\boldsymbol{\theta} = \left[C_i,\varphi_i,\tau_i,f_{d,i}\right]^T. \tag{B.2}$$

Assuming that the measurement vector x is formed by N consecutive samples:

$$x = \left[y[0], y[1], \ldots, y[N-1] \right]^T, \tag{B.3}$$

and letting C_w denote the $N \times N$ covariance matrix of the noise samples, the likelihood function is given by (Kay 1993):

$$f_{x|\theta}\left(x|\theta \right) = \pi^{-N} \left| C_w \right|^{-1} \exp\left(-\left[x - s(\theta) \right]^H C_w^{-1} \left[x - s(\theta) \right] \right), \tag{B.4}$$

where $(\cdot)^H$ denotes the combined operation of transposition and complex conjugation on the complex vector often called the Hermitian transpose, and $|C_w|$ is the determinant of C_w. Given now the model of the likelihood function, we assume that the noise samples are mutually independent with variance σ^2, so that the covariance matrix is given by $C_w^2 = 2\sigma^2 I$, where I denotes the $N \times N$ identity matrix. Then, maximizing the likelihood function requires maximizing:

$$-\left[x - s(\theta) \right]^H \left[x - s(\theta) \right] = -|x|^2 + 2\mathbb{R}e\{ x \cdot s(\theta) \} - |s(\theta)|^2, \tag{B.5}$$

where $\mathbb{R}e\{\cdot\}$ denotes the real part of the complex number. In Eq.(B.5) the first term on the right hand side, $|x|^2$, is independent of θ, therefore the ML estimation problem can be reduced to the following expression:

$$\hat{\theta}_{ML} = \arg\max_{\theta} \left(2\mathbb{R}e\{ x \cdot s(\theta) \} - |s(\theta)|^2 \right), \tag{B.6}$$

which is referred to as the decision statistic. It consists of two components, the first is given by twice the real part of the correlation between the observation vector and the signal vector, the second is a measure of the energy in the signal vector, and can be viewed as a biasing term (O'Driscoll 2007).

Of the four elements of the parameter vector $\boldsymbol{\theta}$, we are only interested in the last two, namely the code delay, τ_i, and the carrier Doppler frequency, $f_{d,i}$. Denoting the vector of the desired parameters as $\boldsymbol{\theta}_d$, and the vector of the nuisance parameters $\boldsymbol{\theta}_n$, so that

$$\begin{aligned} \boldsymbol{\theta}_d &= \left[\tau_i,\, f_{d,i}\right]^T \\ \boldsymbol{\theta}_n &= \left[C_i, \varphi_i\right]^T \end{aligned}, \tag{B.7}$$

it can be shown that the ML of the desired parameters is given by:

$$\hat{\boldsymbol{\theta}}_{d,ML} = \arg\max_{\boldsymbol{\theta}_d} \left(\left| x \cdot \tilde{s}\left(\boldsymbol{\theta}\right) \right|^2 \right). \tag{B.8}$$

In Eq.(B.8), $\tilde{s}\left(\boldsymbol{\theta}\right) = \left[\tilde{s}_n\right]^T$, where

$$\tilde{s}_n = c_i \left[n - \frac{\hat{\tau}_i}{T_s} \right] \exp\left\{ -j2\pi \left(f_{IF} + \hat{f}_{d,i} \right) n T_s \right\}. \tag{B.9}$$

It is important to note that to derive Eq.(B.8) several assumptions have been made. In particular, it has been assumed that the received power is constant over the observation interval, also the effect of all other satellites, multipath and interference have been assumed to contribute only to the noise process. Furthermore, the time delay is approximated by a

first order Taylor series expansion (initial delay plus Doppler). Higher order effects are neglected.

This thesis focuses only on the problem of Doppler frequency, $f_{d,i}$, estimation. Thus, assuming that the receiver is able to correctly estimate the code delay, τ_i, and successfully wipe-off the code $c_i(\cdot)$, and neglecting the effect of the navigation message $d(\cdot)$, the above ML estimation problem is reduced to the classical problem of estimating the frequency of a sinusoid in noise. In this case, we have the signal at the input of the processing block responsible for Doppler frequency estimation given as:

$$r[n] = \sqrt{2C}\, d\left[n - \frac{\tau}{T_s} \right] \cos\left(2\pi\left(f_{IF} + f_d \right) \cdot nT_s + \varphi\right) + \tilde{w}[n]. \tag{B.10}$$

In Eq.(B.10) subscript i has been dropped since only a single useful component is considered. Following the derivation strategy presented above, it can be shown that the ML frequency estimator for a sinusoid in noise is given by:

$$f_{ML}[n] = \arg\max_{f_d} \left| \sum_{n=0}^{N-1} r[n] \exp\left\{ -j2\pi\left(f_{IF} + f_d \right) nT_s \right\} \right|, \tag{B.11}$$

where N is the number of samples used for frequency estimation and $r[n]$ is the signal after code wipe-off. Note that Eq. (B.11) is valid only if the navigation data message, $d(\cdot)$, is constant during the integration time period, $T_c = NT_s$.

REFERENCES

Abatzoglou T.J., (1986) "Fast maximum likelihood joint estimation of frequency and frequency rate," IEEE Trans. Aerosp. Electron. Syst., vol. 22, no. 6, pp. 708–715, Nov.

Antoniou, A. (1993) *Digital Filters: Analysis, Design and Applications*, New York: McGraw-Hill Inc.

Bancroft, J.B., G. Lachapelle, M.E. Cannon and M.G. Petovello (2008) "Twin IMU-HSGPS Integration for Pedestrian Navigation," in *Proceedings of GNSS08*, Savannah, GA, 16-19 Sep, The Institute of Navigation

Borio, D. (2009) *Velocity Estimates from Digital Tracking Loop*, Notes, 3 March, Calgary

Borio, D. (2008) FFT Sign Search with Secondary Code Constraints, IEEE VTC2008 Fall Conference, Calgary, 22-25 September

Borio, D., C. O'Driscoll (2008) *Discriminator based approaches for increasing the Integration Time in Digital Tracking Loops*, Progress report presentation. 9 July, Calgary

Borio, D., C. O'Driscoll (2010) *GNSS Receiver Design*, ENGO 638 Lecture Notes, Department of Geomatics Engineering, University of Calgary, Canada

Borio, D., and G. Lachapelle (2009) "A Non-Coherent Architecture for GNSS Digital Tracking Loops," *Annals of Telecommunications*, *Springer*, in press

Borio, D., N. Sokolova, G. Lachapelle (2009a) “Memory Discriminators for Non-Coherent Integration in GNSS Tracking Loops,” in proceedings of the *European Navigation Conference*, May 3- 6, Naples

Borio, D., N. Sokolova and G. Lachapelle (2009b) “Doppler Measurements and Velocity Estimation: a Theoretical Framework with Software Receiver Implementation,” *Proceedings of GNSS09*, Savannah, GA, 22-25 Sep, The Institute of Navigation, in preparation

Borio, D., N. Sokolova and G. Lachapelle (2010) Doppler Measurement Accuracy in Standard and High-Sensitivity GNSS Receivers, accepted for publication at *IET Radar, Sonar & Navigation journal*, 2010

Bruton, A.M. (2000) *Improving the Accuracy and Resolution of SINS/DGPS Airborne Gravimetry*. Ph.D. Thesis, Report No. 20145, Department of Geomatics Engineering, University of Calgary

Bruton A.M., Glennie C.L. and Schwarz K.P. (1999) “Differentiation for High-Precision GPS Velocity and Acceleration Determination.” *GPS solutions* 2(4), pp. 7-21

Cannon, M.E., G. Lachapelle, M. Szarmes, J. Hebert, J. Keith and S. Jokerst (1997) “DGPS Kinematic Carrier Phase Signal Simulation Analysis for Precise Velocity and Position Determination,” in *Proceedings of National Technical Meeting*, Santa Monica, January 14-16, The Institute of Navigation, Alexandria, VA., 335-350

Chan, Y. T., Ma, Q., So, C. H., and Inkol, R.: ‘Evaluation of various methods for single tone detection and frequency estimation’. In Proc. of IEEE Canadian Conference on Electrical and Computer Engineering, pp. 211–214. St. Johns, Nfld, May 1997

Cheney, W. and D. Kincaid (1985) “Numerical Mathematics and Computing,” 2nd Edition, Brooks/Cole Publishing: Pacific Grove, CA

Collins, J.P., and R.B. Langley (1999) “Possible Weighting Schemes for GPS Carrier Phase Observations in the Presence of Multipath,” Geodetic Research Laboratory, University of New Brunswick, Canada, Report to the United States Army Corps of Engineers, Topographic Engineering Center

Curran J.T, G. Lachapelle, and C.C. Murphy (2010) “Digital GNSS PLL design conditioned on thermal and oscillator phase noise.” *Aerospace and Electronic Systems, IEEE Transactions on Aerospace and Electronic Systems,* in press

Curran, J.T, G. Lachapelle, and C. C. Murphy (2011) “Improving the Design of Frequency Lock Loops for GNSS Receivers.” *IEEE Transactions on Aerospace and Electronic Systems*, in press

Djurić P.M. and S. M. Kay, (1990) “Parameter estimation of chirp signals,” IEEE Trans. Acoust., Speech, Signal Process., vol. 38, no. 12, pp. 2118–2126,

El-Sheimy, N., (2006) Inertial *Techniques and INS/DGPS Integration*, ENGO623 Course Notes, Department of Geomatics Engineering, University of Calgary

Enge, Per and Pratap Misra (2001) “Global Positioning System: Signals, Measurements, and Performance”, Ganga-Jamuna Press

FCC. *Fact sheet: FCC wireless 911 requirements*, Available at: http://www.fcc.gov/pshs/services/911-services/enhanced911/ , last accessed in June 2008

Filler, R. L. (1988) “The acceleration sensitivity of quartz crystal oscillators: A review.” IEEE Transactions on Ultrasonics, Ferroelectronics and Frequency Control, 35(3):297–305

Flower, M. L.: ‘Phase-based frequency estimation: A review’. Digital Signal Processing, vol. 12, no. 4 pp. 590–615, Oct. 2002

Fugger, T. J., B. C. Randles, A. C. Stein, W. C. Whiting, and B. Gallagher, (2000) “Analysis of pedestrian gait and perception/reaction at signal controlled crosswalk intersections,” *in Proc. of the 79th Annual Meeting, Transportation Research Board,* Washington, DC, pp. 20–25

Gaggero, P. and D. Borio (2008) “Ultra-stable Oscillators: Limits of GNSS Coherent Integration,” in *Proceedings of GNSS08*, Savannah, GA, 16-19 Sep, the Institute of Navigation

Gardner F. M., (2005) *Phaselock Techniques*, 3rd ed. Wiley-Interscience

Gelb, A. (1974) *Applied Optimal Estimation*, The Massachusetts Institute of Technology Press, USA

Hartinger, H., and F.K. Brunner (1999) “Variances of GPS Phase Observations: the SIGMA-e Model,” *GPS Solutions*, 2, pp. 35-43

Hebert, J. (1997) “High Accuracy GPS Velocity Using the Carrier Phase Observable,” in *Proceedings of International Symposium on Kinematic Systems in Geodesy*, Geomatics and Navigation (KIS97), Banff, Canada, June 3-6, pp. 265-269

Hebert, J., J. Keith, S. Ryan, M. Szarmes, G. Lachapelle and M.E. Cannon (1997) "GPS Carrier Phase Signal Simulation Analysis for Aircraft Velocity Determination," in *Proc. of 53rd Annual Meeting of the Institute of Navigation,* Albuquereque, N.M., June 30 - July 2, pp. 607-617

Julien, O. (2008) *GNSS Receiver Design*, ENGO 638 Lecture Notes, Department of Geomatics Engineering, University of Calgary, Canada

Kaplan E. D. and C. J. Hegarty (2005), Eds., Understanding *GPS: Principles and Applications*, 2nd ed. Norwood, MA, USA: Artech House Publishers

Kazemi P. L. and C. O'Driscoll (2008) "Comparison of Assisted and Stand-Alone Methods for Increasing Coherent Integration Time for Weak GPS Signal Tracking," in *Proc. of ION/GNSS'08*, Savannah, GA

Kay, S. M.: Fundamentals of Statistical Signal Processing. Volume 1: Estimation Theory. Prentice Hall, 1st ed., Apr. 1993

Kennedy S. (2002) Precise Acceleration Determination from Carrier Phase Measurements. In *Proceeding of the ION GPS 2002*, Portland Oregon, USA, 962-972

Kornfeld R.P., Hansman, R.J., and Deyst, J.J., (1998) "Single Antenna GPS Based Aircraft Attitude Determination," *Proceedings of the Institute of Navigation National Technical Meeting*, Jan. 21-23, 1998, Long Beach, CA, pp. 345-354

Lachapelle, G. (2008) *Advanced GNSS Theory*, ENGO 625 Lecture Notes. Department of Geomatics Engineering, University of Calgary, Chapter 6

Lachapelle, G., H. Kuusniemi, D. Dao, G. MacGougan and M.E. Cannon (2004) "HSGPS Signal Analysis and Performance Under Various Indoor Conditions", Navigation, U.S. Institute of Navigation, 51, 1, 29-43

Lindsey W. and C. M. Chie (1981) "A survey of digital phase-locked loops," Proc. IEEE, vol. 69, no. 4, pp. 410–431, Apr. 1981

MacGougan, G. (2003) *High Sensitivity GPS Performance Analysis in Degraded Signal Environments*, MSc Thesis, published as UCGE Report No. 20176, Department of Geomatics Engineering, University of Calgary, Canada

Misra, P. and Enge, P.: Global Positioning System: Signals, Measurements and Performance. Ganga-Jamuna Press, P. O. Box 633, Lincoln, MA 01773, 2nd ed., 2006

Moafipoor, S., Grejner-Brzezinska, D.A. and Toth, C.K. (2004) "Tightly coupled GPS/INS integration based on GPS carrier phase velocity update," *ION NTM 2004*, San Diego CA, pp. 1094-1102

O'Driscoll, C. (2007) *Performance analysis of the parallel acquisition of weak GPS signals*, Ph.D. dissertation, National University of Ireland, Cork

O'Driscoll, C., D. Borio, M.G. Petovello, T. Williams and G. Lachapelle (2009) "The Soft Approach: A Recipe for a Multi-System, Multi-Frequency GNSS Receiver," *Inside GNSS Magazine*, Volume 4, Number 5, pp. 46-51

NovAtel: *OEMV Family Installation and Operation User Manual*, http://www.novatel.com/Documents/Manuals/om-20000093.pdf, last accessed September 3, 2009

Pany, T., J.-H. Won, G. Hein (2006) “GNSS Software Defined Radio: Real Receiver or Just a Tool for Experts?” InsideGNSS, vol. 1, no. 5, Gibbons Media&Research

Parkinson B.W., J.J. Spiker, Jr., P. Axelrad and P. Enge (1996) “Global Positioning System: Theory and Applications,” AIAA, Washington, DC

Peleg and B. Porat, (1991) “The cramer-rao lower bound for signals with constant amplitude and polynomial phase,” IEEE Trans. Signal Process., vol. 39, no. 3, pp. 749–752, Mar.

Peterson, B., D. Bruckner, and S. Heye (1997) “Measuring GPS Signals Indoors,” in *Proceedings of ION GPS 1997*, September 16-19, Kansas City, Missouri, pp. 615–624, Institute of Navigation, Alexandria, VA, USA

Petovello, M.G. and C. O’Driscoll (2007) *GSNRx™ Algorithm Design Document,* Position, Location And Navigation (PLAN) Group, Department of Geomatics Engineering, University of Calgary, Canada

Petovello, M.G., C. O. Driscoll, and G. Lachapelle (2008) “Weak signal carrier tracking using extended coherent integration with an ultra-tight GNSS/IMU receiver,” in *Proc. of the European Navigation Conference*, Apr. Toulouse, France

Petovello, M.G., C. O’Driscoll, G. Lachapelle, D. Borio, and H. Murtaza (2008), “Architecture and Benefits of an Advanced GNSS Software Receiver,” in *Proc. of International Symposium on GPS/GNSS*, Tokyo, Japan

Petovello, M.G., O. Mezentsev, G. Lachapelle and M.E. Cannon (2003) “High Sensitivity GPS Velocity Updates For Personal Indoor Navigation Using Inertial Navigation Systems,” in *Proceedings of GPS2003*, Session F6, Portland, OR, 9-12 September, The Institute of Navigation

Proakis J.G., P.R. Drouilhet, Jr., and R. Price (1964) “Performance of Coherent Detection Systems Using Decision-Directed Channel Measurement”, *IEEE Transactions on Communication Systems*, vol. CS-12, pp.54-63

Psiaki M.L. (2001) “Block Acquisition of Weak GPS Signals in a Software Receiver”, *ION GPS 2001*, Sep. 11-14, 2001, pp. 2838-2850, Salt Lake City, UT, USA

Psiaki M.L., S.P. Powell, and P.M. Kintner, Jr., (2000) "Accuracy of the Global Positioning System-Derived Acceleration Vector," *Journal of Guidance, Control, and Dynamics,* Vol. 23, No. 3, May-June 2000, pp. 532-538

Raquet, J. (1998) *Development of a Method for Kinematic GPS Carrier-Phase Ambiguity Resolution Using Multiple Reference Receivers*, Ph.D. Thesis, UCGE Report No. 20116, Department of Geomatics Engineering, University of Calgary

Rife, D. C. and Boorstyn, R. R. (1974) "Single-tone parameter estimation for discrete-time observations". IEEE Trans. Inf. Theory, vol. 20, no. 5 pp. 591–598

Ryan, S., G. Lachapelle, and M.E. Cannon (1997) “DGPS Kinematic Carrier Phase Simulation Analysis in the Measurement and Position Domain,” in *Proceedings of GPS97*, Session D3, The Institute of Navigation, Kansas City, 16-19 September, pp. 1035-1045

Satyanarayana, S., D. Borio and G. Lachapelle (2010) “Power Levels and Second Order Statistics for Indoor Fading Using a Calibrated A-GPS Software Receiver. “ *Proceedings of GNSS10*, (Portland, OR, 21-24 Sep), The Institute of Navigation, 13 pages

Savitzky A. and Marcel J.E. Golay (1964) “Smoothing and Differentiation of Data by Simplified Least Squares Procedures,” Analytical Chemistry, 36: 1627–1639

Serrano, L., D. Kim, R. B. Langley, K. Itani and M. Ueno (2004) “A GPS Velocity Sensor: How Accurate Can It Be? - A First Look,” in *Proceedings of ION NTM 2004*, San Diego, California, USA, pp. 875-885

Serrano L., Kim D. and Langley R. B. (2004a) “A single GPS receiver as a real-time, accurate velocity and acceleration sensor,” in *Proceedings of ION/GNSS*, Long Beach, CA, pp. 2021–2034, September

Sokolova, N. (2009) Doppler Measurements and Velocity Estimation: Comparison of Standard and High Sensitivity Receivers. MSc Thesis, published as Report No. 20299, Department of Geomatics Engineering, The University of Calgary, Canada

Sokolova, N., D. Borio, B. Forssell, and G. Lachapelle (2010) Doppler Rate Measurements in Standard and High Sensitivity (HS) GPS Receivers: Theoretical Analysis and Comparison. Proceedings of IEEE/2010 International Conference on Indoor Positioning and Indoor Navigation (IPIN), Zurich, 15-17 September 2010, 9 pp

Soloviev A., S. Gunawardena, and F. van Graas (2004) “Deeply Integrated GPS/Low-Cost IMU for Low CNR Signal Processing: Flight Test Results and Real Time Implementation,” in *Proc. of ION/GNSS*, Long Beach, CA, pp. 1598 – 1608

Soloviev, A., F. Van Grass and S. Gunawardena (2008) "Decoding Navigation Data Messages from Weak GPS Signals," *IEEE Transactions on Aerospace and Electronic Systems*, Accepted for publication

Stephens S.A. and J. Thomas (1995) "Controlled root formulation for digital phase-locked loops," *IEEE Trans. Aerosp. Electron. Syst.*, vol. 31, no. 1, pp. 78 – 95

Strässle C., D. Megnet, H. Mathis, and C. Bürgi (2007) "The squaring loss paradox," in *Proc. of ION/GNSS*, FortWorth, TX, pp. 2715 – 2722

Szarmes, M., S. Ryan, G. Lachapelle and P. Fenton (1997) "GPS High Accuracy Aircraft Velocity Determination Using Doppler Measurements," in *Proceedings of International Symposium on Kinematic Systems in Geodesy*, Geomatics and Navigation - KIS97, Banff, June 3-6, Dept of Geomatics Engineering, the University of Calgary, 167-174

Tsui, J. B.-Y. (2005) "Fundamentals of global positioning system receivers: a software approach", *John Wiley & Sons Inc. 2nd ed., pp. 39-41*

Turunen, S. (2007) "Network Assistance: What Will New GNSS Signals Bring to It?" *Inside GNSS*, pp. 35–41

u-blox: *AEK-4P-4H-4T Product Summary*, http://www.amtechs.co.jp/2_gps/download/catalog/u-blox/ **,** last accessed June 20, 2009

van Dierendonck A. J. (1996) "GPS Receivers," in Global Positioning System: Theory and Applications, B. W. Parkinson and J. J. Spilker Jr, Eds., Vol. 1. American Institute of Aeronautics and Astronautics (AIAA), 1996

van Diggelen F. (2001) “Global Locate Indoor GPS Chipset & Services,” in *Proceedings of the ION GPS*, Salt Lake City

van Graas, F., A. Soloviev (2004) “Precise Velocity Estimation Using a Stand-Alone GPS Receiver,” Navigation, *Journal of the Institute of Navigation*, Vol. 51 No. 4

van Grass F., Soloviev A., de Haag M. U., Gunawardena S. and Braasch M. (2005) “Comparison of two approaches for GNSS receiver algorithms: batch processing and sequential processing considerations” in Proc.of ION/GNSS, Long Beach, CA, pp. 200-211, September

Ward P.W., J.W.Betz and C.J.Hegarty (2005) “Satellite Signal Acquisition, Tracking, and Data Demodulation,” [Chapter 5] in Kaplan E. D. and C. J. Hegarty (2005), Eds., *Understanding GPS: Principles and Applications*, *2nd ed*. Norwood, MA, USA: Artech House Publishers

Watson, R., G. Lachapelle, R. Klukas, S. Turunen, S. Pietilä and I. Halivaara (2006) “Investigating GPS Signals Indoors with Extreme High-Sensitivity Detection Techniques,” *NAVIGATION*, 52(4), pp. 199-213

Wieser, A., M. Gaggl and H. Hartinger (2005) “Improved positioning accuracy with high-sensitivity GNSS receivers and SNR aided integrity monitoring of pseudo-range observations,” *in Proceedings ION GNSS 2005*, 18th Int. Technical Meeting of the Satellite Division, Sept.13-16, Long Beach, CA

Wieser A. (2007) “Development of a GNSS Odometer” in *Proc. of the 20th ION/GNSS*, Forth Worth, TX, pp. 1466-1476, September

Wendel, J., Meister, O., Moenikes, R. and G.F. Trommer, (2006) “Time-differenced carrier phase measurements for tightly coupled GPS/INS integration,” *PLANS 2006*, San Diego CA, pp. 54-60

Zhang J., K. Zhang, R. Grenfell, Y. Li and R. Deakin, (2005) “Real-time Doppler/Doppler rate derivation for dynamic applications,” Journal of Global Positioning System (JGPS), vol. 4, no. 1, pp. 95–105

2.7 GHz RF Vector Signal Analyzer with Digital Downconversion, National Instruments, http://www.ni.com/pdf/products/us/catvectorsignalanalyzer.pdf, 2006